

SERIES EXPANSIONS AND DIRECT INVERSION FOR THE HESTON MODEL*

SIMON J. A. MALHAM[†], JIAQI SHEN[†], AND ANKE WIESE[†]

Abstract. Efficient sampling for the conditional time integrated variance process in the Heston stochastic volatility model is key to the simulation of the stock price based on its exact distribution. We construct a new series expansion for this integral in terms of double infinite weighted sums of particular independent random variables through a change of measure and the decomposition of squared Bessel bridges. When approximated by series truncations, this representation has exponentially decaying truncation errors. We propose feasible strategies to largely reduce the implementation of the new series to simulations of simple random variables that are independent of any model parameters. We further develop direct inversion algorithms to generate samples for such random variables based on Chebyshev polynomial approximations for their inverse distribution functions. These approximations can be used under any market conditions. Thus, we establish a strong, efficient and almost exact sampling scheme for the Heston model.

Key words. Series expansion, Direct inversion, Chebyshev approximation, Stochastic volatility

AMS subject classifications. 91G60, 41A58, 34E05, 41A10, 60H30

1. Introduction. Stochastic volatility models involving a pair of stochastic differential equations, with the diffusion term of the first one governed by the evolution of the second equation, are immensely popular in the pricing of derivatives. Among the existing stochastic volatility models, the Heston model plays an important role and is used widely. It can be expressed in the form of a two-dimensional system

$$(1.1) \quad \frac{dS_t}{S_t} = \mu dt + \sqrt{V_t} \left(\rho dW_t^1 + \sqrt{1 - \rho^2} dW_t^2 \right),$$

$$(1.2) \quad dV_t = \kappa (\theta - V_t) dt + \sigma \sqrt{V_t} dW_t^1,$$

where W^1 and W^2 are two independent standard Brownian motions, and κ, θ, σ and typically also μ are positive constants with $\rho \in [-1, 1]$. The component S characterises the dynamics of the stock price while the component V specifies the variances of its returns. The introduction of randomness to the volatility has been used to explain the long-observed features of the implied volatility surface in a self-consistent way. The variance process follows a mean-reverting square-root or Cox-Ingersoll-Ross (CIR) process (Cox, Ingersoll and Ross [13]).

Closed form solutions for standard vanilla option prices under the Heston model are available; see Heston [21] and Kahl and Jäckel [25]. However for exotic options, especially path-dependent options, such closed form solutions are not known in general and Monte Carlo simulation is often employed. Typically, continuous stochastic processes are approximated by paths simulated on discrete time grids. It is normally natural to consider the Euler-Maruyama scheme which converges weakly with convergence rate one under certain regularity conditions; see Section 14.5 in Kloeden and Platen [26], or other standard higher-order discretization approaches such as the Milstein [30] and Itô-Taylor schemes introduced in Chapter 14 and 15 in Kloeden and

*Submitted to the editors DATE.

Funding: James Watt Scholarship.

[†]Maxwell Institute for Mathematical Sciences and School of Mathematical and Computer Sciences, Heriot-Watt University, Edinburgh, EH14 4AS, UK (S.J.A.Malham@hw.ac.uk, js46@hw.ac.uk, A.Wiese@hw.ac.uk).

Platen [26]; see Section 6.2 in Glasserman [17] as well. However, these conditions do not hold in the Heston model, which will be discussed in detail below.

Discretization schemes such as those have several drawbacks for the Heston model. The first issue is that the probability of the discretised variance process becoming negative is nonzero, which will bring considerable biases to the simulation estimators. Correction techniques such as absorption and reflection are designed to overcome this problem, see Gatheral [15], Bossy and Diop [11] and Higham and Mao [22]. Lord, Koekkoek and Van Dijk [27] unify a large number of traditional correction techniques and design a new scheme, the full truncation method, which seems to perform well in many situations. Taking advantage of the qualitative properties of the true distributions, Andersen [5] proposes two new time-discretization algorithms based on moment-matching strategies, namely the truncated Gaussian scheme and the quadratic-exponential scheme. These positivity-preserving schemes are reported to have substantial improvements in efficiency and robustness over other existing methods; see Andersen [5], Lord, Koekkoek and Van Dijk [27] and Haastrecht and Pelsser [39].

The second issue is related to convergence, which requires the drift and diffusion coefficients to be globally Lipschitz, see Kloeden and Platen [26]. However, the square root functions embedded in the Heston model are not Lipschitz. Thus, convergence of these discretization schemes is difficult to establish; see Glasserman [17] and Andersen [5]. Recently, Altmayer and Neuenkirch [4] have studied the weak convergence rate for a numerical scheme under the Heston model, which typically reaches order one with mild assumptions. Hefter and Jentzen [20] consider the one-dimensional CIR process and show that equidistant discretization methods may have an arbitrary slow convergence rate in the strong sense. See Alfonsi [3] and Berkaoui, Bossy and Diop [7] for more discussions on the convergence of the discretised univariate variance process.

Apart from discretization schemes, there are also (almost) exact simulation methods based on the exact distributions of the stock price and variance processes. The respective transition laws of these follow a conditional lognormal distribution and a conditional scaled noncentral chi-square distribution; see Cox, Ingersoll and Ross [13]. Broadie and Kaya [12] take this approach to generate sample variance and stock price. They apply an acceptance-rejection method to the noncentral chi-square sampling for the variance process. Malham and Wiese [28] propose an exact acceptance-rejection method and a high-accuracy direct inversion method for the simulation of the generalised Gaussian distribution, which are then applied to the noncentral chi-squared sampling. Haastrecht and Pelsser [39] focus on the efficient approximation of the variance. They explore the features of the distribution for the variance process and suggest a cache for its inverse distribution functions, leading to an almost exact simulation scheme.

To realise the stock price, the key task of Broadie and Kaya [12] is to sample from the time integrated variance conditional at the endpoints, i.e. $\left(\int_0^t V_s ds \middle| V_0, V_t\right)$. They build on the results (2.m) and (6.d) in Pitman and Yor [32] to derive the explicit form for the corresponding characteristic function. Fourier inversion techniques in conjunction with the trapezoidal rule are applied to numerically evaluate the probability distribution function. This is followed by inverse transform sampling to simulate the value of the above integral. Their numerical results imply that the proposed method has a faster convergence rate compared to the Euler scheme with bias-free simulation.

Because of the dependence on V_0 and V_t , Broadie and Kaya [12] compute the characteristic function for each step and path in the Monte Carlo simulation. At the

expense of a small bias, Smith [37] presents an approximation to the characteristic function, which makes it possible to precalculate and store the values of the characteristic function for all the points required in advance. Glasserman and Kim [18] provide another sampling method for the time integrated conditional variance, which relies on an explicit representation as infinite sums and mixtures of gamma random variables. When combined with the exact simulation method suggested by Broadie and Kaya [12], their method is highly effective in terms of both accuracy and computational speed for pricing non-path-dependent options across a full range of model parameter values.

Motivated by the decomposition in Glasserman and Kim [18] (Theorem 2.2), we simplify the variance process to a squared Bessel process by a measure transformation and construct a new series expansion for its conditional integral under the new measure with exponentially decaying truncation errors. We demonstrate that the task of sampling the new series can be largely reduced to simulations of simple random variables, which are independent of any model parameters. We provide highly accurate Chebyshev polynomial approximations to the inverse distribution functions of such random variables and design direct inversion algorithms to generate their samples. Thus, we establish a flexible, efficient and almost exact simulation scheme for the Heston model. To summarise, the advantages of our method are that truncation errors decay exponentially, high-accuracy samples can be generated efficiently by direct inversions and approximations of inverse distribution functions can be used under any market conditions.

The paper is organised as follows. In section 2, we present our new representation under the new probability measure and the acceptance-rejection algorithm for changing back to the original measure. In section 3, we detail the simulation methods for each individual part of the representation. We include the derivation of asymptotic expansions for the corresponding distribution functions and the construction of Chebyshev polynomial approximations for their inverse. We apply our method for pricing purposes and we compare its efficiency and accuracy to Glasserman and Kim [18] with numerical results reported in section 4. Conclusions are drawn in section 5.

2. Main results. The method we propose closely follows the lead of Broadie and Kaya [12] and Glasserman and Kim [18] with the key difference for the simulation of the conditional integral of the variance process. To complete the understanding of the motivation for sampling from the conditional integral, we first quote some properties with regard to the Heston model.

We start with the variance process governed by (1.2), which is a CIR process (Cox, Ingersoll and Ross [13]) with transition probability given explicitly as a scaled noncentral chi-squared distribution. With the degrees of freedom for this process defined to be $\delta := 4\kappa\theta/\sigma^2$, we have

$$(2.1) \quad V_t \sim \frac{\sigma^2(1 - \exp(-\kappa t))}{4\kappa} \chi_\delta^2 \left(\frac{4\kappa \exp(-\kappa t)}{\sigma^2(1 - \exp(-\kappa t))} V_0 \right), \quad t > 0,$$

where $V_0 > 0$ is the initial value and $\chi_\delta^2(\lambda)$ denotes a noncentral chi-squared random variable with degrees of freedom δ and noncentrality parameter λ . This means that conditional on V_0 , V_t is distributed as $\sigma^2(1 - \exp(-\kappa t))/(4\kappa)$ multiplied by a noncentral chi-squared distribution with degrees of freedom δ and noncentrality parameter

$$\lambda := \frac{4\kappa \exp(-\kappa t)}{\sigma^2(1 - \exp(-\kappa t))} V_0.$$

The above law provides a way of exactly simulating V_t from V_0 , see Broadie and Kaya [12], Scott [35] and Malham and Wiese [28] for details.

By employing the explicit solution of the stock price process (1.1) and Itô's formula, we obtain

$$\log S_t = \log S_0 + \mu t - \frac{1}{2} \int_0^t V_s ds + \rho \int_0^t \sqrt{V_s} dW_s^1 + \sqrt{1-\rho^2} \int_0^t \sqrt{V_s} dW_s^2.$$

Integrating the variance process (1.2) also gives

$$\int_0^t \sqrt{V_s} dW_s^1 = \int_0^t \frac{1}{\sigma} (dV_s - \kappa(\theta - V_s) ds) = \frac{V_t - V_0 - \kappa\theta t}{\sigma} + \frac{\kappa}{\sigma} \int_0^t V_s ds.$$

Combining these two results, Broadie and Kaya [12] observe that given V_0 , V_t and $\int_0^t V_s ds$, the distribution of $\log(S_t/S_0)$ is Gaussian with known moments since the process V is independent of the Brownian motion W^2 , i.e.

$$\log \frac{S_t}{S_0} \sim N \left(\mu t + \frac{\rho}{\sigma} (V_t - V_0 - \kappa\theta t) + \left(\frac{\rho\kappa}{\sigma} - \frac{1}{2} \right) \int_0^t V_s ds, (1-\rho^2) \int_0^t V_s ds \right).$$

Hence, an exact simulation for the stock price S_t given the initial conditions S_0 and V_0 is now reduced to sampling a conditional normal random variable given above provided there is a way to sampling from the joint distribution $(V_t, \int_0^t V_s ds)$. As V_t can be simulated using the transition law in (2.1), the main challenge is now to develop a tractable method for sampling from the time integral of the variance process V_s over $[0, t]$ given its endpoints V_0 and V_t , i.e.

$$\left(\int_0^t V_s ds \middle| V_0, V_t \right).$$

In what follows we focus on developing a new representation for the above integral building upon the decomposition suggested by Glasserman and Kim [18], which applies the decomposition of the squared Bessel bridges from Pitman and Yor [32].

Before proceeding, we reduce the model to a special case by time-rescaling and a measure transformation. First, define $\tilde{A}_t = V_{4t/\sigma^2}$. Then, \tilde{A}_t satisfies the following stochastic differential equation (Glasserman and Kim [18])

$$d\tilde{A}_t = (\delta - 2q\tilde{A}_t) dt + 2\sqrt{\tilde{A}_t} d\tilde{W}_t^1,$$

where $q := 2\kappa/\sigma^2$ and $\tilde{W}_t^1 := \sigma W_{4t/\sigma^2}^1/2$ becomes a standard Brownian motion. In order to consider a new probability measure, we suppose that the original model is established under measure \mathbb{Q} , meaning that our target now is to simulate

$$\left[\int_0^t V_s ds \middle| V_0 = v_0, V_t = v_t \right] \stackrel{d}{=} \left[\frac{4}{\sigma^2} \int_0^\tau \tilde{A}_s ds \middle| \tilde{A}_0 = a_0, \tilde{A}_\tau = a_\tau \right]$$

under \mathbb{Q} with $\tau = \sigma^2 t/4$, $a_0 = v_0$ and $a_\tau = v_t$.

Second, we further simplify the model by introducing a new probability measure \mathbb{P} (Pitman and Yor [32] and Glasserman and Kim [18]) such that

$$(2.2) \quad \frac{d\mathbb{P}}{d\mathbb{Q}} = \exp \left(q \int_0^\tau \sqrt{\tilde{A}_s} d\tilde{W}_s^1 - \frac{q^2}{2} \int_0^\tau \tilde{A}_s ds \right).$$

By the Girsanov theorem, $W_\tau^\mathbb{P} := \tilde{W}_\tau^1 - \int_0^\tau q \sqrt{\tilde{A}_s} ds$ is a standard Brownian motion under \mathbb{P} . With this replacement, the rescaled process \tilde{A} satisfies

$$(2.3) \quad d\tilde{A}_t = \delta dt + 2\sqrt{\tilde{A}_t} dW_t^\mathbb{P},$$

which is a δ -dimensional squared Bessel process under \mathbb{P} . Hence, our objective is to sample from the time integral of a squared Bessel process \tilde{A} given its values at the endpoints, denoted by I , under the new probability measure \mathbb{P} , i.e.

$$(2.4) \quad I = \left(\int_0^\tau \tilde{A}_s ds \mid \tilde{A}_0 = a_0, \tilde{A}_\tau = a_\tau \right),$$

and to find a connection between the distributions for the conditional integral under \mathbb{P} and \mathbb{Q} .

Next, we state our main result which relies on decomposing the conditional integral as introduced by Glasserman and Kim [18].

THEOREM 2.1. *Under the new probability measure \mathbb{P} , the conditional integral of the rescaled variance process \tilde{A} is equivalent in distribution to the sum of three infinite series of random variables*

$$I = \left(\int_0^\tau \tilde{A}_s ds \mid \tilde{A}_0 = a_0, \tilde{A}_\tau = a_\tau \right) \stackrel{d}{=} X_1 + X_2 + \sum_{j=1}^\eta Z_j,$$

where $X_1, X_2, \eta, Z_1, Z_2, \dots$ are mutually independent, and η is a Bessel random variable with parameters $\nu = \delta/2 - 1$ and $z = \sqrt{a_0 a_\tau}/\tau$, i.e. $\eta \sim \text{Bessel}(\nu, z)$. Moreover, $X_1, X_2, Z_1, Z_2, \dots$ admit the following representations:

(a) We have

$$X_1 \stackrel{d}{=} \sum_{n=0}^\infty \frac{\tau^2}{4^n} \sum_{k=1}^{P_n} S_{n,k},$$

where for $n = 0, 1, \dots$, the P_n are independent Poisson random variables with mean $(a_0 + a_\tau) 2^{n-1}/\tau$ and for $k = 1, 2, \dots, P_n$, the $S_{n,k}$ are independent copies of the random variable $S := (2/\pi^2) \sum_{l=1}^\infty \epsilon_l/l^2$ and $\epsilon_l \sim \text{Exp}(1)$ are independent exponential random variables for $l = 1, 2, \dots$;

(b) Further we have

$$X_2 \stackrel{d}{=} \sum_{n=1}^\infty \frac{\tau^2}{4^n} C_n^{\delta/2},$$

where for $n = 1, 2, \dots$, the $C_n^{\delta/2}$ are independent copies of the random variable $C^{\delta/2} := (2/\pi^2) \sum_{l=1}^\infty \Gamma_{\delta/2,l}/(l-1/2)^2$ and $\Gamma_{\delta/2,l} \sim \text{Gamma}(\delta/2, 1)$ are independent gamma random variables with shape $\delta/2$ and rate 1 for $l = 1, 2, \dots$;

(c) And also we have the $Z_j, j = 1, 2, \dots, \eta$, which are independent copies of the random variable Z such that

$$Z \stackrel{d}{=} \sum_{n=1}^\infty \frac{\tau^2}{4^n} C'_n,$$

where for $n = 1, 2, \dots$, the C'_n are independent copies of the random variable $C'^2 := (2/\pi^2) \sum_{l=1}^\infty \Gamma_{2,l}/(l-1/2)^2$ and $\Gamma_{2,l} \sim \text{Gamma}(2, 1)$ are independent gamma random variables with shape 2 and rate 1 for $l = 1, 2, \dots$

Proof. We work on the probability measure \mathbb{P} throughout this proof. We note that for a fixed $\tau > 0$,

$$(2.5) \quad \left(\int_0^\tau \tilde{A}_s ds \middle| \tilde{A}_0 = a_0, \tilde{A}_\tau = a_\tau \right) = \left(\tau^2 \int_0^1 A_s ds \middle| A_0 = x, A_1 = y \right),$$

where A_s is defined by setting $A_s = \tilde{A}_{s\tau}/\tau$ for $0 \leq s \leq 1$ and $x = a_0/\tau, y = a_\tau/\tau$. Then using equation (2.3), the process A satisfies

$$dA_s = \delta ds + 2\sqrt{A_s} dW_s,$$

where $W_s := W_{s\tau}/\sqrt{\tau}$ is a standard Brownian motion. We observe that $\{A_s\}_{0 \leq s \leq 1}$ is a δ -dimensional squared Bessel process. Conditional on the end points, the process $(A_s, 0 \leq s \leq 1 | A_0 = x, A_1 = y)$ is then a squared Bessel bridge, denoted by $A_{x,y}^{\delta,1} = \{A_{x,y}^{\delta,1}(s)\}_{0 \leq s \leq 1}$. Then the right hand side of (2.5) has the same distribution as

$$(2.6) \quad \left(\tau^2 \int_0^1 A_{x,y}^{\delta,1}(s) ds \right).$$

We prove the result in three steps.

First, the integral (2.6) can be decomposed into the sum of three independent parts as follows:

$$\tau^2 \int_0^1 A_{x,y}^{\delta,1}(s) ds \stackrel{d}{=} X'_1 + X'_2 + \sum_{j=1}^{\eta} Z'_j,$$

where

$$\begin{aligned} X'_1 &= \tau^2 \int_0^1 A_{x+y,0}^{0,1}(s) ds, \\ X'_2 &= \tau^2 \int_0^1 A_{0,0}^{\delta,1}(s) ds, \end{aligned}$$

and for $j = 1, 2, \dots, \eta$, Z'_j are independent copies of

$$Z' = \tau^2 \int_0^1 A_{0,0}^{4,1}(s) ds,$$

and η is an independent Bessel random variable with parameters $\nu = \delta/2 - 1$ and $z = \sqrt{xy} = \sqrt{a_0 a_\tau}/\tau$, i.e. $\eta \sim \text{Bessel}(\nu, z)$. This is a direct result from Glasserman and Kim [18], who apply the decomposition of squared Bessel bridges proposed by Pitman and Yor [32] to the transformed variance process.

Second, it follows from Glasserman and Kim [18] that the Laplace transforms of X'_1 , X'_2 and Z' for $b \geq 0$ are given by

$$(2.7) \quad \Phi'_1(b) = \exp \left(\frac{a_0 + a_\tau}{2\tau} \left(1 - \sqrt{2b\tau} \coth(\sqrt{2b\tau}) \right) \right),$$

$$(2.8) \quad \Phi'_2(b) = \left(\frac{\sqrt{2b}\tau}{\sinh(\sqrt{2b}\tau)} \right)^{\delta/2},$$

$$(2.9) \quad \Phi'_3(b) = \left(\frac{\sqrt{2b}\tau}{\sinh(\sqrt{2b}\tau)} \right)^2.$$

Third, to verify the random variables X'_1 , X'_2 and Z' have the same distribution as the series expansions which define X_1 , X_2 and Z respectively, it is sufficient to show that they have identical Laplace transforms. To do this, let us first rewrite Φ'_i , $i = 1, 2, 3$ using some important identities regarding the hyperbolic functions \coth and \sinh ; see Malham and Wiese [29]. Specifically, we observe

$$\begin{aligned}\coth \zeta &\equiv \coth \frac{\zeta}{2} - \frac{1}{\sinh \zeta}, \\ \sinh \zeta &\equiv 2 \sinh \frac{\zeta}{2} \cosh \frac{\zeta}{2}.\end{aligned}$$

Iterating N times gives us

$$(2.10) \quad \coth \zeta \equiv \coth \frac{\zeta}{2^{N+1}} - \sum_{n=0}^N \frac{1}{\sinh \frac{\zeta}{2^n}},$$

$$(2.11) \quad \sinh \zeta \equiv 2^N \sinh \frac{\zeta}{2^N} \prod_{n=1}^N \cosh \frac{\zeta}{2^n}.$$

Substituting (2.10) into (2.7) and rearranging the terms, we get

$$\exp \left(\frac{a_0 + a_\tau}{2\tau} (1 - \zeta \coth \zeta) \right) = \prod_{n=0}^N \exp \left(\frac{a_0 + a_\tau}{2\tau} 2^n \frac{\frac{\zeta}{2^n}}{\sinh \frac{\zeta}{2^n}} \right) I_N(\zeta, \tau, a_0, a_\tau),$$

where $I_N(\zeta, \tau, a_0, a_\tau) := \exp \left(-(a_0 + a_\tau) (\zeta \coth(\zeta/2^{N+1}) - 1) / (2\tau) \right)$. On the other hand, it follows from $\sum_{n=0}^N 2^n = 2^{N+1} - 1$ that

$$I_N(\zeta, \tau, a_0, a_\tau) = \prod_{n=0}^N \exp \left(-\frac{a_0 + a_\tau}{2\tau} 2^n \right) \exp(\varepsilon_{1,N}(\zeta, \tau, a_0, a_\tau)),$$

where $\varepsilon_{1,N}(\zeta, \tau, a_0, a_\tau) := -(a_0 + a_\tau) (\zeta \coth(\zeta/2^{N+1}) - 2^{N+1}) / (2\tau) \rightarrow 0$ as $N \rightarrow \infty$. Thus, for $\zeta = \sqrt{2b}\tau$, we have an alternative form for Φ'_1 given by

$$\Phi'_1(b) = \prod_{n=0}^{\infty} \exp \left(\frac{a_0 + a_\tau}{2\tau} 2^n \left(\frac{\frac{\sqrt{2b}\tau}{2^n}}{\sinh \frac{\sqrt{2b}\tau}{2^n}} - 1 \right) \right).$$

Similarly, for Φ'_2 after substitution and rearrangement, we have

$$\left(\frac{\zeta}{\sinh \zeta} \right)^{\delta/2} = \prod_{n=1}^N \left(\cosh \frac{\zeta}{2^n} \right)^{-\delta/2} \varepsilon_{2,N}(\zeta, \delta),$$

where $\varepsilon_{2,N}(\zeta, \delta) := ((\zeta/2^N) / \sinh(\zeta/2^N))^{\delta/2} \rightarrow 1$ as $N \rightarrow \infty$. As a result, plugging $\zeta = \sqrt{2b}\tau$ into this expression yields

$$\Phi'_2(b) = \prod_{n=1}^{\infty} \left(\cosh \frac{\sqrt{2b}\tau}{2^n} \right)^{-\delta/2}.$$

Next, we derive the Laplace transforms of X_1 , X_2 and Z , denoted by Φ_1 , Φ_2 and Φ_3 respectively. For any $b \geq 0$, we have

$$\Phi_1(b) = \mathbb{E}[\exp(-bX_1)]$$

$$\begin{aligned}
&= \prod_{n=0}^{\infty} \mathbb{E} \left[\exp \left(-b \frac{\tau^2}{4^n} \sum_{k=1}^{P_n} S_{n,k} \right) \right] \\
&= \prod_{n=0}^{\infty} \mathbb{E} \left[\prod_{k=1}^{P_n} \mathbb{E} \left(\exp \left(-b \frac{\tau^2}{4^n} S_{n,k} \right) \right) \right] \\
&= \prod_{n=0}^{\infty} \mathbb{E} \left[\left(\frac{\sqrt{\frac{2b\tau^2}{4^n}}}{\sinh \sqrt{\frac{2b\tau^2}{4^n}}} \right)^{P_n} \right] \\
&= \prod_{n=0}^{\infty} \exp \left(\frac{a_0 + a_\tau}{2\tau} 2^n \left(\frac{\frac{\sqrt{2b}\tau}{2^n}}{\sinh \frac{\sqrt{2b}\tau}{2^n}} - 1 \right) \right),
\end{aligned}$$

where the second equality comes from the interchange of expectation and limit by the Bounded Convergence Theorem and the fourth equality holds due to the fact that $\mathbb{E} [\exp(-bS_{n,k})] = \sqrt{2b}/\sinh \sqrt{2b}$ for all $n \geq 0$ and $k \geq 1$ (see Biane, Pitman and Yor [8, formula (1.8)]).

Following similar arguments, we now determine the Laplace transform Φ_2 for X_2 . Indeed, from $\mathbb{E} [\exp(-bC_n^{\delta/2})] = (\cosh \sqrt{2b})^{-\delta/2}$ for any $n \geq 1$ (see Biane, Pitman and Yor [8, formula (1.8)]), we conclude that

$$\begin{aligned}
\Phi_2(b) &= \mathbb{E} [\exp(-bX_2)] \\
&= \prod_{n=1}^{\infty} \mathbb{E} \left[\exp \left(-b \frac{\tau^2}{4^n} C_n^{\delta/2} \right) \right] \\
&= \prod_{n=1}^{\infty} \left(\cosh \frac{\sqrt{2b}\tau}{2^n} \right)^{-\delta/2}.
\end{aligned}$$

Hence, we can now deduce that $X'_i \stackrel{d}{=} X_i$ as $\Phi'_i = \Phi_i$ for $i = 1, 2$. In line with the steps explained above, $Z' \stackrel{d}{=} Z$ follows since this is a special case when $\delta = 4$, completing the proof. \square

Remark 2.2. We notice that after separating the time parameter τ , the dependence of X_1 on model parameters is only through the Poisson random variable P_n and X_2 depends only on one parameter δ . This feature provides us with a possibility that the task of sampling the conditional integral I can be largely reduced to the simulations of simple random variables, whose distributions remain unchanged as we change the values for the model parameters; see [section 3.1](#) and [section 3.5](#).

We have represented the conditional time integral I by double infinite weighted sums and mixtures of simple independent random variables under the new probability measure \mathbb{P} , which serves as a theoretical basis for the exact simulation from the distribution of (2.4) under \mathbb{P} . However, our goal is set up under the probability measure \mathbb{Q} . We now focus on the task of generating a sample from the distribution of the conditional integral I under \mathbb{Q} once we have generated a sample under \mathbb{P} . In particular, we explore the relationship between the probability density functions of the integral under these two probability measures. We specify the details in the following theorem.

THEOREM 2.3. *Suppose that f_P and f_Q are the probability density functions of I*

under the probability measures \mathbb{P} and \mathbb{Q} , respectively. Then, we have

$$f_Q(x) = L(q, \nu, \tau, a_0, a_\tau) \exp\left(-\frac{q^2}{2}x\right) f_P(x),$$

where

$$L(q, \nu, \tau, a_0, a_\tau) = \frac{\sinh(q\tau)}{q\tau} \exp\left(\frac{a_0 + a_\tau}{2\tau} (q\tau \coth(q\tau) - 1)\right) \frac{I_\nu\left(\frac{\sqrt{a_0 a_\tau}}{\tau}\right)}{I_\nu\left(\frac{q\sqrt{a_0 a_\tau}}{\sinh(q\tau)}\right)}$$

with $I_\nu(\cdot)$ denoting the modified Bessel function of the first kind.

Proof. We will make use of the shift property of the Laplace transform to justify the theorem. We first establish a connection between their respective Laplace transforms. For any $b \geq 0$, consider the Laplace transform $\mathcal{L}\{f_Q\}(b)$ of f_Q at b , which is the \mathbb{Q} -expectation of $\exp(-bI)$. Thus, we get

$$\begin{aligned} \mathcal{L}\{f_Q\}(b) &= \mathbb{E}^\mathbb{Q} \left[\exp\left(-b \int_0^\tau \tilde{A}_s ds\right) \middle| \tilde{A}_0 = a_0, \tilde{A}_\tau = a_\tau \right] \\ &= \frac{\mathbb{E}^\mathbb{P} \left[\exp\left(-\left(b + \frac{q^2}{2}\right) \int_0^\tau \tilde{A}_s ds\right) \middle| \tilde{A}_0 = a_0, \tilde{A}_\tau = a_\tau \right]}{\mathbb{E}^\mathbb{P} \left[\exp\left(-\frac{q^2}{2} \int_0^\tau \tilde{A}_s ds\right) \middle| \tilde{A}_0 = a_0, \tilde{A}_\tau = a_\tau \right]} \\ &= \frac{\mathcal{L}\{f_P\}\left(b + \frac{q^2}{2}\right)}{\mathcal{L}\{f_P\}\left(\frac{q^2}{2}\right)} \\ &= \mathcal{L}\left\{ \frac{f_P}{\mathcal{L}\{f_P\}\left(\frac{q^2}{2}\right)} \right\} \left(b + \frac{q^2}{2}\right). \end{aligned}$$

The second equality is a result of the change of law formula (6.d) from Pitman and Yor [32], see the Appendix of Broadie and Kaya [12] as well. Now by the application of the shift property, we can write

$$f_Q(x) = \frac{f_P(x)}{\mathcal{L}\{f_P\}\left(\frac{q^2}{2}\right)} \exp\left(-\frac{q^2}{2}x\right).$$

Using the formula (2.m) in Pitman and Yor [32] for the Laplace transform $\mathcal{L}\{f_P\}$ of f_P at $q^2/2$ given by

$$\mathcal{L}\{f_P\}\left(\frac{q^2}{2}\right) = \frac{q\tau}{\sinh(q\tau)} \exp\left(\frac{a_0 + a_\tau}{2\tau} (1 - q\tau \coth(q\tau))\right) \frac{I_\nu\left(\frac{q\sqrt{a_0 a_\tau}}{\sinh(q\tau)}\right)}{I_\nu\left(\frac{\sqrt{a_0 a_\tau}}{\tau}\right)}$$

and setting $L(q, \nu, \tau, a_0, a_\tau) := (\mathcal{L}\{f_P\}(q^2/2))^{-1}$ establishes the stated result. \square

The above theorem relates the density f_P of the distribution explicitly given by Theorem 2.1 in terms of infinite sums to the density f_Q of the distribution we are interested in. This means we can simulate the random variable I under the measure \mathbb{Q} provided we have an observation from its distribution under the measure \mathbb{P} . In

general, we construct the acceptance-rejection algorithm outlined in [Algorithm 2.1](#) to generate samples from f_Q .

On average, the probability of accepting a proposed sample is

$$\mathbb{P}\left(U \leq \exp\left(-\frac{q^2 Y}{2}\right)\right) = \frac{1}{L(q, \nu, \tau, a_0, a_\tau)},$$

where $U \sim \text{Unif}(0, 1)$ and independently Y follows the distribution of I under \mathbb{P} . Consequently, we require $L(q, \nu, \tau, a_0, a_\tau) \geq 1$ due to the fact that a probability only takes values between zero and one. In practice, we prefer a value of L closer to one as it indicates higher acceptance probability on average, and thus fewer iteration steps needed.

Algorithm 2.1 Acceptance-Rejection

- 1: Simulate a realisation Y of the random variable I under \mathbb{P} using [Theorem 2.1](#).
 - 2: Obtain a sample U independently from the uniform distribution $\text{Unif}(0, 1)$ over unit interval.
 - 3: If $U \leq \exp(-q^2 Y/2)$, accept Y as a sample drawn from the distribution of I under \mathbb{Q} ; otherwise reject the value of Y and return to the first step.
-

Remark 2.4. The requirement $L(q, \nu, \tau, a_0, a_\tau) \geq 1$ is fulfilled under any market conditions. In fact, because the support for the random variable I is $(0, +\infty)$, we have $\int_0^\infty L(q, \nu, \tau, a_0, a_\tau) \exp(-q^2 x/2) f_P(x) dx = \int_0^\infty f_Q(x) dx = 1$. Noticing that $\exp(-q^2 x/2) \leq 1$ for $x \geq 0$ and $0 < \int_0^\infty \exp(-q^2 x/2) f_P(x) dx \leq \int_0^\infty f_P(x) dx = 1$ then leads to $L(q, \nu, \tau, a_0, a_\tau) \geq 1$.

So far, we have described the theories behind the simulation of the time integral conditional variance. It is a matter of sampling infinite series, combined with the acceptance-rejection method. For the next stage, we will address some issues concerning the practical implementation of the theory. In particular, strategies are required to deal with infinite summations of random variables. We propose direct inversion algorithms based on approximating the corresponding inverse distribution functions to tackle this problem. Further, the dependence between the series and the model parameters implies that the recomputation of the inverse distribution functions when using a new set of model coefficients is inevitable. We show that the series can be decomposed as the sum of simple random variables, whose distributions do not depend on any market conditions. We specify the details in the next section.

3. Simulation. In this section, we outline how to generate an exact sample for I under \mathbb{P} by [Theorem 2.1](#) introduced earlier. In particular, we discuss the sampling techniques corresponding to X_1 and X_2 . We note that Z is a special case of X_2 with $\delta = 4$. In order to apply the decomposition theorem to sample the conditional integral, we need to determine a point at which the infinite summation is terminated. We consider the truncation for the outer summation now, leaving the inner one to be discussed further in the following contexts. Let us denote the truncation level by K and the resulting *remainder* random variables of X_1 and X_2 by R_1^K and R_2^K

respectively, i.e.

$$R_1^K := \sum_{n=K+1}^{\infty} \frac{\tau^2}{4^n} \sum_{k=1}^{P_n} S_{n,k},$$

$$R_2^K := \sum_{n=K+1}^{\infty} \frac{\tau^2}{4^n} C_n^{\delta/2}.$$

We evaluate the effect of truncation by summarising the means and variances of the remainder terms in the next lemma; see [Appendix A](#) for a detailed proof.

LEMMA 3.1. *Given the truncation level $K > 0$, we have*

$$\begin{aligned} \mathbb{E}[R_1^K] &= \frac{(a_0 + a_\tau)\tau}{6} \frac{1}{2^K}, & \text{Var}[R_1^K] &= \frac{(a_0 + a_\tau)\tau^3}{90} \frac{1}{8^K}, \\ \mathbb{E}[R_2^K] &= \frac{\delta\tau^2}{6} \frac{1}{4^K}, & \text{Var}[R_2^K] &= \frac{\delta\tau^4}{45} \frac{1}{16^K}. \end{aligned}$$

Remark 3.2. The above lemma implies that the truncation errors decay exponentially. This is an appealing property of the new series in [Theorem 2.1](#) as the truncation error will decrease so quickly that the Monte Carlo error will dominate the total error even for small truncation level K . Hence, including the terms at lower levels will be enough to produce an accurate approximation. This is supported by our numerical simulations in [section 4](#).

3.1. Simulation of X_1 . Recall that by dropping the remainders, we approximate X_1 by X_1^K where

$$X_1^K = \sum_{n=0}^K \frac{\tau^2}{4^n} \sum_{k=1}^{P_n} S_{n,k}.$$

Notice that the $S_{n,k}$ are independently and identically distributed as $S = (2/\pi^2) \sum_{l=1}^{\infty} \epsilon_l/l^2$. To reduce the truncation error further, we simulate the tail sum R_1^K as well. Glasserman and Kim [18] use the central limit theorem to show the validity of a normal approximation for the remainders. They also point out that a gamma approximation is feasible and better in the sense that its cumulant generating function is closer to that of the remainder random variable compared with that of a normal approximation. Therefore, inspired by this, the approximation to X_1 with tail simulation for a given truncation level K is

$$X_1 \approx X_1^K + \Gamma_1^K,$$

where Γ_1^K is a gamma random variable such that its first two moments match those of the remainder R_1^K from [Lemma 3.1](#).

We now detail our sampling strategy for X_1^K . The series which defines X_1^K suggests two potential problems. First, the random variables $S_{n,k} \stackrel{d}{=} S$ are represented by an infinite weighted sum of independent exponential random variables, which requires an efficient simulation method. Second, given a Poisson sample $P_n = P$ for a fixed level $n = 0, \dots, K$, sampling the sum of P independent random variables S becomes increasingly computationally demanding when the sample P tends to be larger.

Thus, we now incorporate these two tasks with each other and consider simulating the sum of P independent random variables S directly, denoted by S^P , i.e.

$$S^P = \sum_{k=1}^P S_k,$$

where S_k are independent copies of S . Using the Laplace transform for S given in Biane, Pitman and Yor [8], S^P has the following Laplace transform:

$$(3.1) \quad \Phi_{S^P}(b) = \mathbb{E}[\exp(-bS^P)] = \left(\frac{\sqrt{2b}}{\sinh \sqrt{2b}} \right)^P,$$

for $b > 0$.

We observe that any positive integer P can be expressed in the form

$$P = p_1 + 10p_{10} + 50p_{50} + 5000p_{5000} + 10^4p_{10^4} + 10^5p_{10^5} + 10^6p_{10^6}.$$

Here p_{10^6} is the multiples of 10^6 present in the integer P , i.e. $p_{10^6} = \lfloor P/10^6 \rfloor$, p_{10^5} is the multiples of 10^5 present in the remainder of the division of P by 10^6 , i.e. $p_{10^5} = \lfloor (P - 10^6 p_{10^6}) / 10^5 \rfloor$, and so forth. As the law of S^P is infinitely divisible for any $P > 0$ (see Section 3.2 of Biane, Pitman and Yor [8]), the sum S^P admits the representation

$$S^P \stackrel{d}{=} \sum_{k \in \mathbb{S}} \sum_{i=1}^{p_k} S_i^k,$$

where $\mathbb{S} = \{1, 10, 50, 5000, 10^4, 10^5, 10^6\}$ and for $i = 1, \dots, p_k$, S_i^k are independent copies of S^k , i.e. the sum of k independent random variables S , with $k \in \mathbb{S}$. Then, the above representation can be intended as a basis for an efficient sampling scheme for S^P for all $P > 0$ if we can realise S^k effectively for $k \in \mathbb{S}$. Indeed, we apply the direct inversion method to simulate S^k with their inverse distribution functions approximated by predetermined Chebyshev polynomials for each $k \in \mathbb{S}$. In general, the direct inversion algorithm for generating the samples of S^P for any $P > 0$ is described as follows.

Algorithm 3.1 Direct inversion for S^P

- 1: For each $k \in \mathbb{S}$, sample p_k independent random variables S_i^k , $i = 1, \dots, p_k$ from the distribution of S^k using the inverse distribution functions based on the corresponding Chebyshev polynomial approximations.
 - 2: Compute the accumulated sum, i.e. $\sum_k \sum_{i=1}^{p_k} S_i^k \sim S^P$.
-

The advantage of this algorithm is that we only need to construct the Chebyshev polynomial approximations for the inverse distribution function of S^k for $k \in \mathbb{S}$. With this replacement, the complicated inverse distribution function becomes very easy to compute at arbitrary points. Moreover, since S^k does not depend on any model parameters, the coefficients of the polynomials can be computed and tabulated in advance. As such, when a sample for X_1 is needed, we truncate the series representation to include the terms at $n \leq K$ with the tail approximated by a gamma distribution. For each $n = 0, \dots, K$, we generate Poisson samples P_n and simulate the

sums S^{P_n} directly by [Algorithm 3.1](#), which requires evaluating some prescribed polynomials with coefficients drawn directly from the cached table; see the supplementary materials. To make the above process fast for implementation, we take advantage of the direct inversion to obtain Poisson samples when the mean is less than 10. For larger means, the PTRD transformed rejection method suggested by Hörmann [\[23\]](#) will be used.

To obtain the Chebyshev coefficients, it is crucial to determine the values of the inverse distribution functions at several points efficiently and accurately. For large P , we derive an asymptotic series expansion for the distribution function of S^P when $P \rightarrow +\infty$ through the inverse Fourier transform of its characteristic function. While for small P , we utilise the explicit expression for the density function given by Biane and Yor [\[9\]](#), which involves the parabolic cylinder functions. To derive the representation for the distribution function, we use a routine consisting of the power series and asymptotic expansions for the parabolic cylinder functions to evaluate the density function followed by term-wise integration. With these expansions computed, we apply root-finding algorithms to calculate the required values.

3.2. Asymptotic expansion for the distribution function of S^P for large P . Before proceeding, it is worth noticing that in the limit $P \rightarrow \infty$, the expectation $\mathbb{E}[S^P] = P/3$ and variance $\text{Var}[S^P] = 2P/45$ of S^P will diverge. Thus, we standardise the random variable S^P by $Z^P = (S^P - P/3) / \sqrt{2P/45}$, so that the new random variable Z^P has mean zero and variance one. As S^P is non-negative, the support of Z^P is $[-\sqrt{5P}/\sqrt{2}, +\infty)$. Then, taking the inverse Fourier transform of the characteristic function, the probability density function f_{Z^P} of Z^P has the form

$$\begin{aligned} f_{Z^P}(x) &= \sqrt{\frac{2P}{45}} f_{S^P}\left(\frac{P}{3} + x\sqrt{\frac{2P}{45}}\right) \\ &= \sqrt{\frac{2P}{45}} \frac{1}{2\pi} \int_{-\infty}^{+\infty} \exp\left(-iz\left(\frac{P}{3} + x\sqrt{\frac{2P}{45}}\right)\right) \left(\frac{\sqrt{-2zi}}{\sinh\sqrt{-2zi}}\right)^P dz, \end{aligned}$$

where f_{S^P} denotes the probability density function of S^P and the first equality follows from the classical theorem on transforming density functions. By introducing $\beta = x\sqrt{2/45}/\sqrt{P}$, the above equation can be written as

$$(3.2) \quad f_{Z^P}(x) = \frac{1}{4\pi} \sqrt{\frac{2P}{45}} \int_{-\infty}^{+\infty} \exp(P\rho(z; \beta)) dz,$$

where $\rho(z; \beta)$ satisfies

$$(3.3) \quad \rho(z; \beta) = \log\left(\frac{\sqrt{zi}}{\sinh\sqrt{zi}}\right) + zi\left(\frac{1}{6} + \frac{1}{2}\beta\right).$$

We apply the standard technique of the steepest descent method to develop the asymptotic approximation for f_{Z^P} , where all the higher order terms are given in reciprocal powers of P , see Bender and Orszag [\[6\]](#), Bleistein and Handelsman [\[10\]](#) and Ablowitz and Fokas [\[1\]](#). The expansion is then integrated term-wise to generate the asymptotic representation for the distribution function. The general procedure is given below. We first identify the critical points including saddle points z_0 of $\rho(z; \beta)$ such that $\rho'(z_0; \beta) = 0$. Note that since $\rho(z; \beta)$ depends on the parameter

β , the saddle point z_0 will also depend on β . Due to the fact that β is quite small as $P \rightarrow +\infty$, we can establish a useful expression for z_0 as a Taylor series in β . Afterwards, we demonstrate that the original contour of integration, i.e. the real line, can be deformed onto the steepest descent paths, obtained by considering the contour defined by $\text{Im}(\rho(z; \beta)) = \text{Im}(\rho(z_0; \beta))$ and $\text{Re}(\rho(z; \beta)) < \text{Re}(\rho(z_0; \beta))$, in the domain where the integrand is analytic. In this way, the rapid oscillations of the integrand can be removed when P is large, whence the asymptotic behaviour of the integral can be determined locally depending only on a small neighbourhood of the critical points. We present the results in the next theorem, which is proved in [Appendix B](#).

THEOREM 3.3. *As $P \rightarrow +\infty$ for fixed x with $x > -\sqrt{5P/2}(1 + 3/\pi^2 - 3 \coth \pi/\pi)$ and $|x|$ sufficiently small, we have*

$$(3.4) \quad f_{Z^P}(x) \sim \frac{1}{4\pi} \sqrt{\frac{2}{45}} \exp \left(P \sum_{l=2}^{\infty} \hat{\rho}_l \beta^l \right) \sum_{j=0}^{\infty} \sum_{l=0}^{\infty} \sum_{n=0}^{\lfloor \frac{2}{3}j \rfloor} \hat{\alpha}_{n,l,j} \Gamma \left(j + \frac{1}{2} \right) \beta^l P^{n-j},$$

where $\hat{\rho}_l$ and $\hat{\alpha}_{n,l,j}$ are constants with explicit form derived in the proof and $\Gamma(c)$ is the gamma function.

Remark 3.4. The constant $\hat{\rho}_l$ is defined in the proof in equation (B.16) using constants \hat{r}_k , $\hat{\xi}_k$ and $\hat{v}_{l,j}$ defined in equations (B.3), (B.5) and (B.9), respectively. The constant $\hat{\alpha}_{n,l,j}$ is defined in equation (B.30), which depends on constants $\hat{\omega}_{n,j}$, $\hat{\xi}_{l,k,n}$, \hat{K}_k , $\hat{\gamma}_{l,k}$, $\hat{C}_{l,k_1,k_2,\dots,k_n}$, $\hat{\omega}_l$, $\hat{\phi}_{l,n}$, $\hat{\varphi}_{k,n}$, $\hat{v}_{l,j}$, \hat{r}_k and $\hat{\xi}_k$ defined in equations (B.28)-(B.29), (B.20)-(B.23), (B.27), (B.18), (B.19), (B.26), (B.11), (B.7), (B.9), (B.3) and (B.5), respectively.

Having developed the large P asymptotic approximation for the probability density function f_{Z^P} with all the higher order terms given in reciprocal powers of P , the next stage is to derive an asymptotic representation for the corresponding distribution function. Before that, we first consider the asymptotic expansion for the probability $\mathbb{P}(z_1 < Z^P \leq z_2)$ for some $z_1, z_2 > -\sqrt{5P/2}(1 + 3/\pi^2 - 3 \coth \pi/\pi)$ with $|z_1|$ and $|z_2|$ sufficiently small, which can be accomplished by taking the integration of (3.4) on the finite interval $(z_1, z_2]$. We then explain how this expression can be used to approximate the distribution function. The results are summarised in the next theorem with the proof given in [Appendix C](#).

THEOREM 3.5. *For $z_1, z_2 > -\sqrt{5P/2}(1 + 3/\pi^2 - 3 \coth \pi/\pi)$ and $|z_1|, |z_2|$ sufficiently small, the following asymptotic series expansion holds as $P \rightarrow +\infty$. For $z_1 < z_2 < 0$, we have*

$$\begin{aligned} \int_{z_1}^{z_2} f_{Z^P}(x) dx &\sim \frac{1}{4\pi} \sqrt{\frac{2}{45}} \sum_{j=0}^{\infty} P^{-\frac{j}{2}} \sum_{r=0}^j \sum_{n=0}^r \sum_{l=0}^{j-r} \hat{\eta}_{n,r} \hat{\lambda}_{l,j-r} (-1)^{r+l} \left(\sqrt{2} \right)^{2n+r+l-1} \\ &\quad \cdot \left(\gamma \left(\frac{2n+r+l+1}{2}, \frac{(z_1)^2}{2} \right) - \gamma \left(\frac{2n+r+l+1}{2}, \frac{(z_2)^2}{2} \right) \right). \end{aligned}$$

For $z_1 < 0 \leq z_2$, we have

$$\int_{z_1}^{z_2} f_{Z^P}(x) dx \sim \frac{1}{4\pi} \sqrt{\frac{2}{45}} \sum_{j=0}^{\infty} P^{-\frac{j}{2}} \sum_{r=0}^j \sum_{n=0}^r \sum_{l=0}^{j-r} \hat{\eta}_{n,r} \hat{\lambda}_{l,j-r} \left(\sqrt{2} \right)^{2n+r+l-1}$$

$$\cdot \left((-1)^{r+l} \gamma \left(\frac{2n+r+l+1}{2}, \frac{(z_1)^2}{2} \right) + \gamma \left(\frac{2n+r+l+1}{2}, \frac{(z_2)^2}{2} \right) \right).$$

Here, $\hat{\eta}_{n,r}$ and $\hat{\lambda}_{l,j-r}$ are constants explicitly given in (C.5)-(C.6) and (C.7)-(C.8) in the proof and $\gamma(s, z)$ is the lower incomplete gamma function.

Remark 3.6. We have thus established a large P asymptotic series expansion for the probability that the random variable Z^P takes values in $(z_1, z_2]$. Notice that this representation is valid when $z_i > -\sqrt{5P/2} (1 + 3/\pi^2 - 3 \coth \pi/\pi)$ with $|z_i|$ sufficiently small for $i = 1, 2$. This restriction can be traced back to Theorem 3.3, where the saddle point is given in a Taylor series in β for small $|\beta|$. Hence for practical applications, we truncate the Taylor series to generate an accurate approximation for the saddle point when $|\beta|$ is sufficiently small. More precisely, there is a region centred around zero with width $\tilde{\beta}$, throughout which the error of the approximation is below a given threshold. The range of validity can be determined by numerical comparisons using for example Maple in practice. This range of validity turns out to be large enough so that the error in computing the distribution function for large P is negligible. More precisely, we take the error below 10^{-12} for all the cases considered here and the corresponding values for $\tilde{\beta}$ are 0.0596, 0.0421, 0.0133 and 0.0042 for $P = 5000, 10^4, 10^5$ and 10^6 , respectively.

In summary, we have so far developed a tractable method to evaluate the distribution function $F_{Z^P}(z)$. This is approximated by integration of the corresponding density function on some restricted interval $(-\tilde{z}, z]$ with \tilde{z} carefully chosen for each P . We derive an asymptotic expansion for the integral in reciprocal powers of P for all orders following the steepest descent method. In practice, we compute enough terms for the expansion to achieve the desirable accuracy in Maple with 50 digit accuracy for $P = 5000, 10^4, 10^5$ and 10^6 , along with the root-finding for $F_{Z^P}^{-1}$ values at nodal points required by Chebyshev polynomial approximations.

3.3. Series expansion for the distribution function of S^P for small P .

In this section, we turn to the specifics of the series expansion for the distribution function of S^P for small P . Recall from (3.1) that S^P has the Laplace transform $\Phi_{S^P}(b) = \left(\sqrt{2b}/\sinh \sqrt{2b} \right)^P$ for $b > 0$. Biane and Yor [9, formula (3x)] have given an explicit expression for the probability density function with such a Laplace transform. Namely, for arbitrary $P > 0$, the probability density function f_{S^P} is of the form

$$f_{S^P}(y) = \frac{1}{\sqrt{2\pi}} \frac{2^P}{\Gamma(P)} y^{-\frac{1}{2}(P+2)} \sum_{n=0}^{\infty} \frac{\Gamma(n+P)}{\Gamma(n+1)} \exp \left(-\frac{(2n+P)^2}{4y} \right) D_{P+1} \left(\frac{2n+P}{\sqrt{y}} \right),$$

where $D_{P+1}(z)$ is the parabolic cylinder function with order $P+1$. We use different strategies to calculate these functions according to different ranges of z . For small z , the power series is preferable while for large z an asymptotic expansion will be applied. We summarise these properties here. First, the series expansion for the parabolic cylinder function can be written as

$$(3.5) \quad D_{P+1}(z) = \sum_{k=0}^{\infty} \hat{d}_k(P) z^k,$$

with the coefficients $\hat{d}_k(P)$ satisfying some recurrence relations, that can be found in Gil, Segura and Temme [16] or Abramowitz and Stegun [2]. We use Maple for their

practical implementation. Second, in the limit $z \rightarrow +\infty$, $D_{P+1}(z)$ has the following asymptotic behaviour (Gil, Segura and Temme [16, formula (23), (24), (25)]):

$$(3.6) \quad D_{P+1}(z) \sim \exp\left(-\frac{1}{4}z^2\right) z^{P+1} \sum_{k=0}^{\infty} (-1)^k \frac{(-(P+1))_{2k}}{k! (2z^2)^k},$$

where $(a)_k$ denotes the Pochhammer symbol $(a)_k = \Gamma(a+k)/\Gamma(a)$. For comparisons of different computational methods, see Temme [38] and Gil, Segura and Temme [16]. Finally, integrating the density function f_{S^P} term-wise yields the series representation for the distribution function F_{S^P} of S^P stated below. See Appendix D for a detailed proof.

THEOREM 3.7. *For any $0 \leq x < \infty$ and $P \in (0, 1) \cup \mathbb{N}$, the distribution function $F_{S^P}(x)$ can be written as the following convergent series*

$$(3.7) \quad F_{S^P}(x) = \frac{1}{\sqrt{2\pi}} \frac{2^{P+1}}{\Gamma(P)} \sum_{n=0}^{\infty} \frac{\Gamma(n+P)}{\Gamma(n+1)} (2n+P)^{-P} G\left(\frac{2n+P}{\sqrt{x}}\right),$$

where the function $G(y)$ for $y > 0$ is given by

$$G(y) = \int_y^{+\infty} z^{P-1} \exp\left(-\frac{1}{4}z^2\right) D_{P+1}(z) dz.$$

Further, G satisfies

$$G(y) = G_1(y, y^*) + G_2(y^*)$$

for all $y^* \geq y$ that are sufficiently large, where G_1 can be expressed as the convergent series

$$G_1(y, y^*) = \sum_{k=0}^{\infty} \hat{d}_k(P) 2^{P+k-1} \left(\Gamma\left(\frac{P+k}{2}, \frac{y^2}{4}\right) - \Gamma\left(\frac{P+k}{2}, \frac{(y^*)^2}{4}\right) \right),$$

and G_2 has the asymptotic expansion

$$G_2(y^*) \sim \sum_{k=0}^{\infty} (-1)^k \frac{(-(P+1))_{2k}}{k!} 2^{P-2k-\frac{1}{2}} \Gamma\left(P-k+\frac{1}{2}, \frac{(y^*)^2}{2}\right), \quad \text{as } y^* \rightarrow +\infty.$$

Here, $\Gamma(s, z)$ is the upper incomplete gamma function.

The previous theorem provides an effective approach to calculate the distribution function F_{S^P} for small P across its support with high precision. In practice, we choose to use the asymptotic expansion for the parabolic cylinder function $D_{P+1}(z)$ whenever $z \geq \Delta(P+3/2)$ for some positive constant $\Delta \gg 1$, suggested by Gil, Segura and Temme [16, Section 5]. Accordingly, we set $y^* = \max\{\Delta(P+3/2), y\}$ when computing the function $G(y)$ for fixed $y > 0$. This means only asymptotic series is involved in the computation of $G(y) = G_2(y)$ for sufficiently large y such that $y \geq \Delta(P+3/2)$. The constant Δ , which may vary depending on the value of P , can be determined by numerical trials of comparing the accuracy and efficiency of evaluating both the power series and asymptotic representations at particular points. As in the case for large P , we compute the above series representation for F_{S^P} and perform the root-finding for $F_{S^P}^{-1}$ in Maple for $P = 1, 10$ and 50 . Notice that the series expansion developed here is valid for any $P \in (0, 1)$, not only for integer P . This will be useful in the simulation of X_2 later on.

3.4. Chebyshev polynomial approximation for the inverse distribution function of S^P . As presented above, for any positive integer P , the simulation of S^P is based on generating a series of random variables S^k for $k \in \mathbb{S}$ by direct inversion. This method takes a uniform sample $u \sim \text{Unif}(0, 1)$ and returns the quantile function evaluated at u as a sample for the associated distribution, which requires computing the inverse of the distribution function. However, it is often the case that the inverting process is computationally inefficient due to many factors such as poor initial guess and the lack of an analytical expression for the corresponding quantile function. Since a large number of samples is needed for the Monte Carlo simulation when the same number of inversions of the distribution will be performed, we now look for a more tractable technique to complete this step.

Indeed, we employ the method of Chebyshev polynomials explained below to approximate the inverse distribution function $F_{S^P}^{-1}$ for $P \in \mathbb{S}$. Despite the fact that the polynomial is just an approximation, we can still obtain highly accurate results by restricting the error, which is controlled by the degrees of the polynomials we construct. In practice, we require the uniform error to be far smaller than the Monte Carlo error, e.g. of order 10^{-12} .

Recall that a degree n Chebyshev polynomial approximation has the form

$$c_0 T_0(z) + c_1 T_1(z) + \cdots + c_n T_n(z) - \frac{1}{2} c_0,$$

where $T_k(z) = \cos(k \arccos z)$ for $k = 1, \dots, n$ are the Chebyshev polynomials of degree k defined on $[-1, 1]$ and c_k for $k = 1, \dots, n$ are the Chebyshev coefficients computed in the standard way following Press *et al.* [33]. Since polynomials often exhibit more rapid changes than the distribution functions, approximations by polynomials might not be able to fully capture the behaviour of the inverse function $F_{S^P}^{-1}(u)$. Hence, identifying appropriate scaling schemes of the argument u is of great importance to allow the application of the Chebyshev polynomial approximation. The choices of the scales are mainly characterised by the behaviour of the function depending on the range of P . We briefly state the scaling and its rationale behind for large P and small P separately.

Large P . Instead of the sum S^P , we take the normalised random variable Z^P with zero mean and unit variance into consideration. For the approximation of the inverse distribution function $F_{Z^P}^{-1}$, we focus on the sub-interval $[F_{Z^P}(0), 1)$ of its support $[0, 1]$ first, corresponding to the region where the random variable Z^P takes positive values. In the limit of large P , the distribution function of Z^P resembles that of a standard normal distribution. Thus, we generalise and apply the ideas underlying the Beasley-Springer-Moro direct inversion method for standard normal random variables; see Moro [31], Joy, Boyle and Tan [24] and Malham and Wiese [29]. The normal distribution function has three regions exhibiting different characteristic behaviours on the positive real line. Accordingly, we roughly split the interval $[F_{Z^P}(0), 1)$ into three regimes: the central $[F_{Z^P}(0), u_1]$, the middle $(u_1, u_2]$ and the tail $(u_2, 1 - 10^{-12}]$ regimes. In general, the central regime roughly represents the area where the decreasing density function has a increasing slope while the middle regime represents the area where the decreasing density function has a declining slope with the tail regime representing the region where the density function is flat taking values close to zero. We neglect the regimes from $1 - 10^{-12}$ to 1.

Remark 3.8. It should be pointed out here that the above rule is just for reference only. In reality, we can choose optimal values for the boundaries u_1 and u_2 by a small

number of trials in Maple to ensure that the resulting Chebyshev polynomial approximations have moderate degrees while retaining the accuracy for all three regimes. We may come across the circumstance that the approximations which achieves the desired accuracy have degrees of say 15 for both the central and middle regimes but a higher degree of say 50 for the tail regime for some given u_1 and u_2 . Such a case should be avoided from the perspective of efficiency as higher degree often comes with higher computational cost. Hence, it is necessary to set the values u_1 and u_2 again through further investigations so that the degrees of the approximation for all regions are balanced with each other. If both of the degrees of the Chebyshev polynomials constructed for two neighbouring regions are at relative lower level, we may combine those two regimes to one and produce a unified approximation.

In the central regime, we follow Malham and Wiese [29] to scale and shift the variable. Define $U(u) := \sqrt{2\pi}(u - F_{Z^P}(0))$ and $z(u) := k_1 U(u) + k_2$, where the parameters k_1 and k_2 are chosen to make sure $z(F_{Z^P}(0)) = -1$ and $z(u_1) = 1$. Then, we approximate the inverse distribution function by

$$F_{Z^P}^{-1}(u) \approx U(u) \cdot \left(c_0 T_0(z(u)) + c_1 T_1(z(u)) + \cdots + c_n T_n(z(u)) - \frac{1}{2} c_0 \right).$$

In the middle and tail regimes, we approximate

$$F_{Z^P}^{-1}(u) \approx c_0 T_0(z(u)) + c_1 T_1(z(u)) + \cdots + c_n T_n(z(u)) - \frac{1}{2} c_0,$$

where $U(u) := \log(-\log(1-u))$ and $z(u) := k_1 U(u) + k_2$ with the parameters k_1 and k_2 chosen such that $z(u) = -1$ at the left endpoint and $z(u) = 1$ at the right endpoint. The ansatz for U follows from inverting the asymptotic tail approximation for the standard normal, which is equivalent in distribution to Z^P when $P \rightarrow +\infty$ by the central limit theorem; see Moro [31].

The above serves as a general discussion for choosing the scaled variables and approximations in the region of $[F_{Z^P}(0), 1 - 10^{-12}]$ for large P . We apply this procedure to the cases $P = 10, 50, 5000, 10^4, 10^5$ and 10^6 , the inverse distribution functions of which are roughly anti-symmetric. For the remaining half sub-interval $[10^{-12}, F_{Z^P}(0))$ of its support, we can apply similar results to the scaling and approximation following the arguments mentioned above.

Small P . In the Chebyshev polynomial approximation for small P , the idea remains the same as above. Notice that the random variable S^P takes positive values only. Since the distribution has a heavy right tail, we break down the support of $F_{S^P}^{-1}$ into four regimes: the left $[10^{-12}, u_1]$, the central $(u_1, u_2]$, the middle $(u_2, u_3]$ and the right tail $(u_3, 1 - 10^{-12}]$ regimes. We neglect the regimes at a distance of 10^{-12} from its endpoints. In theory, these boundary points are determined in accordance with the behaviour of the distribution function, but again it is better to set them via empirical studies in practice.

The central limit theorem tells us the asymptotic distribution of the sum S^P when P is large. However, for small P we have to analyse the limiting behaviour of the distribution function F_{S^P} and its inverse $F_{S^P}^{-1}$ in order to help us find the proper scaled variables when we construct Chebyshev polynomial approximations. We build on the series representation for F_{S^P} given in Theorem 3.7 to derive the results below; see Appendix E for a detailed proof.

COROLLARY 3.9. *For any $P \in (0, 1) \cup \mathbb{N}$, the distribution function F_{S^P} has the*

following asymptotic expansion

$$(3.8) \quad F_{S^P}(x) \sim \frac{1}{\sqrt{\pi}} 2^{P+\frac{1}{2}} P^{P-1} x^{-P+\frac{1}{2}} \exp\left(-\frac{P^2}{2x}\right), \quad \text{as } x \rightarrow 0^+.$$

The above expression describes the behaviour of the distribution function $F_{S^P}(x)$ as $x \rightarrow 0^+$. Now, our goal is to invert this relation to obtain the asymptotic approximation for the inverse distribution function $F_{S^P}^{-1}(u)$ as $u \rightarrow 0^+$. Let $u = F_{S^P}(y)$, then from (3.8) it is clear

$$(3.9) \quad \frac{u\sqrt{\pi}}{2^{P+\frac{1}{2}} P^{P-1}} \sim y^{-P+\frac{1}{2}} \exp\left(-\frac{P^2}{2y}\right), \quad \text{as } y \rightarrow 0^+.$$

Introducing the new variable $v := u\sqrt{\pi}/(2^{P+\frac{1}{2}} P^{P-1})$ and taking logarithm on both sides, we can rewrite (3.9) as

$$\log v \sim \left(P - \frac{1}{2}\right) \log \frac{1}{y} - \frac{P^2}{2y}, \quad \text{as } y \rightarrow 0^+.$$

After rearrangement, the above expression becomes

$$\frac{1}{y} \sim \frac{2}{P^2} \left(P - \frac{1}{2}\right) \log \frac{1}{y} - \frac{2}{P^2} \log v, \quad \text{as } y \rightarrow 0^+.$$

Since $\log y^{-1}/y^{-1} \rightarrow 0$ as $y \rightarrow 0^+$, we have $-2 \log v/P^2 \sim y^{-1}$ in the limit $y \rightarrow 0^+$. This relation further gives

$$\log\left(-\frac{2}{P^2} \log v\right) = o\left(\frac{1}{y}\right), \quad \text{as } y \rightarrow 0^+.$$

Hence, taking advantage of order relations we can write y in terms of v as

$$(3.10) \quad \begin{aligned} \frac{1}{y} &\sim -\frac{2}{P^2} \log v + \frac{2}{P^2} \left(P - \frac{1}{2}\right) \log\left(-\frac{2}{P^2} \log v\right) \\ &= -\frac{2}{P^2} \log v + \frac{2}{P^2} \left(P - \frac{1}{2}\right) \log\left(\frac{2}{P^2}\right) + \frac{2}{P^2} \left(P - \frac{1}{2}\right) \log(-\log v) \end{aligned}$$

when $y \rightarrow 0^+$. In particular by the fact that $\log(-\log v) = o(y^{-1})$ as $y \rightarrow 0^+$, its leading order behaviour yields

$$\begin{aligned} y &\sim \left(\frac{2}{P^2} \left(P - \frac{1}{2}\right) \log \frac{2}{P^2} - \frac{2}{P^2} \log v\right)^{-1} \\ &= \left(\frac{2}{P^2} \left(P - \frac{1}{2}\right) \log \frac{2}{P^2} - \frac{2}{P^2} \log\left(\frac{u\sqrt{\pi}}{2^{P+\frac{1}{2}} P^{P-1}}\right)\right)^{-1}, \end{aligned}$$

as $y \rightarrow 0^+$, i.e. $u \rightarrow 0^+$, where the last equation comes from the transformation $v = u\sqrt{\pi}/(2^{P+\frac{1}{2}} P^{P-1})$.

As $u \rightarrow 1$, i.e. $y \rightarrow +\infty$, we adopt a gamma approximation for the tail. This is implied by empirical tests which show that the distribution is positively skewed with a longer right tail. Hence, by matching the mean and variance of S^P with those of a gamma random variable, the shape and rate parameters take the form $s = 5P/2$ and

$r = 15/2$. Then, the distribution function F_{S^P} is approximated by the distribution function F_X of a gamma random variable X with parameters s and r given as follows:

$$F_X(y) = 1 - \frac{1}{\Gamma(\frac{5}{2}P)} \Gamma\left(\frac{5}{2}P, \frac{15}{2}y\right),$$

Making use of the asymptotic relationship given below for the incomplete gamma function (Abramowitz and Stegun [2, formula (6.5.32)])

$$\Gamma(s, z) \sim z^{s-1} \exp(-z) \sum_{k=0}^{\infty} \frac{\Gamma(s)}{\Gamma(s-k)} z^{-k}, \quad \text{as } z \rightarrow +\infty$$

establishes as $y \rightarrow +\infty$,

$$(3.11) \quad F_X(y) \sim 1 - \frac{1}{\Gamma(\frac{5}{2}P)} \left(\frac{15}{2}y\right)^{\frac{5}{2}P-1} \exp\left(-\frac{15}{2}y\right).$$

Set $u = F_X(y)$. After rewriting (3.11), we obtain

$$(1-u) \Gamma\left(\frac{5}{2}P\right) \sim \left(\frac{15}{2}y\right)^{\frac{5}{2}P-1} \exp\left(-\frac{15}{2}y\right), \quad \text{as } y \rightarrow +\infty.$$

To generate an asymptotic expression for y , we start by taking logarithm and defining the new variable $v := (1-u) \Gamma(5P/2)$, which gives

$$(3.12) \quad \log v \sim \left(\frac{5}{2}P - 1\right) \log\left(\frac{15}{2}y\right) - \frac{15}{2}y, \quad \text{as } y \rightarrow +\infty.$$

Rearranging (3.12) leads to

$$y \sim -\frac{2}{15} \log v + \frac{2}{15} \left(\frac{5}{2}P - 1\right) \log\left(\frac{15}{2}y\right), \quad \text{as } y \rightarrow +\infty.$$

By a short calculation analogous to (3.10), we conclude

$$y \sim -\frac{2}{15} \log v + \frac{2}{15} \left(\frac{5}{2}P - 1\right) \log(-\log v), \quad \text{as } y \rightarrow +\infty.$$

On substituting $v = (1-u) \Gamma(5P/2)$, as $y \rightarrow +\infty$, i.e. $u \rightarrow 1$, its leading order is of the form

$$y \sim -\frac{2}{15} \log\left((1-u) \Gamma\left(\frac{5}{2}P\right)\right).$$

The analysis above outlines the asymptotic approximation for $F_{S^P}^{-1}(u)$ as $u \rightarrow 0$ and $u \rightarrow 1$, and provides the ansatz behind the choices of reasonable scaling variables for Chebyshev polynomial approximations for small P , i.e. $P = 1$. Accordingly, we report the routines for approximations of the inverse distribution function $F_{S^P}^{-1}(u)$ through Chebyshev polynomials for the four regimes identified in detail. Note again the parameters k_1 and k_2 given below restrict the ranges of the transformed variable z to the interval $[-1, 1]$.

For all the four regimes, we approximate $F_{S^P}^{-1}(u)$ by a degree n Chebyshev polynomial approximation of a scaled and shifted variable $z(u) := k_1 U(u) + k_2$ as below:

$$F_{S^P}^{-1}(u) \approx c_0 T_0(z(u)) + c_1 T_1(z(u)) + \cdots + c_n T_n(z(u)) - \frac{1}{2} c_0,$$

where $U(u) := ((2/P^2)(P - 1/2) \log(2/P^2) - (2/P^2) \log(u\sqrt{\pi}/(2^{P+1/2}P^{P-1})))^{-1}$ in the left regime $[10^{-12}, u_1]$, $U(u) := (u_2 - u) \sqrt{2P/45}$ in the central regime $(u_1, u_2]$ and $U(u) := (-2/15) \log((1-u)\Gamma(5P/2))$ in the middle regime $(u_2, u_3]$ and right tail regime $(u_3, 1 - 10^{-12}]$.

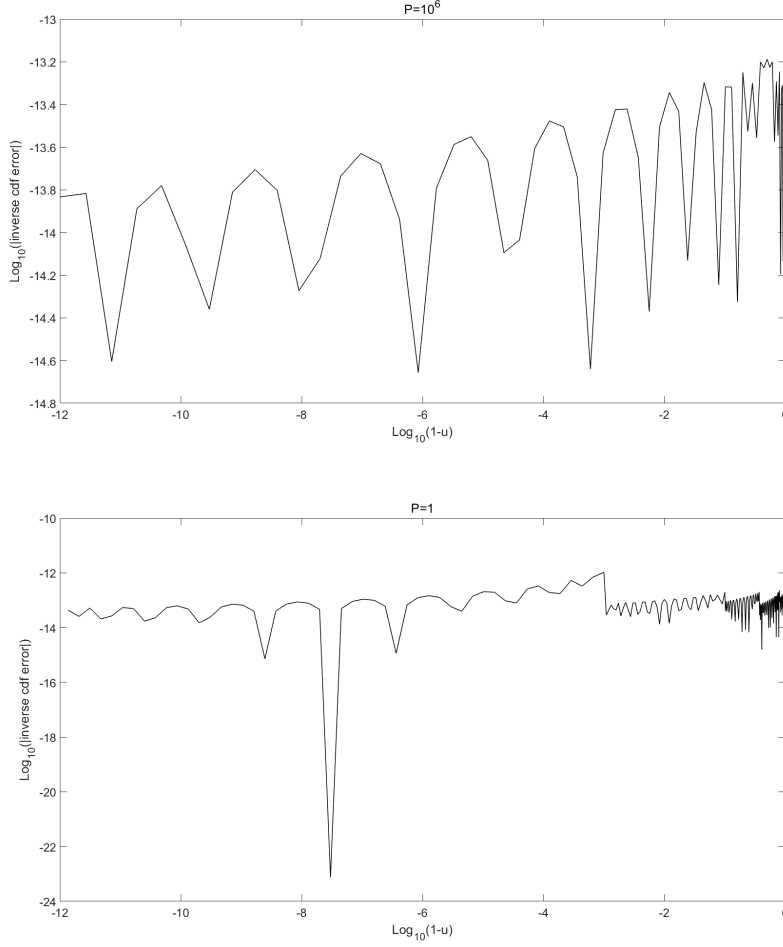


FIG. 1. We plot the errors in the Chebyshev polynomial approximations to the inverse distribution functions $F_{Z^P}^{-1}(u)$ with $P = 10^6$ (top panel) and $F_{S^P}^{-1}(u)$ with $P = 1$ (bottom panel) across all regimes, respectively. Note that to highlight the tail we use a log-log₁₀ scale with $1 - u$ on the abscissa.

We have summarised the approximation techniques for the inverse distribution function $F_{Z^P}^{-1}(u)$ or $F_{S^P}^{-1}(u)$ taking into account the various values that P and u might take. Following this, we compute the coefficients for the Chebyshev polynomial approximations in the standard fashion (see Press *et al.* [33]) for the cases

$P = 1, 10, 50, 5000, 10^4, 10^5, 10^6$ using Maple. With all these accurate and reliable coefficients, quoted in the supplementary materials, then imported to Matlab, subsequent Chebyshev approximations are evaluated by Clenshaw's recurrence formula, which can be found in Press *et al.* [33]. Therefore, for any $P > 0$, S^P can be sampled repeatedly with high efficiency using [Algorithm 3.1](#).

We end this section by showing the respective errors in the Chebyshev polynomial approximations to $F_{Z^P}^{-1}(u)$ and $F_{S^P}^{-1}(u)$ with $u \in [10^{-12}, 1 - 10^{-12}]$ when P is 10^6 and 1 in [Figure 1](#). For each u , the error of the approximation is $c - \hat{c}$, where c is obtained by a high precision root-finding procedure applied to the expansions for the distribution functions and \hat{c} is evaluated by the prescribed Chebyshev polynomials. To highlight the tail we plot the errors on a log-log₁₀ scale with $1 - u$ on the abscissa. For $P = 10^6$, we split the interval $[10^{-12}, 1 - 10^{-12}]$ into two regimes: $[10^{-12}, 0.5001)$ and $[0.5001, 1 - 10^{-12}]$, where both of the Chebyshev polynomials have degrees 16. For $P = 1$, we generate approximations for five regimes as described above where the right tail region is further split into two, the degrees for which are 25 in the left with $u \in [10^{-12}, 0.2)$, 18 in the central with $u \in [0.2, 0.63)$, 15 in the middle with $u \in [0.63, 0.9)$, 18 and 13 in the right tail regimes with $[0.9, 0.999)$ and $[0.999, 1 - 10^{-12}]$, respectively. Notice the error in all cases is of order 10^{-12} . Results for the other values, reported in Shen [36], have similar accuracy as those in [Figure 1](#).

3.5. Simulation of X_2 and Z . Let us first introduce the notation $h = \delta/2$, where $\delta = 4\kappa\theta/\sigma^2$ is the degrees of freedom. Note that for Heston models calibrated to real market data, the zero boundary of the variance process is typically attainable and strongly reflecting; see Haastrecht and Pelsser [39] and Lord, Koekkoek and Van Dijk [27]. By the Feller condition, this requires $\delta < 2$, i.e. $h < 1$. Hence, after separating the time parameter, X_2 can be written in the form

$$X_2 = \sum_{n=1}^{\infty} \frac{\tau^2}{4^n} C_n^h = \tau^2 \sum_{n=1}^{\infty} \frac{1}{4^n} C_n^h = \tau^2 Y_2^h,$$

with $Y_2^h := \sum_{n=1}^{\infty} C_n^h/4^n$ depending only on the parameter h . The structure of the random variable Y_2^h , along with its dependence on the model parameters, provides us with another possibility to sample Y_2^h and thus X_2 , apart from the truncation method. In fact, the Laplace transform of Y_2^h is identical to that for S^h . We can therefore try to extend the direct inversion of S^h for any $h \in \mathbb{N}$ developed above for the simulation of Y_2^h .

Recall that Y_2^h has the Laplace transform

$$\Phi_{Y_2^h}(b) = \mathbb{E} [\exp(-bY_2^h)] = \left(\frac{\sqrt{2b}}{\sinh \sqrt{2b}} \right)^h, \quad \text{for } b > 0,$$

which has the same expression as that of S^h given by (3.1) after replacing P by h . The only difference is that the parameter h now is restricted to $(0, 1)$ rather than positive integers. This suggests the decomposition proposed in [section 3.1](#) for integer h and the resulting S^h is no longer reasonable. However, motivated by Malham and Wiese [28], we have the following alternative formula for $0 < h < 1$, which is given to the first three decimal places

$$h = \frac{h_5}{5} + \frac{h_{10}}{10} + \frac{h_{20}}{20} + \frac{h_{50}}{50} + \frac{h_{100}}{100} + \frac{h_{200}}{200} + \frac{h_{500}}{500} + \frac{h_{1000}}{1000} + \frac{h_{2000}}{2000},$$

where $h_k \in \{0, 1, 2\}$ for $k \in \mathbb{H} = \{5, 10, 20, 50, 100, 200, 500, 1000, 2000\}$. The above decomposition works for the case when h is rounded to three decimal digits, but it can be generalised to $h \in (0, 1)$ given to any decimal places in principle. Next, we give the direct inversion algorithm for generating Y_2^h for any $h \in (0, 1)$ given to the first three decimal places.

Algorithm 3.2 Direct inversion for Y_2^h

- 1: For each $k \in \mathbb{H}$, sample h_k independent random variables $Y_{2,i}^{1/k}$, $i = 1, \dots, h_k$ from the distribution of $Y_2^{1/k}$ by inverse transform sampling based on the corresponding Chebyshev polynomial approximations.
 - 2: Compute the accumulated sum, i.e. $\sum_k \sum_{i=1}^{h_k} Y_{2,i}^{1/k} \sim Y_2^h$.
-

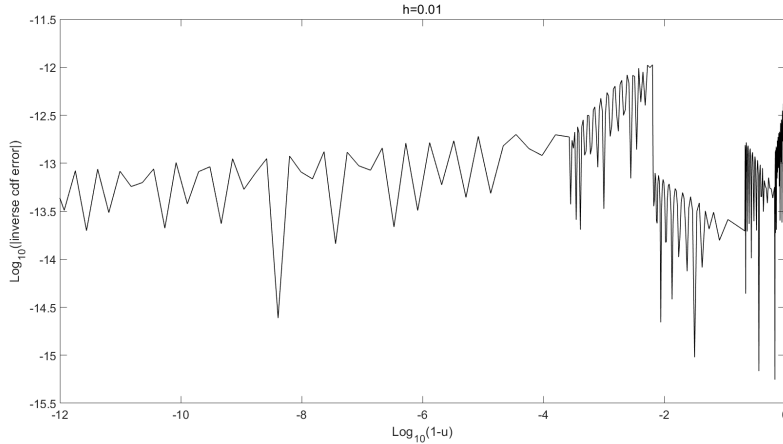


FIG. 2. We plot the errors in the Chebyshev polynomial approximations to the inverse distribution functions $F_{Y_2^h}^{-1}(u)$ with $h = 0.01$ across all regimes. Note as above we use a log-log₁₀ scale with $1 - u$ on the abscissa.

Given [Algorithm 3.2](#), for a general h , the simulation of Y_2^h is reduced to simulating several particular random variables such as $Y_2^{1/5}$, $Y_2^{1/10}$, \dots using their inverse distribution functions, which are approximated by the associated Chebyshev polynomials. To design these Chebyshev polynomial approximations, the approach for S^P with small integer P introduced in [section 3.3](#) and [section 3.4](#) can be fully used here. This is because the series expansion and the asymptotic approximation for the distribution function of S^P remain valid for small non-integer P . Therefore, we apply the same strategy to calculate the Chebyshev polynomial approximations for the inverse distribution function of Y_2^h with fixed $h = 1/k$, $k \in \mathbb{H}$, the values for the coefficients of which are presented in the supplementary materials. [Figure 2](#) shows the errors in the approximation for $F_{Y_2^h}^{-1}$ by Chebyshev polynomials across all regimes when $h = 1/100$. Notice that under such circumstance, because of the heavy tail we further split the right tail region into two smaller regions where different Chebyshev polynomials are developed, making a total of five separate regions: $[10^{-12}, 0.3364)$, $[0.3364, 0.7854)$, $[0.7854, 0.9936)$, $[0.9936, 0.9997)$ and $[0.9997, 1 - 10^{-12}]$ with degrees 24, 19, 18, 19

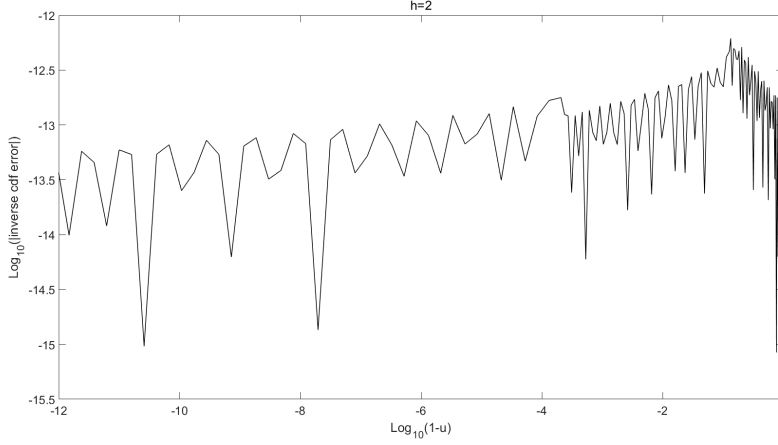


FIG. 3. We plot the errors in the Chebyshev polynomial approximations to the inverse distribution functions $F_{Y_2^h}^{-1}(u)$ with $h = 2$, i.e. $F_{Z'}^{-1}(u)$ across all regimes. Note as above we use a log-log₁₀ scale with $1 - u$ on the abscissa.

and 31, respectively. All errors are fluctuating at the level of 10^{-12} . See Shen [36] for more results of the other cases.

As Z is a special case of X_2 when $h = 2$, the approach to generating samples of X_2 discussed above is fully applicable here. In fact, we directly construct the Chebyshev polynomial approximations for the inverse distribution function $F_{Z'}^{-1}$ with $Z' = Z/\tau^2$ since Z' is independent of any parameters. We plot the resulting errors in Figure 3. The polynomials have degrees between 22 and 27 in the four regions with errors of order 10^{-12} .

TABLE 1
Parameters for the Heston model.

Parameters	European				Path-dependent	
	Case 1	Case 2	Case 3	Case 4	Asian	Barrier
κ	0.5	0.3	1	6.21	1.0407	0.5
θ	0.04	0.04	0.09	0.019	0.0586	0.04
σ	1	0.9	1	0.61	0.5196	1
ρ	-0.9	-0.5	-0.3	-0.7	-0.6747	0
t	10	15	5	1	4	1
v_0	0.04	0.04	0.09	0.010201	0.0194	0.04
S_0	100	100	100	100	100	100
r	0	0	0.05	0.0319	0	0

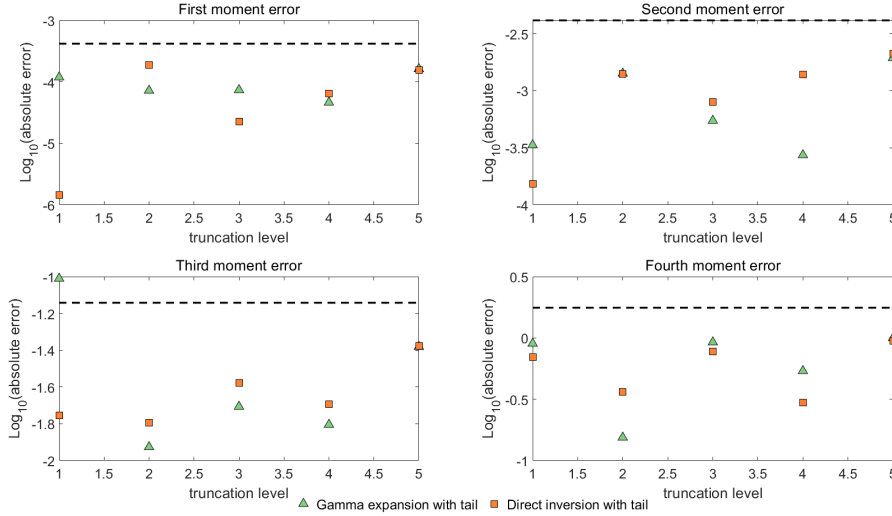
4. Numerical analysis. In this section, we compare our direct inversion method with the gamma expansion of Glasserman and Kim [18] by pricing four challenging European call options in the Heston model. The sets of parameters considered are given in Table 1. These four sets are taken from Glasserman and Kim [18], which are found to be in the typical range of parameter values of the Heston model in practice. Two path-dependent options including an Asian option with yearly fixings (see Smith

[37], Haastrecht and Pelsser [39] and Malham and Wiese [28]) and a digital double no touch barrier option (see Lord, Koekkoek and Van Dijk [27] and Malham and Wiese [28]) are also tested with parameter values shown in Table 1.

4.1. Time integrated conditional variance. Before giving simulation results for option prices, we first illustrate the performance of the above direct inversion method in terms of accuracy based upon the series expansion given in Theorem 2.1. Recall that our objective is to sample from the distribution of the random variable $\int_0^t V_s ds$ given its endpoints V_0 and V_t , denoted by \bar{I} , i.e.

$$\bar{I} = \left(\int_0^t V_s ds \middle| V_0 = v_0, V_t = v_t \right) = \frac{4}{\sigma^2} \left(\int_0^\tau \tilde{A}_s ds \middle| \tilde{A}_0 = a_0, \tilde{A}_\tau = a_\tau \right) = \frac{4}{\sigma^2} I,$$

under the probability measure \mathbb{Q} . We have decomposed the integral into the sum of three independent series after measure transformation. Among the realisation of those three series, the first one is truncated with tail approximated by a gamma random variable and the remaining two series are simulated exactly by direct inversion.

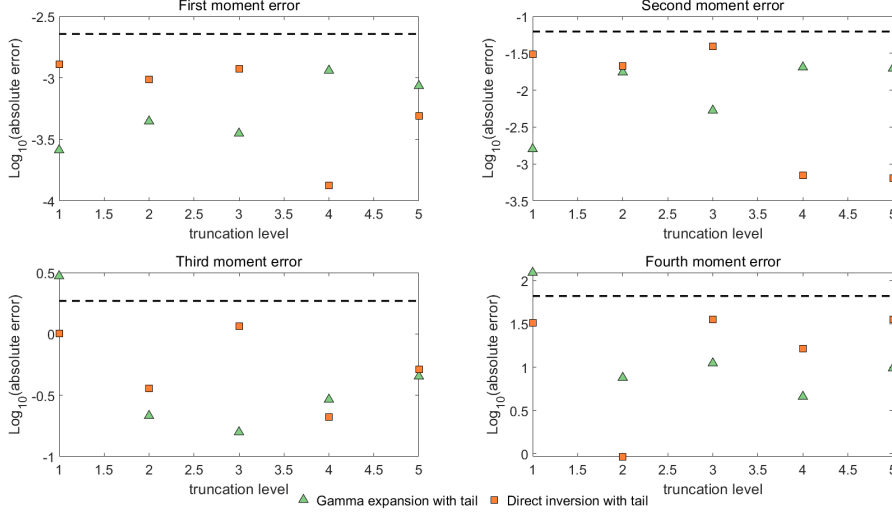


(a) Case 1: $v_0 = v_t = 0.04$

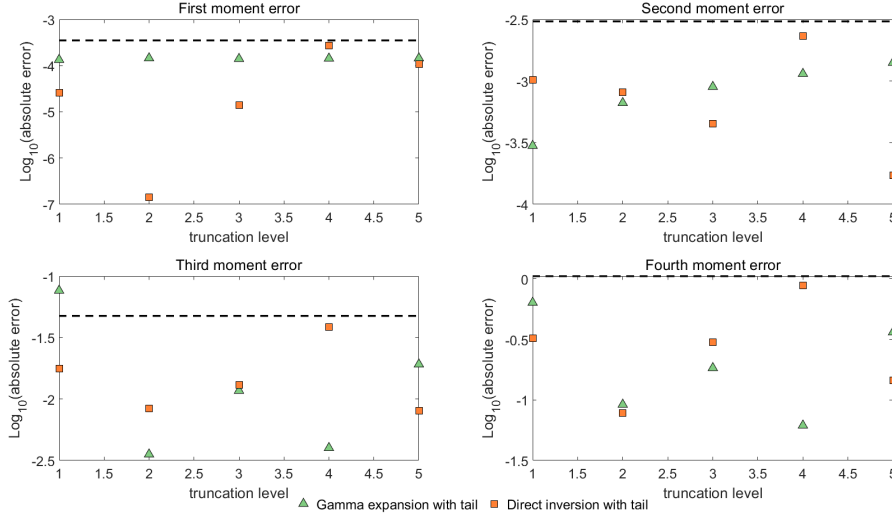
FIG. 4. We indicate the absolute errors in the first four moments of the conditional integral \bar{I} simulated by direct inversion and gamma expansion versus the truncation levels for Case 1 with different values for v_t . Both methods are implemented with tail simulation. We perform $5 \cdot 10^7$ simulations for each case. Below the dashed line, the errors are not statistically significant at the level of three standard deviations.

In Figure 4 and Figure 5 the absolute errors in the first four moments are displayed for simulating the conditional integral \bar{I} with different values of v_t using our method. For comparison, we include the results by employing the gamma expansion from Glasserman and Kim [18] as well. For both methods, we apply tail approximations with truncation level increasing in integers. The number of samples generated in each case is $5 \cdot 10^7$. The three panels shown in Figure 4 from top to bottom correspond to the three representative values $v_t = 0.04, 4, 0.000004$ for Case 1 and the panels in Figure 5 correspond to the three fixed values $v_t = 0.010201, 0.0025, 0.05$ (top to bottom) for Case 4. Note that the true moments can be computed by evaluating

the respective derivatives of the moment generating functions derived by Broadie and Kaya [12] at the origin.



(b) Case 1: $v_0 = 0.04, v_t = 4$



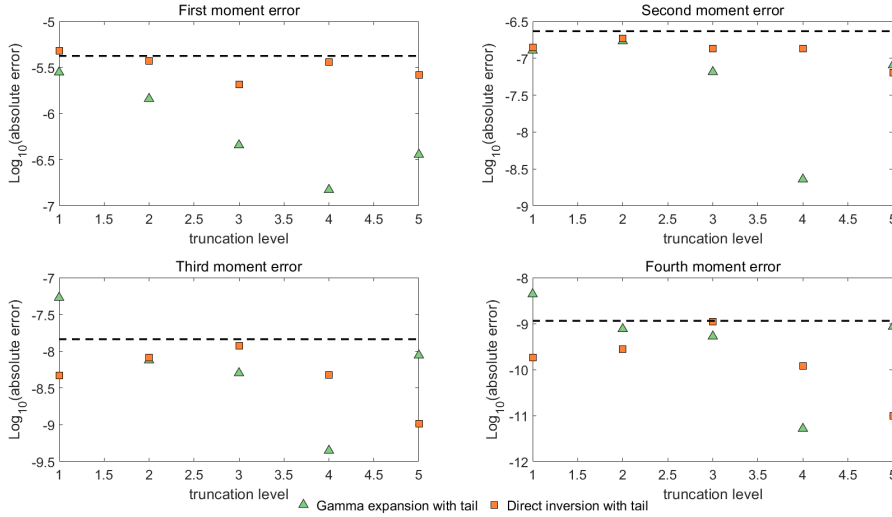
(c) Case 1: $v_0 = 0.04, v_t = 0.000004$

FIG. 4. (cont.) We indicate the absolute errors in the first four moments of the conditional integral \bar{I} simulated by direct inversion and gamma expansion versus the truncation levels for Case 1 with different values for v_t . Both methods are implemented with tail simulation. We perform $5 \cdot 10^7$ simulations for each case. Below the dashed line, the errors are not statistically significant at the level of three standard deviations.

We observe that most errors for the first two moments across different values of v_t and truncation levels for both Case 1 and 4 are not significantly different from zero at the level of three standard deviations, suggesting both methods achieve high accuracy for these two moments as expected. This is consistent with the theory as tail

simulation in each method is designed such that the first two moments are matched. In other words, the simulations should lead to the exact first and second moments in principle, whence only Monte Carlo noise with a scaling as the inverse of the square root of the sample size, i.e. $(5 \cdot 10^7)^{-1/2}$, is observed.

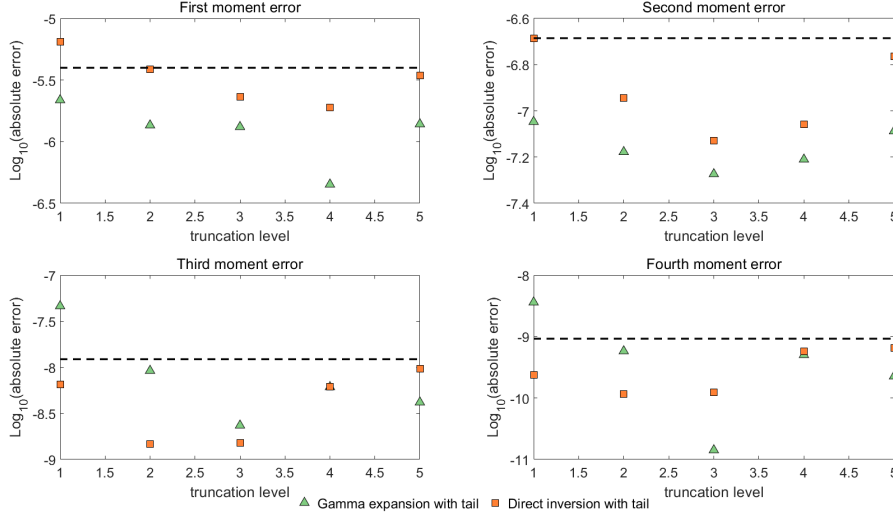
For the higher moments, the errors of the direct inversion are fluctuating at some level below the statistical significance for all circumstances considered. These errors are so small that a decreasing trend is not visible when increasing the truncation level. In contrast, with the increment of the truncation levels, the errors of the gamma expansion first exhibit a decaying pattern until the curves become horizontal. For example, the behaviour of the decreasing errors of the third and fourth moments is obvious when the truncation level is increased from one to two. The falling tendency appears to be more significant when we increase the sample size, thus, reduce the Monte Carlo effect, which will be discussed later. This suggests that there exists some bias in the gamma expansion with small truncation levels while the direct inversion with lower truncation levels has the same accuracy as that with higher ones.



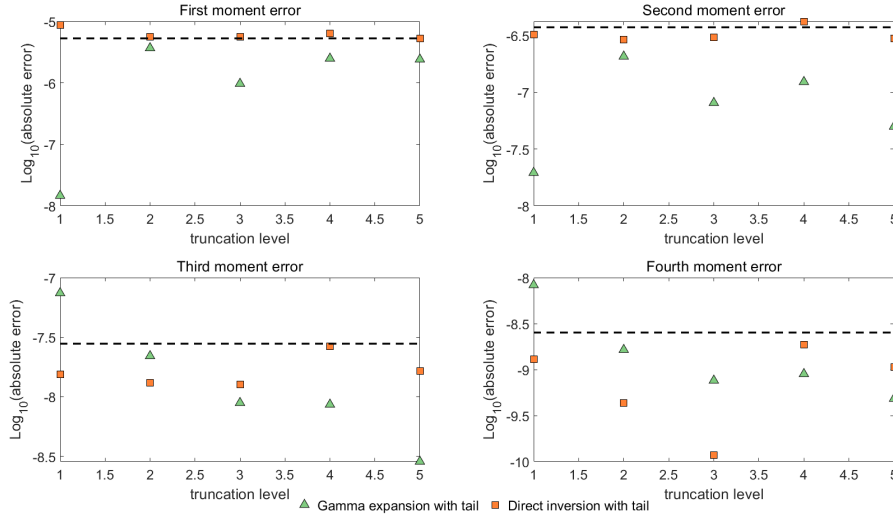
(a) Case 4: $v_0 = v_t = 0.010201$

FIG. 5. We indicate the absolute errors in the first four moments of the conditional integral \bar{I} simulated by direct inversion and gamma expansion versus the truncation levels for Case 4 with different values for v_t . Both methods are implemented with tail simulation. We perform $5 \cdot 10^7$ simulations for each case. Below the dashed line, the errors are not statistically significant at the level of three standard deviations.

While the figures for Case 1 and 4 have many details in common, they also reveal noteworthy differences in the first two moments. As illustrated in the upper panels in Figure 5a, Figure 5b and Figure 5c for Case 4, most of the first and second moment errors in the direct inversion are slightly higher compared to those in the gamma expansion at the same truncation level. Errors of the two schemes considered in the first two moments for Case 1 on the other hand seem to be of the same order to some extent with the same truncation level, which can be seen from the upper panels in Figure 4a, Figure 4b and Figure 4c. In order to find a plausible explanation for this difference, we increase the sample size by a factor of 10 and plot the resulting errors versus the truncation levels in Figure 6 and Figure 7.



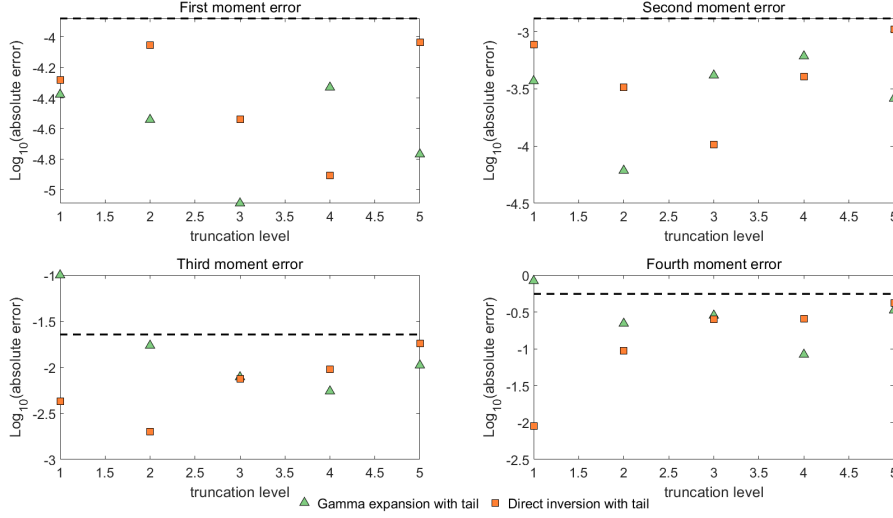
(b) Case 4: $v_0 = 0.010201, v_t = 0.0025$



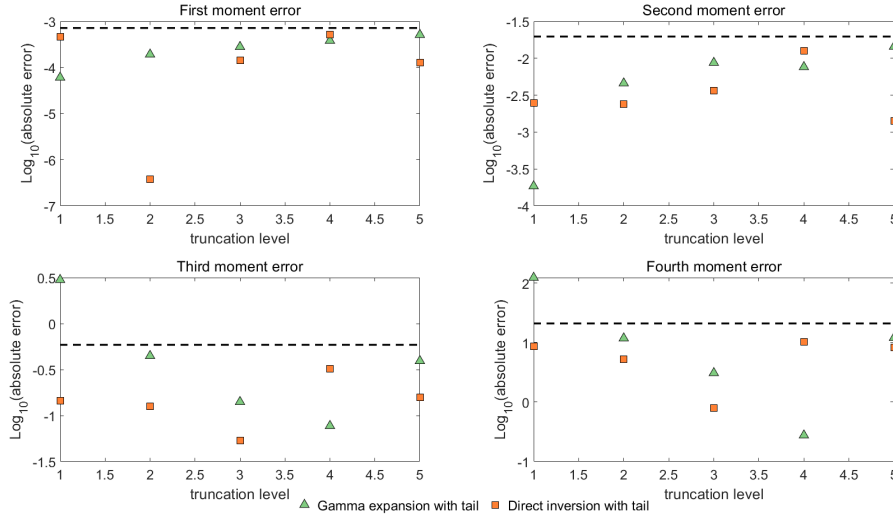
(c) Case 4: $v_0 = 0.010201, v_t = 0.05$

FIG. 5. (cont.) We indicate the absolute errors in the first four moments of the conditional integral \bar{I} simulated by direct inversion and gamma expansion versus the truncation levels for Case 4 with different values for v_t . Both methods are implemented with tail simulation. We perform $5 \cdot 10^7$ simulations for each case. Below the dashed line, the errors are not statistically significant at the level of three standard deviations.

For Case 1, Figure 6 demonstrates the errors in all four moments based on the direct inversion are decreased as expected, i.e. proportional to the reciprocal of the square root of the sample size across all the values of v_t and truncation levels. This confirms that the moment errors observed in Figure 4 using the direct inversion are dominated by the Monte Carlo error. On the other hand, for the gamma expansion we note in the upper panels of each subplots that the first two moments of the simu-



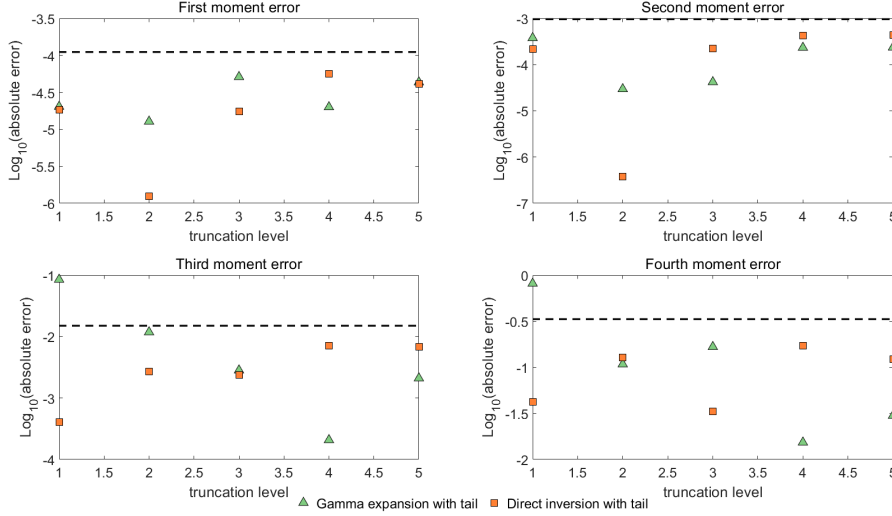
(a) Case 1: $v_0 = v_t = 0.04$



(b) Case 1: $v_0 = 0.04, v_t = 4$

FIG. 6. We indicate the absolute errors in the first four moments of the conditional integral \bar{I} simulated by direct inversion and gamma expansion versus the truncation levels for Case 1 with different values for v_t . Both methods are implemented with tail simulation. We perform $5 \cdot 10^8$ simulations for each case. Below the dashed line, the errors are not statistically significant at the level of three standard deviations.

lations for all five truncation levels are indeed matched with errors improving roughly according to the expected scaling when increasing the sample size. However, we see in the lower panels that the errors in the third and fourth moments hardly show any changes for lower truncation levels such as one and two while the accuracy for the other truncation levels is improved with the increase of the sample size. In fact, after reducing the Monte Carlo noise, there exists an even more clear decreasing trend for



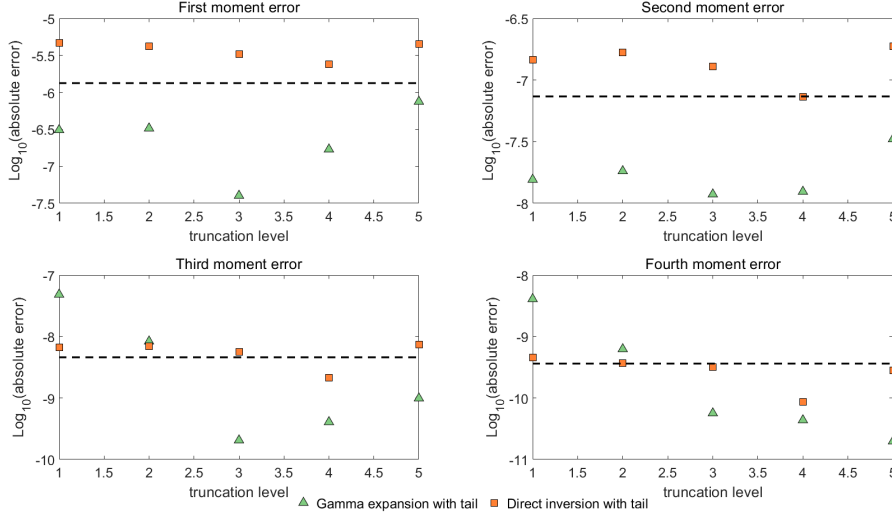
(c) Case 1: $v_0 = 0.04, v_t = 0.000004$

FIG. 6. (cont.) We indicate the absolute errors in the first four moments of the conditional integral \bar{I} simulated by direct inversion and gamma expansion versus the truncation levels for Case 1 with different values for v_t . Both methods are implemented with tail simulation. We perform $5 \cdot 10^8$ simulations for each case. Below the dashed line, the errors are not statistically significant at the level of three standard deviations.

the higher order moment errors with the gamma expansion as the truncation level increases. This seems to corroborate the observations from Figure 4 for Case 1, indicating that the gamma expansion with small truncation levels exhibits some bias while the direct inversion achieves the same accuracy, restricted by the Monte Carlo error, for all truncation levels.

In comparison, Figure 7 shows different behaviour for the errors related to the direct inversion for Case 4 while similar conclusion can be reached for the gamma expansion as Case 1. More specifically, we notice that all moment errors in direct inversion sampling for Case 4 are invariant to increasing the sample size when the truncation levels are fixed. Further we observe that the errors, all remaining steady across a set of different truncation levels, become statistically significant when the number of samples is increased, especially for the first and second moments. Thus, this implies in Case 4 the direct inversion performs equally well for all truncation levels, nevertheless, the accuracy of which is overridden by some bias. We should not fail to mention that the bias is roughly of the same order as the Monte Carlo error with $5 \cdot 10^7$ samples, whence it is not reflected in Figure 5. This accounts for the finding for Case 4 that the first and second moment errors for the direct inversion are always slightly larger than those for gamma expansion, where only Monte Carlo error is in presence. We give a possible explanation for this bias as follows.

The reason for the bias with the direct inversion method for Case 4 lies in the arithmetic precision we use for the parameter h , which is related to the random variable X_2 . Recall that the proposed decomposition requires the rational parameter h is given as a decimal with three significant figures. Let \tilde{h} stand for the rounded number and \tilde{X}_2 denote the approximation to X_2 by replacing h with \tilde{h} . Next, we give the exact errors in the first and second moments of X_2 . Directly computing the first



(a) Case 4: $v_0 = v_t = 0.010201$

FIG. 7. We indicate the absolute errors in the first four moments of the conditional integral \bar{I} simulated by direct inversion and gamma expansion versus the truncation levels for Case 4 with different values for v_t . Both methods are implemented with tail simulation. We perform $5 \cdot 10^8$ simulations for each case. Below the dashed line, the errors are not statistically significant at the level of three standard deviations.

two moments using the series which defines X_2 , we can write

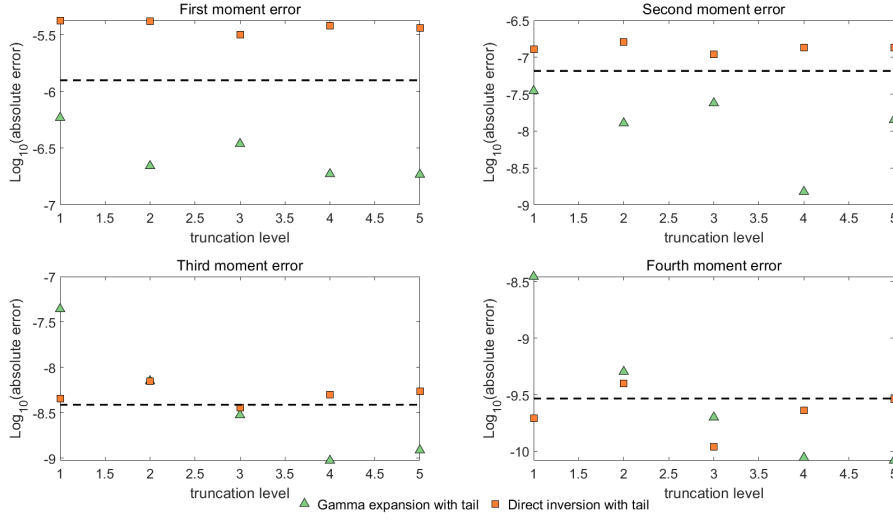
$$\mathbb{E}[X_2] = \frac{1}{3}\tau^2 h, \quad \mathbb{E}[X_2^2] = \frac{2}{45}\tau^4 h + \frac{1}{9}\tau^4 h^2.$$

Then, the corresponding relative errors are

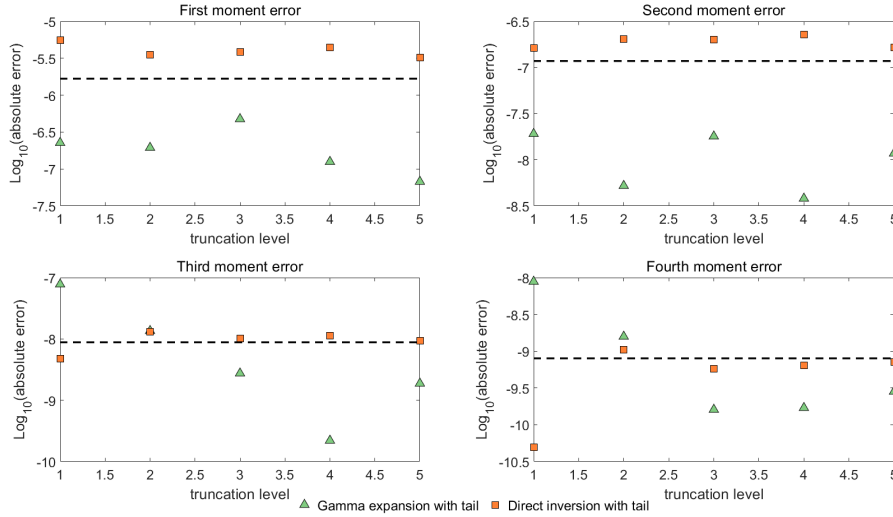
$$\frac{|\mathbb{E}[X_2] - \mathbb{E}[\tilde{X}_2]|}{\mathbb{E}[X_2]} = \frac{|h - \tilde{h}|}{h},$$

$$\frac{|\mathbb{E}[X_2^2] - \mathbb{E}[\tilde{X}_2^2]|}{\mathbb{E}[X_2^2]} = \frac{|2(h - \tilde{h}) + 5(h^2 - \tilde{h}^2)|}{2h + 5h^2}.$$

The above equations shows a linear scaling of the moment errors of X_2 in terms of the discrepancy between the true value h and the approximated value \tilde{h} . Table 2 quotes the values for h and \tilde{h} for all the four European cases. Note that for Case 1 and 3 accurate values of h are used while the relative errors for Case 2 and 4 are of order 10^{-3} and 10^{-4} , respectively. In Figure 8 the panels show the relative errors in the first four moments of X_2 for Case 1 to Case 4 using 10^8 and 10^9 simulations. For Case 1 and Case 3, by successively increasing the sample size the high accuracy for the first four moments of X_2 sampled by direct inversion Algorithm 3.2 is indeed limited by the Monte Carlo error, which improves roughly according to the expected scale. However, the errors are invariant for Case 2 and Case 4 when increasing the sample size. For these two cases, the systematic Monte Carlo error is lower than the bias caused by replacing the true value h with the approximated value \tilde{h} . Hence, the errors reflected in Figure 8, dominated by the bias, fail to show improvement when the sample size is increased by a factor of 10.



(b) Case 4: $v_0 = 0.010201, v_t = 0.0025$



(c) Case 4: $v_0 = 0.010201, v_t = 0.05$

FIG. 7. (cont.) We indicate the absolute errors in the first four moments of the conditional integral \bar{I} simulated by direct inversion and gamma expansion versus the truncation levels for Case 4 with different values for v_t . Both methods are implemented with tail simulation. We perform $5 \cdot 10^8$ simulations for each case. Below the dashed line, the errors are not statistically significant at the level of three standard deviations.

TABLE 2
True value h and rounded value \tilde{h} .

	Case 1	Case 2	Case 3	Case 4
h	0.04000	0.02963	0.18000	0.63418
\tilde{h}	0.04000	0.02950	0.18000	0.63400

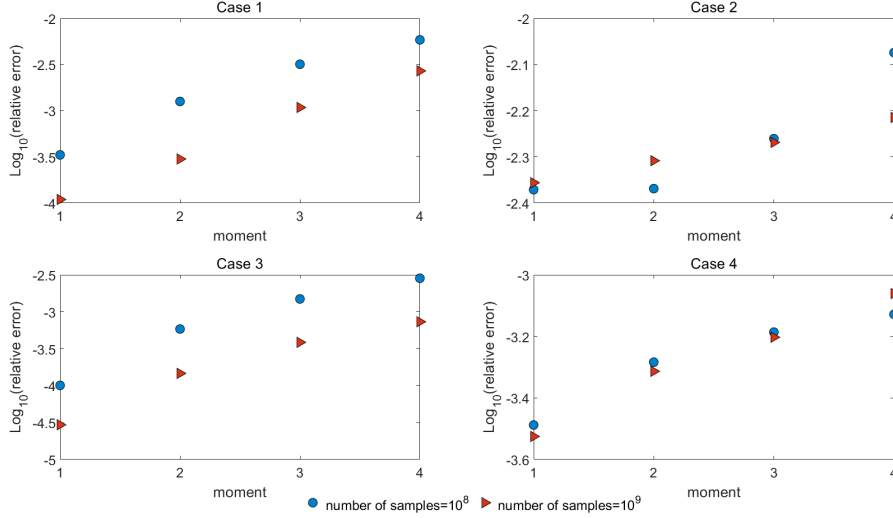
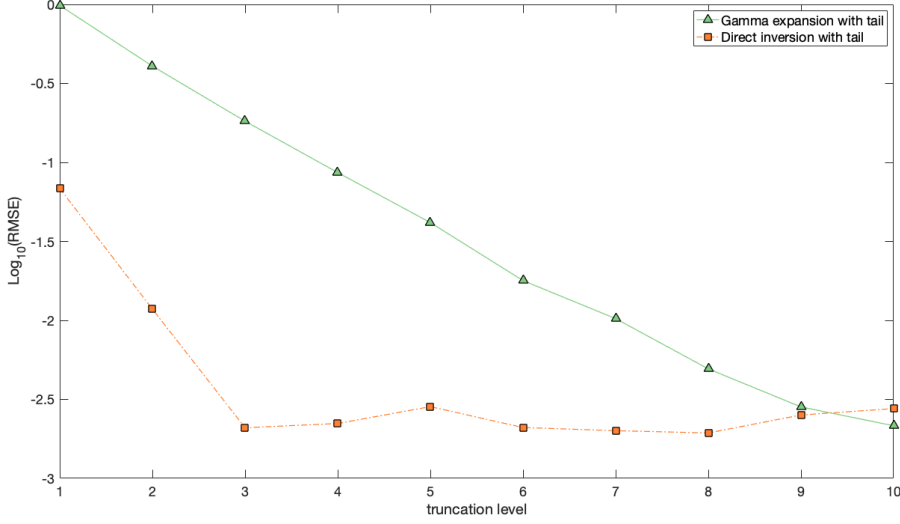


FIG. 8. We plot the relative errors in the first four moments of X_2 simulated by direct inversion Algorithm 3.2 for Case 1 to Case 4. By increasing the sample size by a factor of 10, we note that the accuracy in the moment errors is improved as expected for Case 1 and Case 3. The four moment errors are invariant for Case 2 and Case 4 when increasing the sample size, suggesting possible bias in the direct inversion for these two cases.

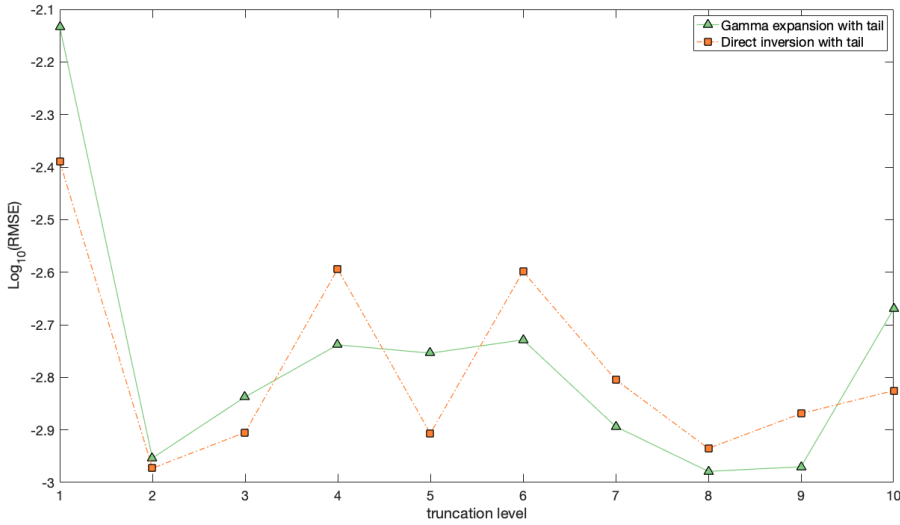
Based on the above analysis, we conclude that the direct inversion method for X_2 exhibits some small bias when approximation of the parameter h is adopted. This can conceivably lead to the bias of the general direct inversion scheme for the conditional integral \bar{I} . However, this bias has nothing to do with the development of the method, but is associated with the decomposition technique and the arithmetic precision involved. Without loss of generality, this method can be extended to allow for a finer decomposition of the parameter h given to any number of decimal places. In this sense, we expect that the accuracy available for this method will become more apparent.

4.2. Option price. In this section, we apply the direct inversion method and the gamma expansion to pricing four European call options and two path-dependent options including an Asian option and a barrier option. These two schemes are both based on the known conditional non-central chi-square distribution for the variance process and the conditional lognormal distribution for the asset price. We further compare the above two methods with the full truncation scheme of Lord, Koekkoek and Van Dijk [27], which is a time stepping method with asset price and variance simulated on discrete time grids. This type of equidistant discretization scheme for the one-dimensional CIR process has been shown to have an arbitrarily slow convergence rate in the strong sense in general; see Hefter and Jentzen [20]. Hence, developing other simulation methods becomes essential for practical purposes.

We first demonstrate the tradeoff between the truncation level and accuracy for the direct inversion scheme and the gamma expansion. Figure 9 plots the root mean square error for the price of an at the money European call option against the truncation level for Case 1 and Case 4. For both methods, we use a sample size of $5 \cdot 10^7$ and truncate after M terms, increasing M in integers from 1 to 10. For Case 1, the direct inversion exhibits a faster convergence rate, revealed by the steeper slope in Figure 9a,



(a) Case 1



(b) Case 4

FIG. 9. We show the root mean square error in the option price (strike 100) versus the truncation level for Case 1 and Case 4. We use a sample size of $5 \cdot 10^7$ with truncation levels increasing in integers from 1 to 10.

in contrast with the gamma expansion. Indeed, truncation after three terms already provides a satisfactory estimator with error curve eventually becoming noisy in the larger M regime. To obtain the same accuracy, many more terms up to $M = 10$ are required for the gamma expansion. For Case 4, increasing M from one to two indeed helps to reduce the error. However, further increase in M does not seem to bring

improvement to the error for both methods, as seen from the horizontal error curves with small fluctuations in Figure 9b. This implies that approximations with small M are sufficient to achieve acceptable accuracy.

Remark 4.1. Similar conclusions as Case 1 can be reached for Case 2 and Case 3 with numerical results presented in Shen [36]. Simulations with different strikes for in the money and out of the money options for the above four test cases are also included there.

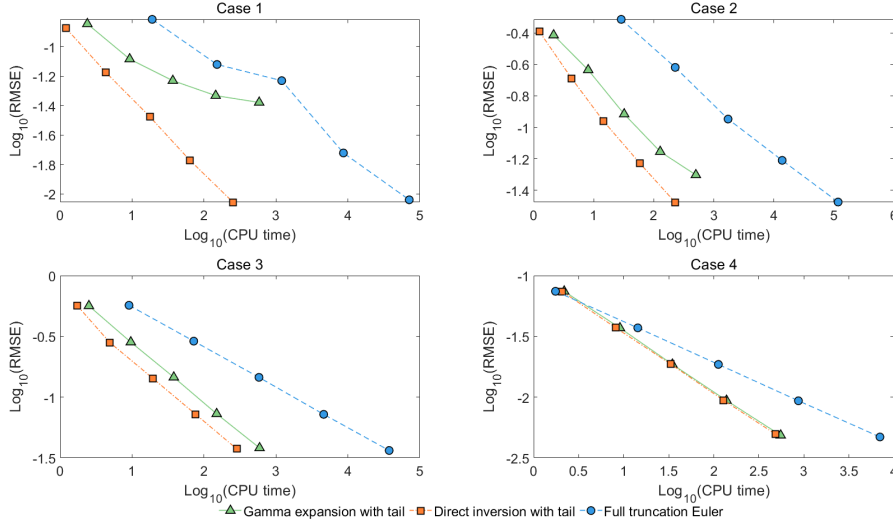


FIG. 10. We show the convergence of the root mean square error in the option price (strike 100) for Case 1 to Case 4 of gamma expansion and direction inversion, both at a truncation level $M = 5$, and full truncation Euler scheme, with number of time steps equal to the square root of the sample size.

Next, we give the comparisons between the direct inversion method, the gamma expansion and the full truncation Euler scheme. In Figure 10, we plot the root mean square error in the option price as a function of the CPU time required on a log-log₁₀ scale for all schemes. For fair comparisons, we implement these three methods as efficiently as possible and generate the CPU time using compiled Matlab code. For the two non-discretization methods, we choose to use truncation level $M = 5$. For the full truncation Euler method, we set the number of time steps equal to the square root of the sample size. This is motivated by the optimal allocation for the number of time steps from Duffie and Glynn [14], which is proportional to the square root of the number of trials for methods with weak order of convergence being equal to one; see Broadie and Kaya [12] and Lord, Koekkoek and Van Dijk [27].

We can see from the upper panels in Figure 10 that the bias in the gamma expansion with $M = 5$ for Case 1 and Case 2 eventually dominates the root mean square error when the number of sample trails increases. By comparison, the root mean square errors for the direct inversion and full truncation Euler scheme are declining monotonically, with the former presenting a more rapid rate with reduced computational cost. For Case 3 and Case 4, the two non-discretization methods both outperform the full truncation Euler scheme, which has a slower convergence rate

reflected by the less steeper slope in the graph.

With regard to the computing time, the gamma expansion is at least two to three times slower than the direct inversion with similar accuracy for Case 1, Case 2 and Case 3. For Case 4, the new method takes much more time compared with Case 1. This is because more effort is needed for the acceptance-rejection sampling of Case 4 due to the slightly unfavourable values for the model parameters. Although the time needed for the direct inversion is marginally more than the gamma expansion for Case 4 with $M = 1$, as the desired accuracy is increased the new method requires less computational budget. In summary, we conclude that the performance of the direct inversion is the best among the three schemes considered here.

Now we turn to the pricing of options with payoffs depending on sample paths. We first consider an at the money Asian option with yearly fixings, the payoff of which is determined by the average of asset prices at the end of each year. We show in Figure 11 the root mean square error of the price versus the CPU time on a log-log₁₀ scale. For the direct inversion and the gamma expansion, we truncate the series after $M = 1$ and simulate the asset prices for each year. Within one year, the terminal value is obtained directly using a single step. For the time discretization scheme, multiple steps are needed for each year. In this test, the number of time steps is taken to be the square root of the sample size in a similar manner to Broadie and Kaya [12] and Smith [37].

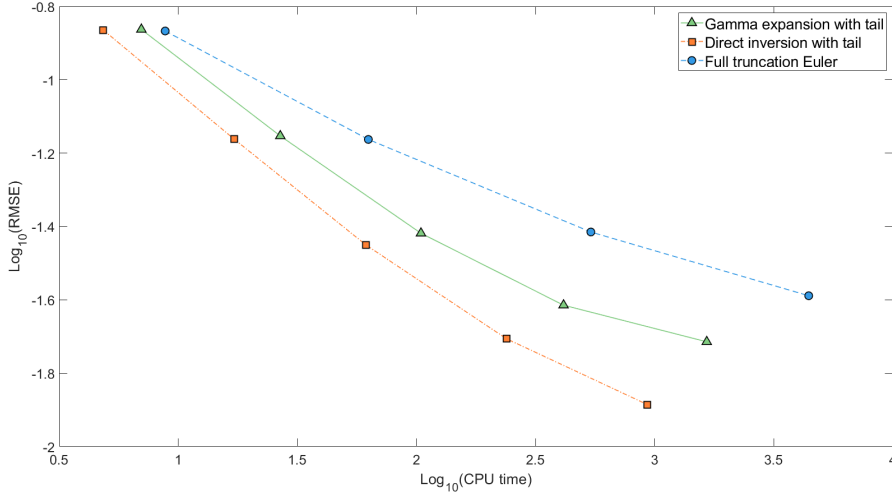


FIG. 11. We show the convergence of the root mean square error in the option price (strike 100) for the Asian option of gamma expansion and direction inversion, both at a truncation level $M = 1$, and full truncation Euler scheme, with number of time steps equal to the square root of the sample size.

We observe that both the gamma expansion and the direct inversion, even with a lower truncation level, deliver similar accuracy compared to the full truncation scheme for small sample sizes. However when the number of simulations increases, bias of the estimated price starts to dominate the root mean square error for all three methods with the standard deviation decreasing according to the expected scaling, i.e. the

TABLE 3
Estimated prices with standard errors and CPU time for the barrier option.

Stepsize		Direct inversion	Gamma expansion
1	Estimated price	0.68944	0.68908
	Standard error	0.00046	0.00046
	CPU time	121.33	179.86
1/2	Estimated price	0.65891	0.65892
	Standard error	0.00047	0.00047
	CPU time	202.52	328.76
1/4	Estimated price	0.63105	0.63182
	Standard error	0.00048	0.00048
	CPU time	353.68	593.03
1/8	Estimated price	0.60544	0.60565
	Standard error	0.00049	0.00049
	CPU time	653.35	1152.22
1/16	Estimated price	0.58364	0.58424
	Standard error	0.00049	0.00049
	CPU time	1224.06	2278.41
1/32	Estimated price	0.56563	0.56556
	Standard error	0.00050	0.00050
	CPU time	2173.38	3952.07
1/64	Estimated price	0.54983	0.54943
	Standard error	0.00050	0.00050
	CPU time	4984.79	9904.97
1/128	Estimated price	0.53743	0.53763
	Standard error	0.00050	0.00050
	CPU time	8020.93	24521.84

inverse of the square root of the sample size. This dominance by the bias eventually decelerates the decrease of the root mean square error. Among the above three methods, the direct inversion produces the smallest bias. In terms of the computing time, very similar conclusions can be drawn as the European option cases. For similar accuracy, the direct inversion is approximately 2 to 7 times faster than the gamma expansion. The time required by the full truncation Euler scheme is by far the largest.

We end this section with a test for pricing a digital double no touch barrier option. The payoff for such an option is either one or zero unit of currency depending on whether the barriers have been crossed. In Table 3, we report the estimated price and standard error together with the CPU time of the direct inversion and the gamma expansion at truncation level $M = 1$ for a double no touch barrier option with barriers 90 and 110. We sample a total of 10^6 paths for each case. We increase the number of time steps per year from 1 to 128 and monitor at each time step if the asset price has hit one of the two barriers.

We see from Table 3 that as we decrease the stepsize, the estimated price of both the direct inversion and the gamma expansion is decreasing monotonically. This is in accordance with our expectation since when more dates are being monitored, there

are more chances for the asset price to cross the barriers. Because of the nature of these two methods, we expect their estimated price will eventually be almost exact with negligible truncation errors when the asset price is monitored on a more frequent basis, for instance, every trading day. The results here are also consistent with those of the four schemes tested in Malham and Wiese [28, Table 5] and the PT, FT and ABR scheme in Lord, Koekkoek and Van Dijk [27, Table 7] in terms of accuracy. Similar conclusions can be reached as the cases for European and Asian options in terms of the computational time. The time required for the gamma expansion is 1.5 to 3 times more than the direct inversion.

5. Conclusion. In this paper, we have designed a new series expansion for the time integrated variance process under the Heston stochastic volatility model. Our expansion is built on a change of measure argument and the decomposition techniques for the integral of squared Bessel bridges by Pitman and Yor [32] and Glasserman and Kim [18]. Acceptance-rejection and direct inversion methods are developed to realise the conditional integral. On combining this result with the method of Broadie and Kaya [12], almost exact simulations of the stock price and variance can be generated on the basis of their exact distributions. We compare our approach with Glasserman and Kim [18] through pricing four practical and challenging options. Apart from that, two path-dependent options including an Asian option and a barrier option are also tested using the above two methods. Further comparisons with a standard time discretization method, i.e. the full truncation Euler scheme, are performed as well. Evidence implies faster computational speed with comparable error in our method.

The series representation and sampling techniques above can also be transferred to the generalised squared Ornstein-Uhlenbeck process x_t with parameters $b \in \mathbb{R}$ and $\delta > 0$ given by

$$dx_t = (\delta + 2bx_t) dt + 2\sqrt{x_t} dW_t,$$

where W_t denotes a standard Brownian motion. Although in this paper we focus only on the case $0 < \delta < 2$, the present result can be applied to other cases $\delta \geq 2$. In essence we need to find an appropriate decomposition for δ and hence establish efficient Chebyshev polynomial approximations required for the resulting direct inversion algorithm. The expansions derived in section 3 will be helpful in determining the coefficients.

Lastly, we recommend a direction for future research. Our method entails an acceptance-rejection algorithm with acceptance probability depending on model parameters. Thus, it is difficult to measure its general computational complexity, i.e. the average number of iterations needed. Besides, in the application of risk management and trading, the acceptance-rejection scheme is less favourable as it will introduce considerable Monte Carlo noise in sensitivity analysis. For these reasons, an alternative should be considered. One realistic way to avoid the use of acceptance-rejection is to sample the Radon-Nikodým derivative directly under the new probability measure instead.

Appendix A. Proof of Lemma 3.1. For the remainder R_1^K , as stated in Theorem 2.1, the $S_{n,k}$ are independent and identically distributed random variables and the P_n are independent Poisson random variables with mean $(a_0 + a_\tau) 2^{n-1}/\tau$. Taking the expectation of R_1^K directly, we have

$$\mathbb{E}[R_1^K] = \sum_{n=K+1}^{\infty} \frac{\tau^2}{4^n} \mathbb{E}[P_n] \mathbb{E}[S_{n,k}]$$

$$\begin{aligned}
&= \sum_{n=K+1}^{\infty} \frac{\tau^2}{4^n} \left(\frac{a_0 + a_\tau}{\tau} 2^{n-1} \right) \left(\frac{2}{\pi^2} \sum_{l=1}^{\infty} \frac{1}{l^2} \right) \\
&= \frac{(a_0 + a_\tau) \tau}{6} \frac{1}{2^K},
\end{aligned}$$

where the last identity holds since $\sum_{l=1}^{\infty} l^{-2} = \pi^2/6$ and $\sum_{n=K+1}^{\infty} 2^{-(n+1)} = 2^{-(K+1)}$. Similarly, we can compute

$$\begin{aligned}
\text{Var} [R_1^K] &= \sum_{n=K+1}^{\infty} \frac{\tau^4}{16^n} \left(\text{Var} [P_n] (\mathbb{E} [S_{n,k}])^2 + \mathbb{E} [P_n] \text{Var} [S_{n,k}] \right) \\
&= \sum_{n=K+1}^{\infty} \frac{\tau^4}{16^n} \left(\frac{a_0 + a_\tau}{\tau} 2^{n-1} \right) \left(\left(\frac{2}{\pi^2} \sum_{l=1}^{\infty} \frac{1}{l^2} \right)^2 + \frac{4}{\pi^4} \sum_{l=1}^{\infty} \frac{1}{l^4} \right) \\
&= \frac{(a_0 + a_\tau) \tau^3}{90} \frac{1}{8^K},
\end{aligned}$$

where we use the formulae $\sum_{l=1}^{\infty} l^{-4} = \pi^4/90$ and $\sum_{n=K+1}^{\infty} 8^{-n} = 8^{-K}/7$.

For the remainder R_2^K , similar to the calculations for the moments of R_1^K , we find

$$\begin{aligned}
\mathbb{E} [R_2^K] &= \sum_{n=K+1}^{\infty} \frac{\tau^2}{4^n} \mathbb{E} [C_n^{\delta/2}] \\
&= \sum_{n=K+1}^{\infty} \frac{\tau^2}{4^n} \left(\frac{2}{\pi^2} \sum_{l=1}^{\infty} \frac{\delta}{2} \frac{1}{(l - \frac{1}{2})^2} \right) \\
&= \frac{\delta \tau^2}{6} \frac{1}{4^K}.
\end{aligned}$$

Note that the last step is a direct result of $\sum_{l=1}^{\infty} (2l-1)^{-2} = \pi^2/8$ and $\sum_{n=K+1}^{\infty} 4^{-n} = 4^{-K}/3$. Further we can proceed with the computation of the variance:

$$\begin{aligned}
\text{Var} [R_2^K] &= \sum_{n=K+1}^{\infty} \frac{\tau^4}{16^n} \text{Var} [C_n^{\delta/2}] \\
&= \sum_{n=K+1}^{\infty} \frac{\tau^4}{16^n} \left(\frac{4}{\pi^4} \sum_{l=1}^{\infty} \frac{\delta}{2} \frac{1}{(l - \frac{1}{2})^4} \right) \\
&= \frac{\delta \tau^4}{45} \frac{1}{16^K},
\end{aligned}$$

in which we apply $\sum_{l=1}^{\infty} (2l-1)^{-4} = \pi^4/96$ and $\sum_{n=K+1}^{\infty} 16^{-n} = 16^{-K}/15$.

Appendix B. Proof of Theorem 3.3. We use the method of steepest descents to find the limiting behaviour as $P \rightarrow +\infty$ of the probability density function f_{Z^P} of the standardised random variable Z^P given by

$$(B.1) \quad f_{Z^P}(x) = \frac{1}{4\pi} \sqrt{\frac{2P}{45}} \int_{-\infty}^{+\infty} \exp(P\rho(z; \beta)) dz,$$

where $\beta = x\sqrt{2/45}/\sqrt{P}$ and

$$\rho(z; \beta) = \log \left(\frac{\sqrt{z}i}{\sinh \sqrt{z}i} \right) + zi \left(\frac{1}{6} + \frac{1}{2}\beta \right).$$

The complex logarithm is chosen to be the principal branch. Note that the support of Z^P is $\left[-\sqrt{5P}/\sqrt{2}, +\infty\right)$ and hence we focus on the case when $\beta \geq -1/3$.

We are interested in the saddle point z_0 such that $\rho'(z_0; \beta) = 0$. Before that, let

$$\varsigma(z) := \frac{\sqrt{zi}}{\sinh \sqrt{zi}},$$

which gives

$$\rho(z; \beta) = \log(\varsigma(z)) + zi \left(\frac{1}{6} + \frac{1}{2}\beta \right).$$

We observe $\varsigma(z)$ and $\rho(z; \beta)$ are analytic when $\text{Im}(z) < \pi^2$ after defining $\varsigma(0) := 1$ and $\rho(0; \beta) := 0$.

Bleistein and Handelsman [10, Chapter 7.6] suggest that we should seek a saddle point near $z = 0$, which will be the dominant one. To obtain an explicit form for the saddle point, we take advantage of the series expansions of $\rho(z; \beta)$ and its differentiation $\rho'(z; \beta)$. Let us first consider the series expansion of $\rho(z; \beta)$ about $z = 0$, which is of the form

$$(B.2) \quad \rho(z; \beta) = \frac{1}{2}\beta iz + \sum_{k=2}^{\infty} \hat{r}_k z^k,$$

where

$$(B.3) \quad \hat{r}_2 = -\frac{1}{180}, \quad \hat{r}_3 = \frac{i}{2835}$$

and so forth. Although we can compute the coefficients \hat{r}_k analytically through Taylor expansion of $\rho(z; \beta)$ up to any order, we compute them using Maple in practice. Hence, its differentiation can be expressed as

$$\rho'(z; \beta) = \frac{1}{2}\beta i + \sum_{k=2}^{\infty} k \hat{r}_k z^{k-1}.$$

The above two series converge pointwise in the domain where $|z| < \pi^2$. It seems that a precise form for the saddle point z_0 such that $\rho'(z_0; \beta) = 0$ is not obtainable. However, we can get a good approximation by making use of the smallness of β . For $\beta \ll 1$, i.e. $|x| \ll \sqrt{P}/\sqrt{2/45}$, we solve the above equation by iteration. In fact, after two iterations, we have the following expression for the desired saddle point

$$z_0 = 45i\beta - \frac{1350}{7}i\beta^2 + O(\beta^3).$$

We show in [Appendix F](#) that the saddle point exists and is unique in the domain of analyticity of $\rho(z; \beta)$, i.e. $\{z \in \mathbb{C} : \text{Im}(z) < \pi^2\}$ for any $\beta > -1/3$, i.e. $x > -\sqrt{5P/2}$. Further since $\rho'(z; \beta)$ is analytic in this region, we can show the solution $z_0 = z_0(\beta)$ is also analytic around $\beta = 0$ by the analytic implicit function theorem and thus $z_0 = z_0(\beta)$ has a Taylor series expansion about $\beta = 0$ valid for sufficiently small $|\beta|$. Hence we can write

$$(B.4) \quad z_0 = \beta \sum_{k=0}^{\infty} \hat{\xi}_k \beta^k$$

for sufficiently small $|\beta|$, where

$$(B.5) \quad \hat{\xi}_0 = 45i, \quad \hat{\xi}_1 = -\frac{1350i}{7}$$

and so on. Again, all these coefficients $\hat{\xi}_k$ are calculated via Maple in practice. Notice that the saddle point z_0 is near the origin and along the imaginary axis.

Now, we can expand $\rho(z; \beta)$ as a Taylor series near the saddle point z_0

$$(B.6) \quad \rho(z; \beta) = \rho(z_0; \beta) + \frac{1}{2!} \rho''(z_0; \beta) (z - z_0)^2 + (z - z_0)^3 \sum_{k \geq 0} \frac{\rho^{(k+3)}(z_0; \beta)}{(k+3)!} (z - z_0)^k,$$

which converges in a neighbourhood of z_0 . For preparations, we must evaluate $\rho^{(k)}(z; \beta)$ for $k \geq 2$ at $z = z_0$. Differentiating the series expansion for ρ in equation (B.2) leads to

$$\rho^{(n)}(z; \beta) = \sum_{k=n}^{\infty} k(k-1) \cdots (k-n+1) \hat{r}_k z^{k-n} = \sum_{k=n}^{\infty} \hat{\varphi}_{k,n} z^{k-n}$$

for $n \geq 2$, where

$$(B.7) \quad \hat{\varphi}_{k,n} := k(k-1) \cdots (k-n+1) \hat{r}_k$$

for $k \geq n$. This series converges in the same domain as the expansion for ρ ; see equation (B.2). To substitute the Taylor series (B.4) regarding the saddle point z_0 into the above equation, we require z_0 to be within its radius of convergence, i.e. $|z_0| < \pi^2$. Hence we restrict β such that $\beta > -1/3 - (1 - \pi \coth \pi) / \pi^2$ (see Remark F.3). By noting that

$$(B.8) \quad z_0^j = \beta^j \sum_{l=0}^{\infty} \hat{v}_{l,j} \beta^l$$

for $j \geq 0$, where

$$(B.9) \quad \begin{aligned} \hat{v}_{0,j} &= \hat{\xi}_0^j, \\ \hat{v}_{l,j} &= \frac{1}{l \hat{\xi}_0} \sum_{k=1}^l (kj - l + k) \hat{\xi}_k \hat{v}_{l-k,j}, \quad \text{for } l \geq 1, \end{aligned}$$

we get that for $n \geq 2$,

$$(B.10) \quad \rho^{(n)}(z_0; \beta) = \sum_{l=0}^{\infty} \hat{\phi}_{l,n} \beta^l$$

for $\beta > -1/3 - (1 - \pi \coth \pi) / \pi^2$ and $|\beta|$ sufficiently small, where

$$(B.11) \quad \hat{\phi}_{l,n} = \sum_{k=0}^l \hat{\varphi}_{n+l-k,n} \hat{v}_{k,l-k}$$

for $l \geq 0$.

With the completion of the foregoing, we are now ready to determine the paths of steepest descent through z_0 given by

$$\operatorname{Im}(\rho(z; \beta)) - \operatorname{Im}(\rho(z_0; \beta)) = 0 \iff \operatorname{Im}(\rho(z; \beta) - \rho(z_0; \beta)) = 0.$$

The condition determining the paths of steepest descent just above, with an error $O((z - z_0)^3)$, is given by

$$(B.12) \quad \operatorname{Im}\left(\frac{1}{2!}\rho''(z_0; \beta)(z - z_0)^2\right) = 0.$$

Direct computation reveals that

$$\rho''(z_0; \beta) < 0.$$

If we set $z := u + iv$ for $u, v \in \mathbb{R}$, then (B.12) implies that the paths of steepest descent and ascent from z_0 lie along the curves

$$2u(v - \operatorname{Im}(z_0)) = 0$$

as z_0 is purely imaginary. These paths, close enough to the saddle point z_0 , that is when $|z - z_0|$ is small, consist of the straight lines $u = 0$ and $v = \operatorname{Im}(z_0)$. To distinguish between the ascent and descent paths, we consider $\operatorname{Re}(\rho(z; \beta))$ along the two lines near $z = z_0$. Along $u = 0$, we have

$$\operatorname{Re}(\rho(z; \beta)) = \operatorname{Re}(\rho(z_0; \beta)) - \frac{1}{2!}\rho''(z_0; \beta)(v - \operatorname{Im}(z_0))^2 + O(|z - z_0|^3) \geq \operatorname{Re}(\rho(z_0; \beta))$$

when z is near z_0 . Along $v = \operatorname{Im}(z_0)$, we have

$$\operatorname{Re}(\rho(z; \beta)) = \operatorname{Re}(\rho(z_0; \beta)) + \frac{1}{2!}\rho''(z_0; \beta)u^2 + O(|z - z_0|^3) \leq \operatorname{Re}(\rho(z_0; \beta))$$

for z close enough to z_0 . Thus, the path of steepest descents from z_0 is $v = \operatorname{Im}(z_0)$, parallel to the real axis.

As z_0 is in the domain of analyticity of $\rho(z; \beta)$, we can deform the original contour of the integration (B.1) onto the steepest descent paths through the saddle point z_0 , denoted by \mathcal{C}_l for $u < 0$ and \mathcal{C}_r for $u > 0$, both pointing a direction away from z_0 . It follows from Cauchy's theorem that

$$f_{Z^P}(x) = \frac{1}{4\pi} \sqrt{\frac{2P}{45}} \int_{-\infty}^{+\infty} \exp(P\rho(z; \beta)) dz = \frac{1}{4\pi} \sqrt{\frac{2P}{45}} \int_{\mathcal{C}_r - \mathcal{C}_l} \exp(P\rho(z; \beta)) dz,$$

whence the main contributions to the asymptotic expansion of the integral now comes from a small neighbourhood of z_0 for large P . We use Laplace's method to evaluate this integral. For some $\epsilon > 0$, we have the following asymptotic relation:

$$(B.13) \quad f_{Z^P}(x) \sim \frac{1}{4\pi} \sqrt{\frac{2P}{45}} \int_{\operatorname{Im}(z_0) - \epsilon}^{\operatorname{Im}(z_0) + \epsilon} \exp(P\rho(z; \beta)) dz, \quad \text{as } P \rightarrow +\infty,$$

where by replacing the contour of integration $\mathcal{C}_r - \mathcal{C}_l$ with a narrow interval centred around z_0 , only exponentially small errors are introduced for large P . Now, ϵ can be chosen so small that we can replace $\rho(z; \beta)$ by its Taylor expansion (B.6), which

converges on the interval $(\operatorname{Im}(z_0)\mathbf{i} - \epsilon, \operatorname{Im}(z_0)\mathbf{i} + \epsilon)$. Then, separating the quadratic term from all the higher-order terms of the series expansion (B.6) in $\exp(P\rho(z; \beta))$ and setting

$$(B.14) \quad g(z; \beta) := \exp \left(P(z - z_0)^3 \sum_{k \geq 0} \frac{\rho^{(k+3)}(z_0; \beta)}{(k+3)!} (z - z_0)^k \right),$$

the integral (B.13) becomes

$$(B.15) \quad f_{Z^P}(x) \sim \frac{1}{4\pi} \sqrt{\frac{2P}{45}} \exp(P\rho(z_0; \beta)) \int_{\operatorname{Im}(z_0)\mathbf{i} - \epsilon}^{\operatorname{Im}(z_0)\mathbf{i} + \epsilon} \exp \left(P \frac{1}{2!} \rho''(z_0; \beta) (z - z_0)^2 \right) g(z; \beta) dz,$$

as $P \rightarrow +\infty$.

To find $\rho(z_0; \beta)$, we use (B.2), (B.4) and (B.8) to write

$$\rho(z_0; \beta) = \frac{1}{2} \beta \mathbf{i} z_0 + \sum_{k=2}^{\infty} \hat{r}_k z_0^k = \sum_{k=2}^{\infty} \hat{\rho}_k \beta^k,$$

where for $k \geq 2$,

$$(B.16) \quad \hat{\rho}_k := \frac{\mathbf{i} \hat{\xi}_{k-2}}{2} + \sum_{m=2}^k \hat{r}_m \hat{v}_{k-m, m}.$$

Since the series in the argument of the exponential function which defines $g(z; \beta)$ in (B.14) is convergent near z_0 , we can write as $z \rightarrow z_0$,

$$(B.17) \quad \begin{aligned} g(z; \beta) &= \exp \left(P(z - z_0)^3 \sum_{k \geq 0} \hat{\sigma}_k(\beta) (z - z_0)^k \right) \\ &= \sum_{n=0}^{\infty} \frac{1}{n!} P^n (z - z_0)^{3n} \left(\sum_{k \geq 0} \hat{\sigma}_k(\beta) (z - z_0)^k \right)^n, \end{aligned}$$

where $\hat{\sigma}_k(\beta) := \rho^{(k+3)}(z_0; \beta)/(k+3)!$ for $k \geq 0$. Further, the Taylor series expansion (B.10) for $\rho^{(k+3)}(z_0; \beta)$ gives us $\hat{\sigma}_k(\beta) = \sum_{l=0}^{\infty} \hat{\gamma}_{l, k} \beta^l$ with

$$(B.18) \quad \hat{\gamma}_{l, k} := \frac{\hat{\phi}_{l, k+3}}{(k+3)!}$$

for $l, k \geq 0$ when $\beta > -1/3 - (1 - \pi \coth \pi)/\pi^2$ and $|\beta|$ is sufficiently small. As an immediate consequence of the properties for Taylor series expansions, we have for $n \geq 2$,

$$\left(\sum_{k \geq 0} \hat{\sigma}_k(\beta) (z - z_0)^k \right)^n = \sum_{k_1=0}^{\infty} \sum_{k_2=0}^{k_1} \cdots \sum_{k_n=0}^{k_{n-1}} \hat{\sigma}_{k_n}(\beta) \hat{\sigma}_{k_{n-1}-k_n}(\beta) \cdots \hat{\sigma}_{k_1-k_2}(\beta) (z - z_0)^{k_1},$$

as $z \rightarrow z_0$. In addition, we observe for $n \geq 2$ and $0 \leq k_n \leq k_{n-1} \leq \cdots \leq k_1$,

$$\hat{\sigma}_{k_n}(\beta) \hat{\sigma}_{k_{n-1}-k_n}(\beta) \cdots \hat{\sigma}_{k_1-k_2}(\beta)$$

$$\begin{aligned}
&= \left(\sum_{l_1=0}^{\infty} \hat{\gamma}_{l_1, k_n} \beta^{l_1} \right) \left(\sum_{l_2=0}^{\infty} \hat{\gamma}_{l_2, k_{n-1}-k_n} \beta^{l_2} \right) \cdots \left(\sum_{l_n=0}^{\infty} \hat{\gamma}_{l_n, k_1-k_2} \beta^{l_n} \right) \\
&= \sum_{l_1=0}^{\infty} \sum_{l_2=0}^{l_1} \cdots \sum_{l_n=0}^{l_{n-1}} \hat{\gamma}_{l_n, k_n} \hat{\gamma}_{l_{n-1}-l_n, k_{n-1}-k_n} \cdots \hat{\gamma}_{l_1-l_2, k_1-k_2} \beta^{l_1} \\
&= \sum_{l_1=0}^{\infty} \hat{\mathcal{C}}_{l_1, k_1, k_2, \dots, k_n} \beta^{l_1}
\end{aligned}$$

for $\beta > -1/3 - (1 - \pi \coth \pi) / \pi^2$ and $|\beta|$ sufficiently small, where

$$(B.19) \quad \hat{\mathcal{C}}_{l_1, k_1, k_2, \dots, k_n} := \sum_{l_2=0}^{l_1} \cdots \sum_{l_n=0}^{l_{n-1}} \hat{\gamma}_{l_n, k_n} \hat{\gamma}_{l_{n-1}-l_n, k_{n-1}-k_n} \cdots \hat{\gamma}_{l_1-l_2, k_1-k_2}$$

for $l_1 \geq 0$. Generally, for $n \geq 0$ we see that

$$\left(\sum_{k \geq 0} \hat{\sigma}_k(\beta) (z - z_0)^k \right)^n = \sum_{k=0}^{\infty} \hat{\theta}_{k,n}(\beta) (z - z_0)^k, \quad \text{as } z \rightarrow z_0.$$

Here $\hat{\theta}_{k,n}(\beta)$ are functions of β satisfying $\hat{\theta}_{k,n}(\beta) = \sum_{l=0}^{\infty} \hat{\mathcal{E}}_{l,k,n} \beta^l$ for $k \geq 0$ with the constants $\hat{\mathcal{E}}_{l,k,n}$ as stated below: for $n = 0$,

$$(B.20) \quad \hat{\mathcal{E}}_{l,k,n} = \hat{\mathcal{E}}_{l,k,0} = \begin{cases} 1, & \text{for } k = l = 0, \\ 0, & \text{otherwise,} \end{cases}$$

for $n = 1$,

$$(B.21) \quad \hat{\mathcal{E}}_{l,k,n} = \hat{\mathcal{E}}_{l,k,1} = \hat{\gamma}_{l,k}, \quad \text{for } k, l \geq 0,$$

for $n = 2$,

$$(B.22) \quad \hat{\mathcal{E}}_{l,k,n} = \hat{\mathcal{E}}_{l,k,2} = \sum_{k_2=0}^k \hat{\mathcal{C}}_{l,k,k_2}, \quad \text{for } k, l \geq 0,$$

for $n \geq 3$,

$$(B.23) \quad \hat{\mathcal{E}}_{l,k,n} = \sum_{k_2=0}^k \sum_{k_3=0}^{k_2} \cdots \sum_{k_n=0}^{k_{n-1}} \hat{\mathcal{C}}_{l,k,k_2, \dots, k_n}, \quad \text{for } k, l \geq 0.$$

Using these factors, we can rewrite $g(z; \beta)$ in (B.17) as

$$\begin{aligned}
g(z; \beta) &= \sum_{n=0}^{\infty} \frac{1}{n!} P^n (z - z_0)^{3n} \left(\sum_{k=0}^{\infty} \hat{\theta}_{k,n}(\beta) (z - z_0)^k \right) \\
&= \sum_{n=0}^{\infty} \sum_{k=0}^{\infty} \frac{1}{n!} P^n \hat{\theta}_{k,n}(\beta) (z - z_0)^{3n+k} \\
&= \sum_{j=0}^{\infty} \sum_{3n+k=j} \frac{1}{n!} P^n \hat{\theta}_{k,n}(\beta) (z - z_0)^j
\end{aligned}$$

$$\begin{aligned}
&= \sum_{j=0}^{\infty} \sum_{n=0}^{\lfloor \frac{j}{3} \rfloor} \frac{1}{n!} P^n \hat{\theta}_{j-3n,n}(\beta) (z - z_0)^j \\
&= \sum_{j=0}^{\infty} \hat{g}_j(\beta) (z - z_0)^j
\end{aligned}$$

in the limit $z \rightarrow z_0$, where $\hat{g}_j(\beta) := \sum_{n=0}^{\lfloor j/3 \rfloor} P^n \hat{\theta}_{j-3n,n}(\beta) / n!$ for $j \geq 0$. Hence, we have

$$g(z; \beta) - \sum_{j=0}^J \hat{g}_j(\beta) (z - z_0)^j = o\left((z - z_0)^J\right), \quad \text{as } z \rightarrow z_0$$

for any $J \geq 0$. From this it follows that for any $\epsilon^* > 0$ there is an interval $|z - z_0| < L$ for some $L > 0$, in which

$$\left| g(z; \beta) - \sum_{j=0}^J \hat{g}_j(\beta) (z - z_0)^j \right| \leq \epsilon^* |(z - z_0)^J|.$$

Therefore for any $0 < \epsilon < L$, we have

$$\begin{aligned}
&\left| \int_{\text{Im}(z_0) - \epsilon}^{\text{Im}(z_0)} \exp\left(P \frac{1}{2} \rho''(z_0; \beta) (z - z_0)^2\right) \left(g(z; \beta) - \sum_{j=0}^J \hat{g}_j(\beta) (z - z_0)^j\right) dz \right| \\
&\leq \int_{\text{Im}(z_0) - \epsilon}^{\text{Im}(z_0)} \exp\left(P \frac{1}{2} \rho''(z_0; \beta) (z - z_0)^2\right) \left| g(z; \beta) - \sum_{j=0}^J \hat{g}_j(\beta) (z - z_0)^j \right| dz \\
&\leq \epsilon^* \int_{\text{Im}(z_0) - \epsilon}^{\text{Im}(z_0)} \exp\left(P \frac{1}{2} \rho''(z_0; \beta) (z - z_0)^2\right) |(z - z_0)^J| dz \\
&= \epsilon^* (-1)^J \int_{\text{Im}(z_0) - \epsilon}^{\text{Im}(z_0)} \exp\left(P \frac{1}{2} \rho''(z_0; \beta) (z - z_0)^2\right) (z - z_0)^J dz.
\end{aligned}$$

Then as $\epsilon \rightarrow 0^+$, we can write

$$\begin{aligned}
&\int_{\text{Im}(z_0) - \epsilon}^{\text{Im}(z_0)} \exp\left(P \frac{1}{2} \rho''(z_0; \beta) (z - z_0)^2\right) g(z; \beta) dz \\
&= \sum_{j=0}^J \hat{g}_j(\beta) \int_{\text{Im}(z_0) - \epsilon}^{\text{Im}(z_0)} \exp\left(P \frac{1}{2} \rho''(z_0; \beta) (z - z_0)^2\right) (z - z_0)^j dz \\
&\quad + o\left(\int_{\text{Im}(z_0) - \epsilon}^{\text{Im}(z_0)} \exp\left(P \frac{1}{2} \rho''(z_0; \beta) (z - z_0)^2\right) (z - z_0)^J dz\right),
\end{aligned}$$

which gives

$$\begin{aligned}
&\int_{\text{Im}(z_0) - \epsilon}^{\text{Im}(z_0)} \exp\left(P \frac{1}{2} \rho''(z_0; \beta) (z - z_0)^2\right) g(z; \beta) dz \\
&\sim \sum_{j=0}^{\infty} \hat{g}_j(\beta) \int_{\text{Im}(z_0) - \epsilon}^{\text{Im}(z_0)} \exp\left(P \frac{1}{2} \rho''(z_0; \beta) (z - z_0)^2\right) (z - z_0)^j dz
\end{aligned}$$

for small ϵ . Now the above integrals can be evaluated by change of variables. For arbitrary $j \geq 0$, the substitution $z = \text{Im}(z_0) i + x$ yields

$$\begin{aligned} & \int_{\text{Im}(z_0)i-\epsilon}^{\text{Im}(z_0)i} \exp\left(P \frac{1}{2} \rho''(z_0; \beta) (z - z_0)^2\right) (z - z_0)^j dz \\ &= \int_{-\epsilon}^0 \exp\left(P \frac{1}{2} \rho''(z_0; \beta) x^2\right) x^j dx \\ &= \frac{1}{2} (-1)^j \left(\frac{-2}{\rho''(z_0; \beta)}\right)^{\frac{1}{2}(j+1)} \cdot \int_0^{-\frac{1}{2} \rho''(z_0; \beta) \epsilon^2} \zeta^{\frac{1}{2}(j-1)} \exp(-P\zeta) d\zeta, \end{aligned}$$

where the last step is a result of the change of variable $\rho''(z_0; \beta) x^2/2 = -\zeta$. Thus as $\epsilon \rightarrow 0^+$, we have

$$\begin{aligned} & \int_{\text{Im}(z_0)i-\epsilon}^{\text{Im}(z_0)i} \exp\left(P \frac{1}{2} \rho''(z_0; \beta) (z - z_0)^2\right) g(z; \beta) dz \\ & \sim \sum_{j=0}^{\infty} \hat{g}_j(\beta) \frac{1}{2} (-1)^j \left(\frac{-2}{\rho''(z_0; \beta)}\right)^{\frac{1}{2}(j+1)} \int_0^{-\frac{1}{2} \rho''(z_0; \beta) \epsilon^2} \zeta^{\frac{1}{2}(j-1)} \exp(-P\zeta) d\zeta. \end{aligned}$$

Similar arguments give us that

$$\begin{aligned} & \int_{\text{Im}(z_0)i}^{\text{Im}(z_0)i+\epsilon} \exp\left(P \frac{1}{2} \rho''(z_0; \beta) (z - z_0)^2\right) g(z; \beta) dz \\ & \sim \sum_{j=0}^{\infty} \hat{g}_j(\beta) \frac{1}{2} \left(\frac{-2}{\rho''(z_0; \beta)}\right)^{\frac{1}{2}(j+1)} \int_0^{-\frac{1}{2} \rho''(z_0; \beta) \epsilon^2} \zeta^{\frac{1}{2}(j-1)} \exp(-P\zeta) d\zeta, \end{aligned}$$

as $\epsilon \rightarrow 0^+$.

Hence, the integration in (B.15) can be expanded in an asymptotic series for small ϵ as follows:

$$\begin{aligned} & \int_{\text{Im}(z_0)i-\epsilon}^{\text{Im}(z_0)i+\epsilon} \exp\left(P \frac{1}{2!} \rho''(z_0; \beta) (z - z_0)^2\right) g(z; \beta) dz \\ & \sim \sum_{j=0}^{\infty} \frac{1}{2} \left(1 + (-1)^j\right) \hat{g}_j(\beta) \left(\frac{-2}{\rho''(z_0; \beta)}\right)^{\frac{1}{2}(j+1)} \int_0^{-\frac{1}{2} \rho''(z_0; \beta) \epsilon^2} \zeta^{\frac{1}{2}(j-1)} \exp(-P\zeta) d\zeta, \end{aligned}$$

where terms with odd j vanish. For large P , we can extend the integration region in each integral to infinity. With this replacement, we introduce only exponentially small errors for large P , whence we have as $P \rightarrow +\infty$,

$$\begin{aligned} \int_0^{-\frac{1}{2} \rho''(z_0; \beta) \epsilon^2} \zeta^{\frac{1}{2}(j-1)} \exp(-P\zeta) d\zeta & \sim \int_0^{+\infty} \zeta^{\frac{1}{2}(j-1)} \exp(-P\zeta) d\zeta \\ & = P^{-\frac{1}{2}(j+1)} \Gamma\left(\frac{j}{2} + \frac{1}{2}\right) \end{aligned}$$

for $j \geq 0$. Assembling the above results, we have the following asymptotic series

(B.24)

$$f_{Z^P}(x) \sim \frac{1}{4\pi} \sqrt{\frac{2P}{45}} \exp\left(P \sum_{l=2}^{\infty} \hat{\rho}_l \beta^l\right) \sum_{j=0}^{\infty} \hat{g}_{2j}(\beta) \left(\frac{-2}{\rho''(z_0; \beta)}\right)^{j+\frac{1}{2}} P^{-(j+\frac{1}{2})} \Gamma\left(j + \frac{1}{2}\right)$$

in the limit $P \rightarrow +\infty$ for fixed x with $x > -\sqrt{5P/2}(1 + 3/\pi^2 - 3 \coth \pi/\pi)$ and $|x|$ sufficiently small.

Lastly, we wish to express the terms involving β , i.e. $\hat{g}_{2j}(\beta)(-2/\rho''(z_0; \beta))^{j+1/2}$ as a Taylor series expansion in β . This can be achieved by collecting the coefficients from the product of their individual series. Assume that

$$(B.25) \quad \sqrt{\frac{-2}{\rho''(z_0; \beta)}} = \sum_{n=0}^{\infty} \hat{K}_n \beta^n$$

for $|\beta|$ sufficiently small and some constants \hat{K}_n for $n \geq 0$. Then taking the square on both sides yields

$$\frac{-2}{\rho''(z_0; \beta)} = \sum_{l=0}^{\infty} \sum_{k=0}^l \hat{K}_k \hat{K}_{l-k} \beta^l = \sum_{l=0}^{\infty} \hat{\mu}_l \beta^l,$$

where $\hat{\mu}_l := \sum_{k=0}^l \hat{K}_k \hat{K}_{l-k}$ for $l \geq 0$. On the other hand, by performing simple arithmetical operations on the Taylor series (B.10) with $n = 2$ for $\rho''(z_0; \beta)$, we see

$$\frac{-2}{\rho''(z_0; \beta)} = \sum_{l=0}^{\infty} \hat{\omega}_l \beta^l$$

for $\beta > -1/3 - (1 - \pi \coth \pi)/\pi^2$ and $|\beta|$ sufficiently small, where

$$(B.26) \quad \begin{aligned} \hat{\omega}_0 &= -\frac{2}{\hat{\phi}_{0,2}}, \\ \hat{\omega}_l &= -\frac{1}{\hat{\phi}_{0,2}} \sum_{m=0}^{l-1} \hat{\omega}_m \hat{\phi}_{l-m,2}, \quad \text{for } l \geq 1. \end{aligned}$$

Hence, by equating the coefficients, we find

$$(B.27) \quad \hat{\omega}_l = \hat{\mu}_l = \sum_{k=0}^l \hat{K}_k \hat{K}_{l-k}, \quad \text{for } l \geq 0,$$

providing the values for the constants \hat{K}_k with $k \geq 0$.

Based on the previous analysis, we are now ready to derive the Taylor series expansion of $(-2/\rho''(z_0; \beta))^{j+1/2}$ for $\beta > -1/3 - (1 - \pi \coth \pi)/\pi^2$ and $|\beta|$ sufficiently small. Indeed, from (B.25) we have for $j \geq 0$,

$$\left(\frac{-2}{\rho''(z_0; \beta)}\right)^{j+\frac{1}{2}} = \left(\sum_{n=0}^{\infty} \hat{K}_n \beta^n\right)^{2j+1} = \sum_{n=0}^{\infty} \hat{\omega}_{n,j} \beta^n,$$

where for $j = 0$,

$$(B.28) \quad \hat{\omega}_{n,j} = \hat{\omega}_{n,0} = \hat{K}_n, \quad \text{for } n \geq 0,$$

for $j \geq 1$,

$$(B.29) \quad \hat{\omega}_{n,j} = \sum_{n_2=0}^n \sum_{n_3=0}^{n_2} \cdots \sum_{n_{2j+1}=0}^{n_{2j}} \hat{K}_{n_{2j+1}} \hat{K}_{n_{2j}-n_{2j+1}} \cdots \hat{K}_{n_2-n_3} \hat{K}_{n-n_2}, \quad \text{for } n \geq 0.$$

If we combine the series for $\hat{g}_{2j}(\beta)$ with the explicit series expansion given above, we obtain for $j \geq 0$,

$$\begin{aligned}
\hat{g}_{2j}(\beta) \left(\frac{-2}{\rho''(z_0; \beta)} \right)^{j+\frac{1}{2}} &= \left(\sum_{n=0}^{\lfloor \frac{2}{3}j \rfloor} \frac{1}{n!} P^n \sum_{l=0}^{\infty} \hat{\mathcal{E}}_{l,2j-3n,n} \beta^l \right) \left(\sum_{n=0}^{\infty} \hat{\omega}_{n,j} \beta^n \right) \\
&= \left(\sum_{l=0}^{\infty} \left(\sum_{n=0}^{\lfloor \frac{2}{3}j \rfloor} \frac{1}{n!} P^n \hat{\mathcal{E}}_{l,2j-3n,n} \right) \beta^l \right) \left(\sum_{k=0}^{\infty} \hat{\omega}_{k,j} \beta^k \right) \\
&= \sum_{l=0}^{\infty} \left(\sum_{k=0}^l \left(\sum_{n=0}^{\lfloor \frac{2}{3}j \rfloor} \frac{1}{n!} P^n \hat{\mathcal{E}}_{k,2j-3n,n} \right) \hat{\omega}_{l-k,j} \right) \beta^l \\
&= \sum_{l=0}^{\infty} \sum_{n=0}^{\lfloor \frac{2}{3}j \rfloor} \sum_{k=0}^l \frac{1}{n!} \hat{\omega}_{l-k,j} \hat{\mathcal{E}}_{k,2j-3n,n} P^n \beta^l \\
&= \sum_{l=0}^{\infty} \sum_{n=0}^{\lfloor \frac{2}{3}j \rfloor} \hat{\alpha}_{n,l,j} P^n \beta^l,
\end{aligned}$$

where

$$(B.30) \quad \hat{\alpha}_{n,l,j} := \frac{1}{n!} \sum_{k=0}^l \hat{\omega}_{l-k,j} \hat{\mathcal{E}}_{k,2j-3n,n}$$

for $0 \leq n \leq \lfloor 2j/3 \rfloor$ and $l \geq 0$. Then (B.24) becomes

$$(B.31) \quad f_{Z^P}(x) \sim \frac{1}{4\pi} \sqrt{\frac{2P}{45}} \exp \left(P \sum_{l=2}^{\infty} \hat{\rho}_l \beta^l \right) \sum_{j=0}^{\infty} \sum_{l=0}^{\infty} \sum_{n=0}^{\lfloor \frac{2}{3}j \rfloor} \hat{\alpha}_{n,l,j} P^n \beta^l P^{-(j+\frac{1}{2})} \Gamma \left(j + \frac{1}{2} \right),$$

as $P \rightarrow +\infty$ for $\beta > -1/3 - (1 - \pi \coth \pi)/\pi^2$ and $|\beta|$ sufficiently small, which completes the proof.

Appendix C. Proof of Theorem 3.5. Before integrating the density function, we first rewrite its asymptotic expansion in Theorem 3.3 in terms of the original variable x by using the identity $\beta = x\sqrt{2/45}/\sqrt{P}$. Accordingly in the limit $P \rightarrow +\infty$ with $x > -\sqrt{5P/2}(1 + 3/\pi^2 - 3 \coth \pi/\pi)$ and $|x|$ sufficiently small, the probability density function has the following asymptotic expansion

$$\begin{aligned}
(C.1) \quad f_{Z^P}(x) &\sim \frac{1}{4\pi} \sqrt{\frac{2}{45}} \exp \left(\sum_{l=2}^{\infty} \hat{\rho}_l \left(\frac{2}{45} \right)^{\frac{l}{2}} P^{1-\frac{l}{2}} x^l \right) \\
&\cdot \sum_{j=0}^{\infty} \sum_{l=0}^{\infty} \sum_{n=0}^{\lfloor \frac{2}{3}j \rfloor} \hat{\alpha}_{n,l,j} \left(\frac{2}{45} \right)^{\frac{l}{2}} \Gamma \left(j + \frac{1}{2} \right) P^{n-\frac{l}{2}-j} x^l.
\end{aligned}$$

To justify that the integrated series is indeed asymptotic to the distribution function, we adjust the terms in (C.1) to form a more appropriate expression for easier computation.

Specifically, we separate the quadratic term $\hat{\rho}_2 (2/45) x^2$ from the argument $\sum_{l=2}^{\infty} \hat{\rho}_l (2/45)^{l/2} P^{1-l/2} x^l$ of the exponential function. As the integration is taken with respect to x , we expand the remaining term in an asymptotic approximation in P with all the coefficients given as polynomials of x . Note that $\hat{\rho}_2 = i\xi_0/2 + \hat{r}_2(\hat{\xi}_0)^2 = -45/4$, which gives

$$(C.2) \quad \exp \left(\sum_{l=2}^{\infty} \hat{\rho}_l \left(\frac{2}{45} \right)^{\frac{l}{2}} P^{1-\frac{l}{2}} x^l \right) = \exp \left(-\frac{1}{2} x^2 \right) \exp \left(\sum_{l=3}^{\infty} \hat{\rho}_l \left(\frac{2}{45} \right)^{\frac{l}{2}} P^{1-\frac{l}{2}} x^l \right).$$

Now note, as $P \rightarrow +\infty$, we have

$$(C.3) \quad \begin{aligned} \exp \left(\sum_{l=3}^{\infty} \hat{\rho}_l \left(\frac{2}{45} \right)^{\frac{l}{2}} P^{1-\frac{l}{2}} x^l \right) &\sim \sum_{n=0}^{\infty} \frac{1}{n!} \left(\sum_{l=3}^{\infty} \hat{\rho}_l \left(\frac{2}{45} \right)^{\frac{l}{2}} P^{1-\frac{l}{2}} x^l \right)^n \\ &\sim \sum_{n=0}^{\infty} \frac{1}{n!} \left(\frac{2}{45} \right)^{\frac{3n}{2}} P^{-\frac{n}{2}} x^{3n} \left(\sum_{k=0}^{\infty} \hat{\rho}_{k+3} \left(\frac{2}{45} \right)^{\frac{k}{2}} P^{-\frac{k}{2}} x^k \right)^n. \end{aligned}$$

Analogous to the previous computations, the generalisation of multiplication of asymptotic expansions tells us for $n \geq 0$,

$$(C.4) \quad \left(\sum_{k=0}^{\infty} \hat{\rho}_{k+3} \left(\frac{2}{45} \right)^{\frac{k}{2}} P^{-\frac{k}{2}} x^k \right)^n \sim \sum_{k=0}^{\infty} \hat{\vartheta}_{k,n} \left(\frac{2}{45} \right)^{\frac{k}{2}} P^{-\frac{k}{2}} x^k,$$

where

$$(C.5) \quad \begin{aligned} \hat{\vartheta}_{0,n} &= (\hat{\rho}_3)^n, \\ \hat{\vartheta}_{k,n} &= \frac{1}{k \hat{\rho}_3} \sum_{m=1}^k (mn - k + m) \hat{\rho}_{k+3} \hat{\vartheta}_{k-m,n}, \quad \text{for } k \geq 1. \end{aligned}$$

Using (C.2)–(C.4) amounts to

$$\begin{aligned} \exp \left(\sum_{l=2}^{\infty} \hat{\rho}_l \left(\frac{2}{45} \right)^{\frac{l}{2}} P^{1-\frac{l}{2}} x^l \right) &\sim \exp \left(-\frac{1}{2} x^2 \right) \sum_{n=0}^{\infty} \frac{1}{n!} \left(\frac{2}{45} \right)^{\frac{3n}{2}} P^{-\frac{n}{2}} x^{3n} \\ &\quad \cdot \sum_{k=0}^{\infty} \hat{\vartheta}_{k,n} \left(\frac{2}{45} \right)^{\frac{k}{2}} P^{-\frac{k}{2}} x^k \\ &\sim \exp \left(-\frac{1}{2} x^2 \right) \sum_{n=0}^{\infty} \sum_{k=0}^{\infty} \frac{1}{n!} \left(\frac{2}{45} \right)^{\frac{3n+k}{2}} \hat{\vartheta}_{k,n} P^{-\frac{n+k}{2}} x^{3n+k} \\ &\sim \exp \left(-\frac{1}{2} x^2 \right) \sum_{j=0}^{\infty} \left(\sum_{n=0}^j \frac{1}{n!} \left(\frac{2}{45} \right)^{\frac{2n+j}{2}} \hat{\vartheta}_{j-n,n} x^{2n+j} \right) P^{-\frac{j}{2}} \\ &\sim \exp \left(-\frac{1}{2} x^2 \right) \sum_{j=0}^{\infty} \hat{A}_j(x) P^{-\frac{j}{2}}, \end{aligned}$$

as $P \rightarrow +\infty$, where

$$\hat{A}_j(x) := \sum_{n=0}^j \frac{1}{n!} \left(\frac{2}{45} \right)^{\frac{2n+j}{2}} \hat{\vartheta}_{j-n,n} x^{2n+j} = \sum_{n=0}^j \hat{\eta}_{n,j} x^{2n+j}, \quad \text{for } j \geq 0$$

with

$$(C.6) \quad \hat{\eta}_{n,j} := \left(\frac{2}{45} \right)^{n+\frac{1}{2}j} \frac{\hat{\vartheta}_{j-n,n}}{n!}$$

for $0 \leq n \leq j$. Further, we see that

$$\begin{aligned} & \sum_{j=0}^{\infty} \sum_{l=0}^{\infty} \sum_{n=0}^{\lfloor \frac{2}{3}j \rfloor} \hat{\alpha}_{n,l,j} \left(\frac{2}{45} \right)^{\frac{l}{2}} \Gamma \left(j + \frac{1}{2} \right) x^l P^{n-\frac{l}{2}-j} \\ & \sim \sum_{m=0}^{\infty} \sum_{l=0}^{\infty} \sum_{j=m}^{3m} \hat{\alpha}_{j-m,l,j} \left(\frac{2}{45} \right)^{\frac{l}{2}} \Gamma \left(j + \frac{1}{2} \right) x^l P^{-(m+\frac{l}{2})} \\ & \sim \sum_{\substack{r=0 \\ r \text{ even}}}^{\infty} \sum_{\substack{l=0 \\ l \text{ even}}}^r \sum_{j=\frac{r-l}{2}}^{\frac{3(r-l)}{2}} \hat{\alpha}_{j-\frac{r-l}{2},l,j} \left(\frac{2}{45} \right)^{\frac{l}{2}} \Gamma \left(j + \frac{1}{2} \right) x^l P^{-\frac{r}{2}} \\ & \quad + \sum_{\substack{r=1 \\ r \text{ odd}}}^{\infty} \sum_{\substack{l=1 \\ l \text{ odd}}}^r \sum_{j=\frac{r-l}{2}}^{\frac{3(r-l)}{2}} \hat{\alpha}_{j-\frac{r-l}{2},l,j} \left(\frac{2}{45} \right)^{\frac{l}{2}} \Gamma \left(j + \frac{1}{2} \right) x^l P^{-\frac{r}{2}} \\ & \sim \sum_{r=0}^{\infty} \hat{B}_r(x) P^{-\frac{r}{2}} \end{aligned}$$

when $P \rightarrow +\infty$ with

$$\hat{B}_r(x) := \sum_{l=0}^r \hat{\lambda}_{l,r} x^l, \quad \text{for } r \geq 0,$$

where for even r ,

$$(C.7) \quad \hat{\lambda}_{l,r} := \begin{cases} 0, & \text{for odd } l, \\ \sum_{j=\frac{r-l}{2}}^{\frac{3(r-l)}{2}} \hat{\alpha}_{j-\frac{r-l}{2},l,j} \left(\frac{2}{45} \right)^{\frac{l}{2}} \Gamma \left(j + \frac{1}{2} \right), & \text{for even } l, \end{cases}$$

and for odd r ,

$$(C.8) \quad \hat{\lambda}_{l,r} := \begin{cases} 0, & \text{for even } l, \\ \sum_{j=\frac{r-l}{2}}^{\frac{3(r-l)}{2}} \hat{\alpha}_{j-\frac{r-l}{2},l,j} \left(\frac{2}{45} \right)^{\frac{l}{2}} \Gamma \left(j + \frac{1}{2} \right), & \text{for odd } l. \end{cases}$$

Following the above discussion, (C.1) can be rearranged as

$$\begin{aligned} f_{Z^P}(x) & \sim \frac{1}{4\pi} \sqrt{\frac{2}{45}} \exp \left(-\frac{1}{2}x^2 \right) \left(\sum_{j=0}^{\infty} \hat{A}_j(x) P^{-\frac{j}{2}} \right) \left(\sum_{r=0}^{\infty} \hat{B}_r(x) P^{-\frac{r}{2}} \right) \\ & \sim \frac{1}{4\pi} \sqrt{\frac{2}{45}} \exp \left(-\frac{1}{2}x^2 \right) \sum_{j=0}^{\infty} \left(\sum_{r=0}^j \hat{A}_r(x) \hat{B}_{j-r}(x) \right) P^{-\frac{j}{2}} \\ & \sim \frac{1}{4\pi} \sqrt{\frac{2}{45}} \exp \left(-\frac{1}{2}x^2 \right) \sum_{j=0}^{\infty} \hat{\psi}_j(x) P^{-\frac{j}{2}}, \end{aligned}$$

where for $j \geq 0$,

$$\hat{\psi}_j(x) := \sum_{r=0}^j \hat{A}_r(x) \hat{B}_{j-r}(x) = \sum_{r=0}^j \sum_{n=0}^r \sum_{l=0}^{j-r} \hat{\eta}_{n,r} \hat{\lambda}_{l,j-r} x^{2n+r+l}.$$

Then, by the definition for asymptotic expansions, we have the order relation given below: for any $J \geq 0$,

$$f_{Z^P}(x) - \frac{1}{4\pi} \sqrt{\frac{2}{45}} \exp\left(-\frac{1}{2}x^2\right) \sum_{j=0}^J \hat{\psi}_j(x) P^{-\frac{j}{2}} = o\left(P^{-\frac{J}{2}}\right),$$

as $P \rightarrow +\infty$ with $x > -\sqrt{5P/2}(1 + 3/\pi^2 - 3 \coth \pi/\pi)$ and $|x|$ sufficiently small. Integrating on finite interval $(z_1, z_2]$ such that $z_i > -\sqrt{5P/2}(1 + 3/\pi^2 - 3 \coth \pi/\pi)$ and $|z_i|$ sufficiently small for $i = 1, 2$, we have

$$\int_{z_1}^{z_2} f_{Z^P}(x) dx = \frac{1}{4\pi} \sqrt{\frac{2}{45}} \sum_{j=0}^J P^{-\frac{j}{2}} \int_{z_1}^{z_2} \exp\left(-\frac{1}{2}x^2\right) \hat{\psi}_j(x) dx + o\left(P^{-\frac{J}{2}}\right).$$

Next, we show the integrals on the right hand side are finite. In fact, for $0 \leq j \leq J$, we can write

$$\begin{aligned} \left| \int_{z_1}^{z_2} \exp\left(-\frac{1}{2}x^2\right) \hat{\psi}_j(x) dx \right| &\leq \int_{z_1}^{z_2} \exp\left(-\frac{1}{2}x^2\right) |\hat{\psi}_j(x)| dx \\ &\leq \sum_{r=0}^j \sum_{n=0}^r \sum_{l=0}^{j-r} |\hat{\eta}_{n,r} \hat{\lambda}_{l,j-r}| \int_{z_1}^{z_2} \exp\left(-\frac{1}{2}x^2\right) |x^{2n+r+l}| dx \\ &< +\infty. \end{aligned}$$

Notice that the constants $\hat{\eta}_{n,r}$ and $\hat{\lambda}_{l,j-r}$ are finite. Hence, we have the following asymptotic expansion: when $P \rightarrow +\infty$,

$$\begin{aligned} \int_{z_1}^{z_2} f_{Z^P}(x) dx &\sim \frac{1}{4\pi} \sqrt{\frac{2}{45}} \sum_{j=0}^{\infty} P^{-\frac{j}{2}} \int_{z_1}^{z_2} \exp\left(-\frac{1}{2}x^2\right) \hat{\psi}_j(x) dx \\ &\sim \frac{1}{4\pi} \sqrt{\frac{2}{45}} \sum_{j=0}^{\infty} P^{-\frac{j}{2}} \int_{z_1}^{z_2} \exp\left(-\frac{1}{2}x^2\right) \sum_{r=0}^j \sum_{n=0}^r \sum_{l=0}^{j-r} \hat{\eta}_{n,r} \hat{\lambda}_{l,j-r} x^{2n+r+l} dx \\ (C.9) \quad &\sim \frac{1}{4\pi} \sqrt{\frac{2}{45}} \sum_{j=0}^{\infty} P^{-\frac{j}{2}} \sum_{r=0}^j \sum_{n=0}^r \sum_{l=0}^{j-r} \hat{\eta}_{n,r} \hat{\lambda}_{l,j-r} \int_{z_1}^{z_2} \exp\left(-\frac{1}{2}x^2\right) x^{2n+r+l} dx. \end{aligned}$$

We apply the change of variable $v = x^2/2$ to compute the above integrals. For $z_1 < z_2 < 0$ and $q \geq 0$, we have

$$\begin{aligned} \int_{z_1}^{z_2} \exp\left(-\frac{1}{2}x^2\right) x^q dx &= (-1)^q (\sqrt{2})^{q-1} \int_{\frac{z_2^2}{2}}^{\frac{z_1^2}{2}} \exp(-v) v^{\frac{q+1}{2}-1} dv \\ &= (-1)^q (\sqrt{2})^{q-1} \left(\gamma\left(\frac{q+1}{2}, \frac{(z_1)^2}{2}\right) - \gamma\left(\frac{q+1}{2}, \frac{(z_2)^2}{2}\right) \right), \end{aligned}$$

where $\gamma(s, z)$ is the lower incomplete gamma function. For $z_1 < 0 \leq z_2$ and $q \geq 0$, we consider the integral on the two sub-intervals $[z_1, 0]$ and $[0, z_2]$ separately. By additivity, we get

$$\begin{aligned} \int_{z_1}^{z_2} \exp\left(-\frac{1}{2}x^2\right) x^q dx &= (-1)^q (\sqrt{2})^{q-1} \int_0^{\frac{z_1^2}{2}} \exp(-v) v^{\frac{q+1}{2}-1} dv \\ &\quad + (\sqrt{2})^{q-1} \int_0^{\frac{z_2^2}{2}} \exp(-v) v^{\frac{q+1}{2}-1} dv \\ &= (\sqrt{2})^{q-1} \left((-1)^q \gamma\left(\frac{q+1}{2}, \frac{(z_1)^2}{2}\right) + \gamma\left(\frac{q+1}{2}, \frac{(z_2)^2}{2}\right) \right). \end{aligned}$$

Substituting the explicit form for the integrals back into (C.9) yields the stated representation, completing the proof.

Appendix D. Proof of Theorem 3.7. Recall that the probability density function f_{S^P} of S^P has the form

$$f_{S^P}(y) = \frac{1}{\sqrt{2\pi}} \frac{2^P}{\Gamma(P)} y^{-\frac{1}{2}(P+2)} \sum_{n=0}^{\infty} \frac{\Gamma(n+P)}{\Gamma(n+1)} \exp\left(-\frac{(2n+P)^2}{4y}\right) D_{P+1}\left(\frac{2n+P}{\sqrt{y}}\right),$$

in which $D_{P+1}(z)$ is a parabolic cylinder function of order $P+1$. The distribution function F_{S^P} is derived by term-wise integration of the above series. First we show that $\sum_{n=0}^{\infty} \int_0^x |f_n(y)| dy < \infty$ for any finite $x \geq 0$, where

$$f_n(y) := \frac{\Gamma(n+P)}{\Gamma(n+1)} \exp\left(-\frac{(2n+P)^2}{4y}\right) D_{P+1}\left(\frac{2n+P}{\sqrt{y}}\right) y^{-\frac{1}{2}(P+2)}.$$

For fixed $n \geq 0$, application of the variable transformation $z = (2n+P)/\sqrt{y}$ gives

$$\int_0^x |f_n(y)| dy = 2 \frac{\Gamma(n+P)}{\Gamma(n+1)} (2n+P)^{-P} \int_{\frac{2n+P}{\sqrt{x}}}^{+\infty} \exp\left(-\frac{1}{4}z^2\right) |D_{P+1}(z)| z^{P-1} dz.$$

Notice that the parabolic cylinder function $D_{P+1}(z)$ is square integrable on $[0, \infty)$ (Gradshteyn and Ryzhik [19, Chapter 7.711]), i.e.

$$\|D_{P+1}\|_2 := \left(\int_0^{+\infty} |D_{P+1}(z)|^2 dz \right)^{\frac{1}{2}} < \infty.$$

By Hölder's inequality, we have

(D.1)

$$\int_y^{+\infty} \exp\left(-\frac{1}{4}z^2\right) |D_{P+1}(z)| z^{P-1} dz \leq \left(\int_y^{+\infty} z^{2(P-1)} \exp\left(-\frac{1}{2}z^2\right) dz \right)^{\frac{1}{2}} \|D_{P+1}\|_2$$

for $y \geq 0$. Next we consider the following two cases for P separately: $P \in (0, 1)$ and $P \in \mathbb{N}$.

For any $P \in (0, 1)$, $z^{2(P-1)}$ is monotonically decreasing, which yields

$$\begin{aligned} \int_y^{+\infty} \exp\left(-\frac{1}{4}z^2\right) |D_{P+1}(z)| z^{P-1} dz &\leq y^{P-1} \left(\int_y^{+\infty} \exp\left(-\frac{1}{2}z^2\right) dz \right)^{\frac{1}{2}} \|D_{P+1}\|_2 \\ &= (2\pi)^{\frac{1}{4}} \|D_{P+1}\|_2 y^{P-1} (1 - \Phi(y))^{\frac{1}{2}} \end{aligned}$$

for $y > 0$, where $\Phi(y)$ is the distribution function of a standard normal random variable. Then, it follows that the sequence $\int_0^x |f_n(y)| dy$ with finite x is bounded by

$$\int_0^x |f_n(y)| dy \leq b_n,$$

where

$$b_n := 2(2\pi)^{\frac{1}{4}} \|D_{P+1}\|_2 x^{\frac{1}{2}(1-P)} \frac{\Gamma(n+P)}{\Gamma(n+1)} \frac{1}{2n+P} \left(1 - \Phi\left(\frac{2n+P}{\sqrt{x}}\right)\right)^{\frac{1}{2}}.$$

By the ratio test, we can deduce that the series $\sum_{n=0}^{\infty} b_n$ is convergent. In fact, we have

$$\left| \frac{b_{n+1}}{b_n} \right| = \frac{n+P}{n+1} \frac{2n+P}{2(n+1)+P} \left(\frac{1 - \Phi\left(\frac{2(n+1)+P}{\sqrt{x}}\right)}{1 - \Phi\left(\frac{2n+P}{\sqrt{x}}\right)} \right)^{\frac{1}{2}} \rightarrow 0, \quad \text{as } n \rightarrow \infty.$$

The comparison test implies that the series $\sum_{n=0}^{\infty} \int_0^x |f_n(y)| dy$ is also convergent for any finite x .

For any $P \in \mathbb{N}$, the integral on the right hand side of (D.1) can be regarded as the moment of some transformation of a standard normal random variable Z , i.e.

$$\begin{aligned} \int_y^{+\infty} z^{2(P-1)} \exp\left(-\frac{1}{2}z^2\right) dz &= \sqrt{2\pi} \mathbb{E} \left[Z^{2(P-1)} \mathbf{1}_{\{Z \geq y\}} \right] \\ &\leq \sqrt{2\pi} \left(\mathbb{E} \left[Z^{4(P-1)} \right] \right)^{\frac{1}{2}} \left(\mathbb{E} \left[(\mathbf{1}_{\{Z \geq y\}})^2 \right] \right)^{\frac{1}{2}} \\ &= \sqrt{2\pi} \left(\mathbb{E} \left[Z^{4(P-1)} \right] \right)^{\frac{1}{2}} (1 - \Phi(y))^{\frac{1}{2}} \end{aligned}$$

for $y \geq 0$, where $\mathbf{1}_{\{z \geq y\}}$ is the indicator function and the inequality follows from Hölder's inequality. Hence, the above argument gives the bounds for $\int_0^x |f_n(y)| dy$ with $x < \infty$ as

$$\int_0^x |f_n(y)| dy \leq b_n,$$

where

$$b_n := 2(2\pi)^{\frac{1}{4}} \|D_{P+1}\|_2 \left(\mathbb{E} \left[Z^{4(P-1)} \right] \right)^{\frac{1}{4}} \frac{\Gamma(n+P)}{\Gamma(n+1)} (2n+P)^{-P} \left(1 - \Phi\left(\frac{2n+P}{\sqrt{x}}\right)\right)^{\frac{1}{4}}.$$

Similarly, the series $\sum_{n=0}^{\infty} b_n$ converges by the fact that

$$\left| \frac{b_{n+1}}{b_n} \right| = \frac{n+P}{n+1} \left(\frac{2n+P}{2(n+1)+P} \right)^P \left(\frac{1 - \Phi\left(\frac{2(n+1)+P}{\sqrt{x}}\right)}{1 - \Phi\left(\frac{2n+P}{\sqrt{x}}\right)} \right)^{\frac{1}{4}} \rightarrow 0, \quad \text{as } n \rightarrow \infty,$$

implying the convergence of the series $\sum_{n=0}^{\infty} \int_0^x |f_n(y)| dy$ for finite x as well.

Thus, for fixed $0 \leq x < \infty$ and $P \in (0, 1) \cup \mathbb{N}$, we have $\sum_{n=0}^{\infty} \int_0^x |f_n(y)| dy < \infty$. Then, applying a corollary of the Dominated Convergence Theorem (Rudin [34, Theorem 1.38]) yields

$$\sum_{n=0}^{\infty} \int_0^x f_n(y) dy = \int_0^x \sum_{n=0}^{\infty} f_n(y) dy,$$

where the integration and summation can be interchanged. This leads to the following convergent series expansion for the distribution function F_{S^P} : for any $x < \infty$,

$$\begin{aligned} F_{S^P}(x) &= \frac{1}{\sqrt{2\pi}} \frac{2^P}{\Gamma(P)} \sum_{n=0}^{\infty} \int_0^x f_n(y) dy \\ &= \frac{1}{\sqrt{2\pi}} \frac{2^P}{\Gamma(P)} \sum_{n=0}^{\infty} \frac{\Gamma(n+P)}{\Gamma(n+1)} \int_0^x y^{-\frac{1}{2}(P+2)} \exp\left(-\frac{(2n+P)^2}{4y}\right) D_{P+1}\left(\frac{2n+P}{\sqrt{y}}\right) dy \\ &= \frac{1}{\sqrt{2\pi}} \frac{2^{P+1}}{\Gamma(P)} \sum_{n=0}^{\infty} \frac{\Gamma(n+P)}{\Gamma(n+1)} (2n+P)^{-P} G\left(\frac{2n+P}{\sqrt{x}}\right), \end{aligned}$$

where the function $G(y)$ is defined as

$$(D.2) \quad G(y) = \int_y^{+\infty} z^{P-1} \exp\left(-\frac{1}{4}z^2\right) D_{P+1}(z) dz.$$

To evaluate the function G , we first follow the methods mentioned earlier to calculate the parabolic cylinder functions D_{P+1} and hence its integrand. We may replace $D_{P+1}(z)$ by its convergent power series on the entire interval of integration to derive the corresponding series expansion for G . However, the power series converges too slowly to be of practical use for large z . Instead, we split the interval of integration $[y, +\infty)$ into two small elements, say $[y, y^*)$ and $[y^*, +\infty)$ for some sufficiently large $y^* \geq y$, where we apply different representations for $D_{P+1}(z)$ depending on the value of z . Then, we have

$$G(y) = G_1(y, y^*) + G_2(y^*),$$

where

$$\begin{aligned} G_1(y, y^*) &:= \int_y^{y^*} z^{P-1} \exp\left(-\frac{1}{4}z^2\right) D_{P+1}(z) dz, \\ G_2(y^*) &:= \int_{y^*}^{+\infty} z^{P-1} \exp\left(-\frac{1}{4}z^2\right) D_{P+1}(z) dz. \end{aligned}$$

On $[y^*, +\infty)$, the asymptotic expansion (3.6) is a convenient way to compute $D_{P+1}(z)$ and hence G_2 . On $[y, y^*)$, the power series (3.5) will be useful for G_1 . Next, we consider the integral on the two sub-intervals case by case.

On $[y^*, +\infty)$, we approximate the parabolic cylinder function $D_{P+1}(z)$ by its asymptotic series (3.6) on the entire interval under consideration. The series is then multiplied by $z^{P-1} \exp(-z^2/4)$ and integrated term by term to generate a series approximation for the integral G_2 . To confirm that the resulting series is the correct asymptotic expansion for the integral with large y^* , we note that

$$z^{P-1} \exp\left(-\frac{1}{4}z^2\right) D_{P+1}(z) \sim z^{2P} \exp\left(-\frac{1}{2}z^2\right) \sum_{k=0}^{\infty} \hat{a}_k z^{-2k}, \quad \text{as } z \rightarrow +\infty,$$

where $\hat{a}_k = (-1)^k 2^{-k} (-(P+1))_{2k} / k!$ for $k \geq 0$. By the definition for asymptotic expansions, we have for each K ,

$$z^{P-1} \exp\left(-\frac{1}{4}z^2\right) D_{P+1}(z) - z^{2P} \exp\left(-\frac{1}{2}z^2\right) \sum_{k=0}^K \hat{a}_k z^{-2k} = o\left(z^{2P} \exp\left(-\frac{1}{2}z^2\right) z^{-2K}\right),$$

as $z \rightarrow +\infty$, meaning that for any $\epsilon > 0$, there exists a $z_0 > 0$ such that for $z > z_0$,

$$\left| z^{P-1} \exp\left(-\frac{1}{4}z^2\right) D_{P+1}(z) - z^{2P} \exp\left(-\frac{1}{2}z^2\right) \sum_{k=0}^K \hat{a}_k z^{-2k} \right| \leq \epsilon \left| z^{2P} \exp\left(-\frac{1}{2}z^2\right) z^{-2K} \right|.$$

Then, properties of integration yield for any $y^* > z_0$,

$$\begin{aligned} & \left| G_2(y^*) - \sum_{k=0}^K \hat{a}_k \int_{y^*}^{+\infty} z^{2P} \exp\left(-\frac{1}{2}z^2\right) z^{-2k} dz \right| \\ & \leq \int_{y^*}^{+\infty} \left| z^{P-1} \exp\left(-\frac{1}{4}z^2\right) D_{P+1}(z) - z^{2P} \exp\left(-\frac{1}{2}z^2\right) \sum_{k=0}^K \hat{a}_k z^{-2k} \right| dz \\ & \leq \epsilon \int_{y^*}^{+\infty} z^{2P} \exp\left(-\frac{1}{2}z^2\right) z^{-2K} dz. \end{aligned}$$

Hence, we have the following asymptotic relation: as $y^* \rightarrow +\infty$,

$$G_2(y^*) - \sum_{k=0}^K \hat{a}_k \int_{y^*}^{+\infty} z^{2P} \exp\left(-\frac{1}{2}z^2\right) z^{-2k} dz = o\left(\int_{y^*}^{+\infty} z^{2P} \exp\left(-\frac{1}{2}z^2\right) z^{-2K} dz\right),$$

which further gives the asymptotic expansion

$$G_2(y^*) \sim \sum_{k=0}^{\infty} \hat{a}_k \int_{y^*}^{+\infty} z^{2P} \exp\left(-\frac{1}{2}z^2\right) z^{-2k} dz, \quad \text{as } y^* \rightarrow +\infty.$$

Introducing a new variable $\zeta = z^2/2$, we find that

$$\begin{aligned} G_2(y^*) & \sim \sum_{k=0}^{\infty} \hat{a}_k 2^{P-k-\frac{1}{2}} \int_{\frac{(y^*)^2}{2}}^{+\infty} \zeta^{P-k-\frac{1}{2}} \exp(-\zeta) d\zeta \\ & \sim \sum_{k=0}^{\infty} \hat{a}_k 2^{P-k-\frac{1}{2}} \Gamma\left(P-k+\frac{1}{2}, \frac{(y^*)^2}{2}\right) \end{aligned}$$

in the limit $y^* \rightarrow +\infty$, where $\Gamma(s, z)$ is the upper incomplete gamma function. Replacing \hat{a}_k by the explicit form given above generates the stated asymptotic expansion for G_2 .

On $[y, y^*)$, approximating the parabolic cylinder function $D_{P+1}(z)$ using the power series (3.5), we can write

$$\begin{aligned} G_1(y, y^*) & = \int_y^{y^*} z^{P-1} \exp\left(-\frac{1}{4}z^2\right) \left(\sum_{k=0}^{\infty} \hat{d}_k(P) z^k\right) dz \\ & = \sum_{k=0}^{\infty} \hat{d}_k(P) \int_y^{y^*} z^{P+k-1} \exp\left(-\frac{1}{4}z^2\right) dz \\ & = \sum_{k=0}^{\infty} \hat{d}_k(P) 2^{P+k-1} \int_{\frac{y^2}{4}}^{\frac{(y^*)^2}{4}} \zeta^{\frac{P+k}{2}-1} \exp(-\zeta) d\zeta \\ & = \sum_{k=0}^{\infty} \hat{d}_k(P) 2^{P+k-1} \left(\Gamma\left(\frac{P+k}{2}, \frac{y^2}{4}\right) - \Gamma\left(\frac{P+k}{2}, \frac{(y^*)^2}{4}\right) \right), \end{aligned}$$

where the interchange of integration and summation in the second step follows from the fact that the power series is uniformly convergent over the interval of integration and a change of variable $\zeta = z^2/4$ is applied for the third step. Notice that the above series is convergent for any $0 < y \leq y^*$.

Appendix E. Proof of Corollary 3.9. Recall from Theorem 3.7 that the distribution function F_{SP} for $P \in (0, 1) \cup \mathbb{N}$ takes the form

$$(E.1) \quad F_{SP}(x) = \frac{1}{\sqrt{2\pi}} \frac{2^{P+1}}{\Gamma(P)} \sum_{n=0}^{\infty} \frac{\Gamma(n+P)}{\Gamma(n+1)} (2n+P)^{-P} G\left(\frac{2n+P}{\sqrt{x}}\right)$$

for any $0 \leq x < \infty$, where the function G has the asymptotic approximation

$$G(y) \sim \sum_{k=0}^{\infty} (-1)^k \frac{(-(P+1))_{2k}}{k!} 2^{P-2k-\frac{1}{2}} \Gamma\left(P-k+\frac{1}{2}, \frac{y^2}{2}\right), \quad \text{as } y \rightarrow +\infty.$$

Then it follows from the definition for asymptotic expansions that

$$G(y) = 2^{P-\frac{1}{2}} \Gamma\left(P+\frac{1}{2}, \frac{y^2}{2}\right) + o\left(\Gamma\left(P+\frac{1}{2}, \frac{y^2}{2}\right)\right), \quad \text{as } y \rightarrow +\infty.$$

Further, by the asymptotic expansion for the incomplete gamma function (Abramowitz and Stegun [2, formula (6.5.32)])

$$\Gamma(s, z) \sim z^{s-1} \exp(-z) \sum_{k=0}^{\infty} \frac{\Gamma(s)}{\Gamma(s-k)} z^{-k}, \quad \text{as } z \rightarrow +\infty,$$

we have

$$\Gamma\left(P+\frac{1}{2}, \frac{y^2}{2}\right) = \left(\frac{y^2}{2}\right)^{P-\frac{1}{2}} \exp\left(-\frac{y^2}{2}\right) + o\left(y^{2P-1} \exp\left(-\frac{y^2}{2}\right)\right), \quad \text{as } y \rightarrow +\infty.$$

The above analysis yields

$$G(y) = y^{2P-1} \exp\left(-\frac{y^2}{2}\right) + o\left(y^{2P-1} \exp\left(-\frac{y^2}{2}\right)\right), \quad \text{as } y \rightarrow +\infty.$$

Hence, we can write

$$\begin{aligned} G\left(\frac{2n+P}{\sqrt{x}}\right) &= (2n+P)^{2P-1} x^{\frac{1}{2}-P} \exp\left(-\frac{(2n+P)^2}{2x}\right) \\ &\quad + o\left((2n+P)^{2P-1} x^{\frac{1}{2}-P} \exp\left(-\frac{(2n+P)^2}{2x}\right)\right) \end{aligned}$$

in the limit $x \rightarrow 0^+$. The observation

$$(2n+P)^{2P-1} \frac{\exp\left(-\frac{(2n+P)^2}{2x}\right)}{\exp\left(-\frac{P^2}{2x}\right)} = (2n+P)^{2P-1} \exp\left(-\frac{4n^2+4nP}{2x}\right) \rightarrow 0, \quad \text{as } x \rightarrow 0^+$$

for any $n \geq 1$ establishes

$$G\left(\frac{2n+P}{\sqrt{x}}\right) = o\left(G\left(\frac{P}{\sqrt{x}}\right)\right), \quad \text{as } x \rightarrow 0^+.$$

Therefore, (E.1) becomes

$$\begin{aligned}
F_{S^P}(x) &= \frac{1}{\sqrt{2\pi}} \frac{2^{P+1}}{\Gamma(P)} \frac{\Gamma(P)}{\Gamma(1)} P^{-P} G\left(\frac{P}{\sqrt{x}}\right) + o\left(G\left(\frac{P}{\sqrt{x}}\right)\right) \\
&= \frac{1}{\sqrt{2\pi}} 2^{P+1} P^{P-1} x^{\frac{1}{2}-P} \exp\left(-\frac{P^2}{2x}\right) + o\left(x^{\frac{1}{2}-P} \exp\left(-\frac{P^2}{2x}\right)\right) \\
&\sim \frac{1}{\sqrt{2\pi}} 2^{P+1} P^{P-1} x^{\frac{1}{2}-P} \exp\left(-\frac{P^2}{2x}\right), \quad \text{as } x \rightarrow 0^+.
\end{aligned}$$

Appendix F. Uniqueness and Existence of Saddle Points. In this section, we show the existence and uniqueness of saddle points, which is used in the proof of Theorem 3.3 in Appendix B.

LEMMA F.1. *For $\beta > -1/3$, there exists a unique solution to $\rho'(z; \beta) = 0$ in the domain $\{z \in \mathbb{C} : \text{Im}(z) < \pi^2\}$, where*

$$\rho(z; \beta) = \log\left(\frac{\sqrt{zi}}{\sinh \sqrt{zi}}\right) + zi\left(\frac{1}{6} + \frac{1}{2}\beta\right).$$

Further, this unique solution lies on the imaginary axis and is at zero when $\beta = 0$.

Proof. Direct differentiation of $\rho(z; \beta)$ gives

$$\begin{aligned}
\rho'(z; \beta) &= \frac{\sinh \sqrt{zi}}{\sqrt{zi}} \frac{\sinh \sqrt{zi} - \sqrt{zi} \cosh \sqrt{zi}}{\sinh^2 \sqrt{zi}} \frac{i}{2\sqrt{zi}} + i\left(\frac{1}{6} + \frac{1}{2}\beta\right) \\
&= \frac{i}{2} \left(\frac{1 - \sqrt{zi} \coth \sqrt{zi}}{zi} + \left(\frac{1}{3} + \beta\right) \right).
\end{aligned}$$

For convenience set $\hat{\beta} := \beta + 1/3$ and

$$\theta(z) := \frac{1 - \sqrt{zi} \coth \sqrt{zi}}{zi}.$$

Then $\rho'(z; \beta)$ becomes

$$\rho'(z; \beta) = \frac{i}{2} \left(\theta(z) + \hat{\beta} \right).$$

First, we note $\theta(z)$ is well-defined for all $z \in \mathbb{C}$ except at a countable set of poles which we discuss now. From Weierstrass Product Theorem in complex variable theory we have the classical identity

$$z \coth z = 1 + 2z^2 \sum_{n=1}^{\infty} \frac{1}{z^2 + n^2 \pi^2}.$$

Hence we know

$$(F.1) \quad \theta(z) = -2 \sum_{n=1}^{\infty} \frac{1}{zi + n^2 \pi^2}.$$

Then we observe the only singularities of $\theta(z)$ and hence of $\rho'(z; \beta)$ are at $z = n^2 \pi^2 i$ for $n \geq 1$.

Second, if we set $z = u + iv$ for $u, v \in \mathbb{R}$, equation (F.1) can be written as

$$\theta(z) = -2 \sum_{n=1}^{\infty} \frac{1}{ui - v + n^2\pi^2} = -2 \sum_{n=1}^{\infty} \frac{n^2\pi^2 - v - iu}{(n^2\pi^2 - v)^2 + u^2},$$

the imaginary part of which is

$$\text{Im}\theta(z) = 2u \sum_{n=1}^{\infty} \frac{1}{(n^2\pi^2 - v)^2 + u^2}.$$

At a zero of $\rho'(z; \beta)$ we must have $\theta(z) = -\hat{\beta}$, where $\hat{\beta} \in \mathbb{R}$. In other words, $\theta(z)$ must be real, i.e. its imaginary part must be zero. Then from the above equation, we see this occurs if and only if $u = 0$, i.e. z is on the imaginary axis. Hence all zeros of $\rho'(z; \beta)$ lie on the imaginary axis.

Third, now let us focus entirely on the imaginary axis and set $z = iv$ for $v \in \mathbb{R}$. Then $\theta(z)$ becomes

$$\theta(iv) = -2 \sum_{n=1}^{\infty} \frac{1}{n^2\pi^2 - v}.$$

Since term by term $(n^2\pi^2 - v)^{-1}$ decreases monotonically in magnitude as v moves in the direction from π^2 to $-\infty$, so $\theta(iv)$ increases monotonically as v moves in the same direction. Further, each term $(n^2\pi^2 - v)^{-1} > 0$ for $v < \pi^2$. Hence $\theta(iv) < 0$ when $v < \pi^2$. If we set $v = -\nu$ with $\nu > 0$ then from its definition, we observe

$$\theta(iv) = \frac{1}{\nu} - \frac{\coth \sqrt{\nu}}{\sqrt{\nu}} \rightarrow 0, \quad \text{as } \nu \rightarrow +\infty$$

since $\coth \sqrt{\nu} \rightarrow 1$ as $\nu \rightarrow +\infty$. This implies $\theta(iv) \rightarrow 0$ as $v \rightarrow -\infty$. At $v = 0$ by using that $\sum_{n=1}^{\infty} n^{-2} = \pi^2/6$, we see

$$\theta(0) = -\frac{1}{3}.$$

Thus $\theta(iv)$ decreases monotonically from zero as $v \rightarrow -\infty$ to $-1/3$ at $v = 0$ and continues to decrease monotonically to $-\infty$ as $v \rightarrow \pi^2$.

Hence for $\beta > -1/3$, i.e. $\hat{\beta} > 0$, there is one and only one solution to $\theta(z) = -\hat{\beta}$, i.e. to $\rho'(z; \beta) = 0$ in the region $\{z \in \mathbb{C} : \text{Im}(z) < \pi^2\}$. This unique solution must lie on the imaginary axis and is at zero when $\beta = 0$. \square

Remark F.2. We note that the condition $\beta > -1/3$ is satisfied in the domain where the density f_{Z^P} is strictly positive, and hence this condition does not constitute a restriction.

Remark F.3. We have shown the imaginary part $v = v(\beta)$ of the solution $z_0 = z_0(\beta)$ to $\rho'(z; \beta) = 0$ is a monotonically increasing function of β . To ensure v is within the radius of convergence of the Taylor series expansion of ρ and ρ' , we must require $v > -\pi^2$, and hence we require $-(\beta + 1/3) = \theta(iv) < \theta(-i\pi^2) = (1 - \pi \coth \pi)/\pi^2$, i.e. $\beta > -1/3 - (1 - \pi \coth \pi)/\pi^2$.

Acknowledgements. We would like to thank the referees for their useful comments and suggestions which helped to improve the original manuscript.

REFERENCES

- [1] M. J. ABLOWITZ AND A. S. FOKAS, *Complex Variables: Introduction and Applications*, Cambridge Texts in Applied Mathematics, 2nd ed., Cambridge University Press, Cambridge, 2003.
- [2] M. ABRAMOWITZ AND I. A. STEGUN, eds., *Handbook of Mathematical Functions with Formulas, Graphs, and Mathematical Tables*, National Bureau of Standards: Applied Mathematics Series, Vol. 55, U.S. Government Printing Office, Washington, DC, 1964.
- [3] A. ALFONSI, *High order discretization schemes for the CIR process: application to affine term structure and Heston models*, Math. Comp., 79 (2010), 209–237.
- [4] M. ALTMAYER AND A. NEUENKIRCH, *Discretising the Heston model: an analysis of the weak convergence rate*, IMA J. Numer. Anal., 37 (2017), 1930–1960.
- [5] L. ANDERSEN, *Simple and efficient simulation of the Heston stochastic volatility model*, J. Comput. Finance, 11 (2008), 1–42.
- [6] C. M. BENDER AND S. A. ORSZAG, *Advanced Mathematical Methods for Scientists and Engineers I: Asymptotic Methods and Perturbation Theory*, Springer-Verlag, New York, 1999.
- [7] A. BERKAOUI, M. BOSSY, AND A. DIOP, *Euler scheme for SDEs with non-Lipschitz diffusion coefficient: strong convergence*, ESAIM Probab. Stat., 12 (2008), 1–11.
- [8] P. BIANE, J. PITMAN AND M. YOR, *Probability laws related to the Jacobi theta and Riemann zeta functions, and Brownian excursions*, Bull. Amer. Math. Soc. (N.S.), 38 (2001), 435–465.
- [9] P. BIANE AND M. YOR, *Valeurs principales associées aux temps locaux Browniens*, Bull. Sci. Math., 111 (1987), 23–101.
- [10] N. BLEISTEIN AND R. A. HANDELSMAN, *Asymptotic Expansions of Integrals*, 2nd ed., Dover Publications, Inc., New York, 1986.
- [11] M. BOSSY AND A. DIOP, *An efficient discretization scheme for one dimensional SDEs with a diffusion coefficient function of the form $|x|^\alpha$, $\alpha \in [1/2, 1)$* , INRIA, (2006).
- [12] M. BROADIE AND O. KAYA, *Exact simulation of stochastic volatility and other affine jump diffusion processes*, Oper. Res., 54 (2006), 217–231.
- [13] J. C. COX, J. E. INGERSOLL, AND S. A. ROSS, *A theory of the term structure of interest rates*, Econometrica, 53 (1985), 385–407.
- [14] D. DUFFIE AND P. GLYNN, *Efficient Monte Carlo simulation of security prices*, Ann. Appl. Probab., 5 (2019), 897–905.
- [15] J. GATHERAL, *The Volatility Surface: A Practitioner’s Guide*, Wiley Finance Series, Vol. 357, John Wiley & Sons, New Jersey, 2006.
- [16] A. GIL, J. SEGURA, AND N. M. TEMME, *Computing the real parabolic cylinder functions $U(a, x)$, $V(a, x)$* , ACM Trans. Math. Software, 32 (2006), 70–101.
- [17] P. GLASSERMAN, *Monte Carlo Methods in Financial Engineering*, Applications of Mathematics, Stochastic Modelling and Applied Probability, Vol. 53, Springer-Verlag, New York, 2003.
- [18] P. GLASSERMAN AND K. K. KIM, *Gamma expansion of the Heston stochastic volatility model*, Finance Stoch., 15 (2011), 267–296.
- [19] I. S. GRADSHTEYN AND I. M. RYZHIK, *Table of Integrals, Series, and Products*, Academic Press, New York, 2014.
- [20] M. HEFTER AND A. JENTZEN, *On arbitrarily slow convergence rates for strong numerical approximations of Cox-Ingersoll-Ross processes and squared Bessel processes*, Finance Stoch., 23 (2019), 139–172.
- [21] S. L. HESTON, *A closed-form solution for options with stochastic volatility with applications to bond and currency options*, Rev. Financ. Stud., 6 (1993), 327–343.
- [22] D. HIGHAM AND X. MAO, *Convergence of Monte Carlo simulations involving the mean-reverting square root process*, J. Comput. Finance, 8 (2005), 35–61.
- [23] W. HÖRMANN, *The transformed rejection method for generating Poisson random variables*, Insurance Math. Econom., 12 (1993), 39–45.
- [24] C. JOY, AND P. P. BOYLE, AND K. S. TAN, *Quasi-Monte Carlo methods in numerical finance*, Manag. Sci., 42 (1996), 926–938.
- [25] C. KAHL AND P. JÄCKEL, *Not-so-complex logarithms in the Heston model*, Wilmott, 19 (2005), 94–103.
- [26] P. E. KLOEDEN AND E. PLATEN, *Numerical Solution of Stochastic Differential Equations*, Applications of Mathematics, Stochastic Modelling and Applied Probability, Vol. 23, Springer-Verlag, New York, 1992.
- [27] R. LORD, R. KOEKKOEK, AND D. VAN DIJK, *A comparison of biased simulation schemes*

- for stochastic volatility models, *Quant. Finance*, 10 (2010), 177–194.
- [28] S. J. A. MALHAM, AND A. WIESE, *Chi-square simulation of the CIR process and the Heston model*, *Int. J. Theor. Appl. Finance*, 16 (2013), 1350014.
 - [29] S. J. MALHAM AND A. WIESE, *Efficient almost-exact Lévy area sampling*, *Statist. Probab. Lett.*, 88 (2014), 50–55.
 - [30] G. N. MILSTEIN, *Numerical Integration of Stochastic Differential Equations*, Springer-Verlag, New York, 1994.
 - [31] B. MORO, *The full Monte*, *Risk*, 8 (1995), 57–58.
 - [32] J. PITMAN AND M. YOR, *A decomposition of Bessel bridges*, *Z. Wahrsch. Verw. Geb.*, 59 (1982), 425–457.
 - [33] W. H. PRESS, S. A. TEUKOLSKY, W. T. VETTERLING, AND B. P. FLANNERY, *Numerical Recipes in C: The Art of Scientific Computing*, 2nd ed., Cambridge University Press, Cambridge, 1992.
 - [34] W. RUDIN, *Real and Complex Analysis*, 3rd ed., McGraw-Hill Book Company, New York, 1987.
 - [35] L. O. SCOTT, *Simulating a multi-factor term structure model over relatively long discrete time periods*, *Proceedings of the IAFE First Annual Computational Finance Conference*, Graduate School of Business, Stanford University, Stanford, CA, 1996.
 - [36] J. SHEN, *Direct Inversion for the Heston model*, PhD thesis, Heriot-Watt University, 2020.
 - [37] R. D. SMITH, *An almost exact simulation method for the Heston model*, *J. Comput. Finance*, 11 (2007), 115–125.
 - [38] N. M. TEMME, *Numerical and asymptotic aspects of parabolic cylinder functions*, *J. Comput. Appl. Math.*, 121 (2000), 221–246.
 - [39] A. VAN HAASTRECHT, AND A. PELSSER, *Efficient, almost exact simulation of the Heston stochastic volatility model*, *Int. J. Theor. Appl. Finance*, 13 (2010), 1–43.

Appendix G. Supplementary Materials. In the tables below, we quote the Chebyshev coefficients of the approximations to the inverse distribution functions for the (standardised) sum $(Z^P) S^P$. Note that the u denotes the right boundary point of each regime.

TABLE 4
Chebyshev coefficients c_n for $P = 1$.

n	left	central	middle
0	1.870164486816790e-01	4.979491420716220e-01	9.481879998153620e-01
1	7.543713026654420e-02	8.479024376573340e-02	1.331260262296900e-01
2	-8.902496689813970e-04	5.515061682001420e-03	-2.432806629044970e-04
3	5.081110592347190e-04	1.234615565280710e-03	7.536358417854170e-05
4	-6.749946441432770e-05	7.826573846201580e-05	-1.832873207509700e-05
5	1.869595919328090e-05	3.190249135857450e-05	3.735655017085910e-06
6	-4.954381513667230e-06	6.911355172727800e-07	-6.763222944593870e-07
7	1.546665396688050e-06	1.101914889591240e-06	1.152436476933680e-07
8	-5.158806635369980e-07	-4.732064488662130e-08	-1.948453255574870e-08
9	1.840226824599990e-07	4.708456855473810e-08	3.380721765672400e-09
10	-6.893572202548840e-08	-5.304437974915840e-09	-6.060338021312360e-10
11	2.688851615671340e-08	2.373716110861710e-09	1.110982538990550e-10
12	-1.083817122960260e-08	-4.052654986799920e-10	-2.059320821371500e-11
13	4.489823790157280e-09	1.347795701927130e-10	3.835128401417810e-12
14	-1.903315339772780e-09	-2.837136223549530e-11	-6.941256697800590e-13
15	8.228619256107180e-10	8.275614752183520e-12	
16	-3.618241198589310e-10	-1.932522965168290e-12	
17	1.614597119724730e-10	4.988201361092360e-13	
18	-7.298521657921080e-11		
19	3.336786065994890e-11		
20	-1.540524697535400e-11		
21	7.165207365475960e-12		
22	-3.335368012294930e-12		
23	1.513427174673910e-12		
24	-5.858440022503530e-13		
u			
	2.000000000000000e-01	6.300000000000000e-01	9.000000000000000e-01
k_1			
	1.059586512649680e+01	-2.206240228024450e+01	1.146497265429040e+01
k_2			
	-1.186186343393790e+00	1.000000000000000e+00	-2.084692506698210e+00

TABLE 4
(cont.) Chebyshev coefficients c_n for $P = 1$.

n	right tail	right tail
0	2.147319302658020e+00	7.301291887179110e+00
1	4.666085467273610e-01	2.110381075693420e+00
2	-5.745397085771070e-06	-3.401385019474830e-12
3	3.926281274449900e-06	3.135451774873670e-12
4	-2.335817034793870e-06	-2.797671851935420e-12
5	1.221893569112290e-06	2.415971255636180e-12
6	-5.676317622953180e-07	-2.018406573717770e-12
7	2.363679020058830e-07	1.629565101375640e-12
8	-8.898571009069280e-08	-1.267921039843530e-12
9	3.052532824574800e-08	9.444179410663350e-13
10	-9.610414759815690e-09	-6.622577811449470e-13
11	2.796013299028150e-09	4.176644424605940e-13
12	-7.568881452656740e-10	-2.012958534474450e-13
13	1.920738140207490e-10	
14	-4.610765872702790e-11	
15	1.059477675547800e-11	
16	-2.363411529421280e-12	
17	4.992754651101120e-13	
18		
19		
20		
21		
22		
23		
24		
	9.990000000000000e-01	
	k_1	k_1
	3.257208614274380e+00	7.201627100158970e-01
	k_2	k_2
	-1.124938736608290e+00	-1.635958636579130e+00

TABLE 5
Chebyshev coefficients c_n for $P = 10$.

n	left tail	left central
0	-4.186236205146250e+00	-1.966613010380010e+00
1	1.605190906754510e+00	-1.483681112879300e-02
2	1.059708264495660e-02	-5.446775372602540e-03
3	-2.569138906164220e-02	2.105452172418740e-06
4	2.657630896552880e-03	-3.250251439573260e-05
5	5.038422707739470e-04	6.250462841383680e-07
6	-1.420477191393670e-04	-2.522741048643350e-07
7	-2.983752657616170e-06	1.026418500454660e-08
8	5.644770851826920e-06	-2.286307882545840e-09
9	-4.127971330420580e-07	1.386590908961820e-10
10	-2.164910928216110e-07	-2.303940103504890e-11
11	3.970382219542570e-08	1.773158449711400e-12
12	8.721275989102100e-09	-2.474347778199780e-13
13	-3.382084859676620e-09	
14	-2.332160758995600e-10	
15	2.833835970869750e-10	
16	-2.159881036758510e-11	
17	-1.980176647976920e-11	
18	5.076230137995960e-12	
19	8.012161542244290e-13	
20	-6.172636726201170e-13	
u		
	3.331451575280440e-01	5.379510893093010e-01
k_1		
	-6.189978932685550e-01	-3.895807869740060e+00
k_2		
	1.058533490397160e+00	1.000000000000000e+00
n	right central	right tail
0	2.105468260211710e+00	1.013961870007640e+01
1	5.526660297932240e-02	5.881348912778960e+00
2	6.562580263096990e-03	1.613214220004240e+00
3	4.554851569107730e-04	3.583662354665820e-01
4	4.959544883969950e-05	6.562610713857870e-02
5	4.554114153141270e-06	1.013276567637800e-02
6	4.895102446478050e-07	1.335612973263590e-03
7	5.011014704681740e-08	1.508499455059680e-04
8	5.446620224111430e-09	1.461564610943890e-05
9	5.859569797393820e-10	1.229129368330510e-06
10	6.466760957427150e-11	9.368122509902420e-08
11	7.143472968048850e-12	6.969255008216930e-09
12	7.892055904355890e-13	5.168922908502960e-10
13		3.395515411597460e-11
14		1.469649165527180e-12
15		-3.35536462420540e-14
16		
17		
18		
19		
20		
	7.168371818502030e-01	
k_1		
	4.460293975175440e+00	6.354110577138770e-01
k_2		
	-1.000000000000000e+00	-1.147724394557630e+00

TABLE 6
Chebyshev coefficients c_n for $P = 50$.

n	left tail	left central
0	-5.288942152307260e+00	-2.000965923235480e+00
1	2.354558187240890e+00	5.027272329447840e-03
2	-2.148300929212860e-01	-5.388241960386400e-03
3	1.167801704830350e-03	1.321210600565510e-04
4	4.271918579401850e-03	-3.328258515654870e-05
5	-7.367600678980360e-04	1.691117475054500e-06
6	3.190352612884990e-05	-2.758671231347400e-07
7	1.049570860070370e-05	2.011261792238410e-08
8	-2.661096411008500e-06	-2.690233651951720e-09
9	2.849363340335400e-07	2.380979895569440e-10
10	6.003686941040730e-09	-2.896342891338410e-11
11	-9.314474427911970e-09	2.851594174388340e-12
12	2.078536143889170e-09	-3.279640552952750e-13
13	-2.199997312217100e-10	
14	-1.383145073419240e-11	
15	1.142880443224370e-11	
16	-2.619066923423380e-12	
17	3.160327088396940e-13	
u		
	3.197003565947650e-01	5.169883337643990e-01
k_1		
	-6.266377357307220e-01	-4.044263478442090e+00
k_2		
	1.082311211678360e+00	9.99999999999990e-01
n	right central	right tail
0	2.062558090116340e+00	8.002513934544340e+00
1	3.614884716178920e-02	4.310172977793670e+00
2	5.905537215326120e-03	9.680044235587960e-01
3	3.302424143714490e-04	1.854270427762370e-01
4	4.120186343509380e-05	3.016976801851500e-02
5	3.385543742585720e-06	4.333887776280000e-03
6	3.843164000781120e-07	5.620910828054070e-04
7	3.717029485793840e-08	6.549643858862510e-05
8	4.112363385448630e-09	6.704595648415990e-06
9	4.289267466426690e-10	5.921631388292800e-07
10	4.741128697087930e-11	4.529653831824030e-08
11	5.137505874838590e-12	3.042863599628060e-09
12	5.647548074791590e-13	1.746343337679330e-10
13		9.109476838228590e-12
14		8.873841036286460e-13
15		
16		
17		
	7.027660432349340e-01	
k_1		
	4.294834741352050e+00	6.327817827711070e-01
k_2		
	-1.000000000000000e+00	-1.122310983565170e+00

TABLE 7
Chebyshev coefficients c_n for $P = 5000$.

n	left tail	left middle
0	-9.007526636815000e+00	-2.320006146407520e+00
1	2.127535755063470e+00	1.266023709561750e+00
2	-1.873229942604270e-01	-1.152857342660610e-01
3	1.220927893353500e-02	9.871525791146420e-03
4	-5.143519783570370e-04	-6.330801524297140e-04
5	1.053201736042580e-05	2.721250039684760e-05
6	2.597870360642370e-07	-5.511437046510560e-07
7	-3.977373581792380e-08	-9.780799116408280e-09
8	2.731783965620670e-09	7.487832322276510e-10
9	-1.221138438089840e-10	-6.846285108906070e-11
10	3.067277829880080e-12	1.419621555779360e-11
11	-1.657314975397310e-13	-1.036284107015480e-12
12		-3.034958826524900e-14
13		
14		
15		
16		
17		
18		
19		
u		
	5.000000000000000e-03	5.016991626360740e-01
k_1		
	-1.210717168704150e+00	-9.809650284289560e-01
k_2		
	3.018736842909130e+00	6.356505843676840e-01
n	right middle	right tail
0	2.350506283752280e+00	9.391788080584070e+00
1	1.288612184352350e+00	2.304276718789270e+00
2	1.238550415075650e-01	2.244838261893660e-01
3	1.126367631985240e-02	1.723724750804200e-02
4	8.113776712522790e-04	1.029865654753350e-03
5	4.574695148394010e-05	5.284626922206710e-05
6	2.146343317877790e-06	2.632282130705390e-06
7	1.059607255591610e-07	1.297109856324030e-07
8	6.522023447796370e-09	6.005448267256560e-09
9	3.433932966389800e-10	3.273100583196690e-10
10	7.415030905551360e-12	5.306924125563730e-11
11	-5.333234673760680e-14	2.645356635940220e-11
12		1.613648499072340e-11
13		9.700093322305410e-12
14		5.663793575999130e-12
15		3.213742114800220e-12
16		1.771549706162470e-12
17		9.437229274020540e-13
18		4.731397672671720e-13
19		1.949505078193680e-13
	9.950000000000000e-01	
k_1		
	9.857057212990940e-01	1.210983500602370e+00
k_2		
	-6.435551648966840e-01	-3.019180921864380e+00

TABLE 8
Chebyshev coefficients c_n for $P = 10^4$.

n	left tail	left middle
0	-8.763208308698120e+00	-2.117708885805710e+00
1	2.272856177544270e+00	1.148679380728190e+00
2	-2.195485611789300e-01	-9.719454925386660e-02
3	1.600603323734860e-02	7.829228309183660e-03
4	-7.913864835076260e-04	-4.795725327622320e-04
5	2.398092020649720e-05	2.045360216276630e-05
6	-1.924215235351760e-07	-5.013317907576720e-07
7	-3.279659242674000e-08	3.503726442772780e-09
8	3.433751594624110e-09	-1.253562317413470e-10
9	-1.944135457019680e-10	-1.311511811147320e-12
10	5.718823252641270e-12	5.140621840511810e-12
11	-3.006387310778820e-13	-4.635014571234970e-13
12		
13		
14		
15		
16		
17		
u		
	1.000000000000000e-02	5.012014905499710e-01
k_1		
	-1.115994743243930e+00	-1.054206693922630e+00
k_2		
	2.704324434390850e+00	6.099629843489590e-01
n	right middle	right tail
0	2.134535481408690e+00	9.022503475215680e+00
1	1.161232186820710e+00	2.401317040413510e+00
2	1.019807405937260e-01	2.487767815506420e-01
3	8.555012569847670e-03	2.028231950132690e-02
4	5.664908014626390e-04	1.266220882300120e-03
5	2.890763831163810e-05	6.623334821975800e-05
6	1.181852005087120e-06	3.326141775983180e-06
7	4.960639757165790e-08	1.667239146689460e-07
8	2.822677760359780e-09	7.705454473071610e-09
9	1.409816724283650e-10	3.768066578229160e-10
10	1.871694274577610e-12	3.560180300524010e-11
11	-1.571409536591980e-13	1.210420538657680e-11
12		7.304190736146010e-12
13		4.532327470602990e-12
14		2.727718438162450e-12
15		1.578085621557310e-12
16		8.497824077877610e-13
17		3.683334903311600e-13
9.900000000000000e-01		
k_1		
	1.058073632931550e+00	1.115994743243930e+00
k_2		
	-6.158684948176150e-01	-2.704324434390850e+00

TABLE 9
Chebyshev coefficients c_n for $P = 10^5$.

n	left tail	right tail
0	-5.706926051399320e+00	5.760300411129710e+00
1	3.395553188579180e+00	3.436321449713240e+00
2	-6.300054999277720e-01	6.483188840749760e-01
3	9.838818354304640e-02	1.035993426134920e-01
4	-1.136750936655030e-02	1.252833208873680e-02
5	9.513883577249630e-04	1.161417162277510e-03
6	-6.015836221231600e-05	9.191380802217640e-05
7	3.618126012554300e-06	7.737590464616790e-06
8	-1.697979831324770e-07	6.400595433239310e-07
9	-1.897253631189280e-08	2.904203939446630e-08
10	3.326071860640010e-09	1.050861883541800e-09
11	2.442263784022650e-10	6.008685289953490e-10
12	-3.833832227759890e-11	6.651321295963480e-11
13	-1.297154428240060e-11	-1.031199486940060e-11
14	1.412983301319550e-12	-9.752972166933010e-13
15	4.089569727968860e-13	5.588332180241710e-13
u		
	5.003799449933160e-01	
	k_1	k_1
	-5.424593574874610e-01	5.427821460191420e-01
	k_2	k_2
	8.005868439521350e-01	-8.016582768171050e-01

TABLE 10
Chebyshev coefficients c_n for $P = 10^6$.

n	left tail	right tail
0	-5.946145460337920e+00	5.964470382846980e+00
1	3.556004911984500e+00	3.570041770711440e+00
2	-6.801894131410160e-01	6.865586194977590e-01
3	1.092510150797910e-01	1.110985275994380e-01
4	-1.307725205702110e-02	1.349685679309470e-02
5	1.160328523663860e-03	1.237761453545620e-03
6	-8.240107479627320e-05	9.434859113712600e-05
7	5.926003936265940e-06	7.508635778142890e-06
8	-3.827985039853400e-07	5.673276390309780e-07
9	-4.939610258605130e-09	1.429761666233160e-08
10	2.191431812357590e-09	-4.002728561697650e-10
11	4.611932833470640e-10	6.107231293159660e-10
12	-4.959733545874770e-11	6.167427914388110e-11
13	-1.701165301087770e-11	-1.590293060974530e-11
14	1.492500677577930e-12	-1.334659663440940e-12
15	5.860252785293660e-13	6.358368604978550e-13
u		
	5.001201491665880e-01	
	k_1	k_1
	-5.310898090226540e-01	5.311876095528130e-01
	k_2	k_2
	8.051645964724630e-01	-8.054970186947690e-01

TABLE 11
Chebyshev coefficients c_n for $h = 2$.

n	left	left
0	3.746732186396810e-01	1.246285546643250e+00
1	1.195997564921540e-01	3.358246308532060e-01
2	-8.070601474351940e-03	2.386732322681120e-02
3	1.339603001568510e-03	1.294898023275990e-02
4	-2.506080830464610e-04	2.637423242240120e-03
5	5.637743633696060e-05	1.091486949977880e-03
6	-1.413866007641720e-05	3.083088185622240e-04
7	3.869664142567620e-06	1.183343193111800e-04
8	-1.132969831139660e-06	3.838648490201040e-05
9	3.501617974093610e-07	1.440406811311990e-05
10	-1.130976314574740e-07	5.002488355310480e-06
11	3.788372056248530e-08	1.869987422785930e-06
12	-1.308238855480900e-08	6.739900491698620e-07
13	4.635781671551490e-09	2.526970560301390e-07
14	-1.679323548784110e-09	9.311688370921460e-08
15	6.200204087490220e-10	3.508754493020290e-08
16	-2.327351020956820e-10	1.311638643142900e-08
17	8.863586972126330e-11	4.968660909382380e-09
18	-3.418842923801670e-11	1.875958145331950e-09
19	1.333107561719920e-11	7.141781072249230e-10
20	-5.234957827868200e-12	2.716166269988070e-10
21	2.035050527498960e-12	1.038650818883500e-10
22	-7.009107859412300e-13	3.972098592976600e-11
23		1.524237223546780e-11
24		5.838842289005870e-12
25		2.206347821363880e-12
26		7.400818875262400e-13
	u	
	4.943694484749030e-02	8.724214735883850e-01
	k_1	k_1
	4.396896568327450e+00	1.265081819857330e+00
	k_2	k_2
	-1.301445639726460e+00	-1.662175466937440e+00

TABLE 11
(cont.) Chebyshev coefficients c_n for $h = 2$.

n	middle	right tail
0	3.527966142386780e+00	1.003328309377590e+01
1	7.472142334253430e-01	2.496706503355630e+00
2	-1.333644417363060e-02	-1.589949448670880e-02
3	2.622018509548740e-03	3.113590178926820e-03
4	-6.027577883155430e-04	-6.963073964368400e-04
5	1.515242268297150e-04	1.678769292503920e-04
6	-4.036373098988620e-05	-4.250114645375870e-05
7	1.119644049107180e-05	1.113756440553480e-05
8	-3.199289309119440e-06	-2.994727316140500e-06
9	9.349240809409510e-07	8.214913272814210e-07
10	-2.779917579878980e-07	-2.289772183834370e-07
11	8.378973634959820e-08	6.466492239429990e-08
12	-2.552869970129400e-08	-1.846256500319380e-08
13	7.845488794437930e-09	5.320336235290850e-09
14	-2.428118880696940e-09	-1.545402456085360e-09
15	7.559005461053680e-10	4.520062644698680e-10
16	-2.364994613022200e-10	-1.330078378584710e-10
17	7.431800136657720e-11	3.934888781070520e-11
18	-2.344374813365950e-11	-1.169587411803260e-11
19	7.415598838082110e-12	3.489114825460500e-12
20	-2.333558791113770e-12	-1.037689978383220e-12
21	6.745346171083730e-13	2.859557405213800e-13
22		
23		
24		
25		
26		
	9.997923134230980e-01	
	k_1	k_1
	2.336282203175340e+00	6.370068451629010e-01
	k_2	k_2
	-6.514171570857550e-01	-1.450272673332570e+00

TABLE 12
Chebyshev coefficients c_n for $h = 1/5$.

n	left	central	middle
0	1.551440631887020e-02	5.965851817537560e-02	2.365922039769380e-01
1	7.154056831584140e-03	1.701537131814850e-02	7.509528018047980e-02
2	1.120793580526900e-04	2.597262497204220e-03	6.749060031298230e-03
3	-2.767589127786680e-05	4.709183006272860e-04	-9.756034732487190e-05
4	5.310776527089690e-06	7.145518311775060e-05	-4.546713797013440e-05
5	-1.242484981459680e-06	1.330260630541950e-05	2.265934249688400e-06
6	3.545760586969740e-07	1.967551836645490e-06	3.137406427278980e-07
7	-1.173714662110980e-07	3.949016650674680e-07	1.344476627067420e-08
8	4.313888580276150e-08	5.420695609123570e-08	-8.390259114557710e-09
9	-1.709037630074550e-08	1.243550067642890e-08	7.380356092377570e-10
10	7.159028761307770e-09	1.439656776199120e-09	-2.253776759627590e-10
11	-3.130641321239270e-09	4.213671249996360e-10	4.735083288679870e-11
12	1.416650107438240e-09	3.320038533665110e-11	-6.226333936166760e-12
13	-6.591639233672150e-10	1.566391114883240e-11	2.369177040131130e-12
14	3.138939220131410e-10	4.052720676134970e-13	-5.354588204982440e-13
15	-1.524291404102210e-10		
16	7.526974215608190e-11		
17	-3.770866706212000e-11		
18	1.912726184698180e-11		
19	-9.801629544246880e-12		
20	5.055418302750250e-12		
21	-2.598617692870460e-12		
22	1.287201224090770e-12		
23	-5.308318388467400e-13		
24			
u			
	2.096913523963960e-01	6.331471212688160e-01	9.308037742250030e-01
k_1			
	1.685718137659840e+02	-5.009544088177860e+01	8.992727193150630e+00
k_2			
	-1.121868009800680e+00	1.000000000000000e+00	-1.516097941825860e+00

TABLE 12
(cont.) Chebyshev coefficients c_n for $h = 1/5$.

n	right tail	right tail
0	9.766531067045780e-01	5.548556192934720e+00
1	3.018335097399800e-01	2.006312378503930e+00
2	1.137764493492600e-02	2.401553462574660e-02
3	-1.796551902064940e-03	-5.827238250950370e-03
4	2.961890615175630e-04	1.564108444981830e-03
5	-3.906140490786650e-05	-4.425250341488140e-04
6	3.228136981746220e-07	1.292806696330280e-04
7	1.990381470117290e-06	-3.860207865611520e-05
8	-7.180791153931000e-07	1.171917601240410e-05
9	1.237304075899040e-07	-3.609533592707940e-06
10	4.797867870237380e-09	1.128193509794600e-06
11	-1.022283804766720e-08	-3.587762176720570e-07
12	3.242766128356910e-09	1.166622015545870e-07
13	-3.934089138513020e-10	-3.905857435831940e-08
14	-1.071903231878940e-10	1.356481292566670e-08
15	7.087360088039800e-11	-4.912140911093550e-09
16	-1.797818306057740e-11	1.854288283705740e-09
17	1.002649821269050e-12	-7.243408051055730e-10
18	1.130725736108390e-12	2.888927287597270e-10
19	-5.251498162236730e-13	-1.156809097791070e-10
20		4.568355593550080e-11
21		-1.746849139303900e-11
22		6.337718113837970e-12
23		-2.123287366692640e-12
24		6.058538275109010e-13
	9.985870051144820e-01	
	k_1	k_1
	3.854817463192980e+00	7.119316740438860e-01
	k_2	k_2
	-2.078549151656860e+00	-1.568565612274160e+00

TABLE 13
Chebyshev coefficients c_n for $h = 1/10$.

n	left	central	middle
0	3.130510092436490e-03	2.226333345761950e-02	1.988982349173310e-01
1	1.417002017122940e-03	1.019151935447450e-02	8.748062377822970e-02
2	2.360674641499860e-05	2.673461828675060e-03	1.322178512127460e-02
3	-6.764554780577100e-06	7.541005867012190e-04	1.783172989082840e-05
4	1.073524111115770e-06	1.825724014495570e-04	-1.742061549930610e-04
5	-2.165240827636890e-07	5.070406265568330e-05	1.493474602053700e-06
6	5.714805445297300e-08	1.156695182629020e-05	3.359055560341550e-06
7	-1.802784817620440e-08	3.413930484845420e-06	5.333580684343860e-08
8	6.351907282247530e-09	6.943759577207300e-07	-5.521667146922240e-08
9	-2.410001034673690e-09	2.411908456774400e-07	-2.276235131191460e-09
10	9.649353406509410e-10	3.679790048414060e-08	-2.893556379100810e-10
11	-4.026554373758090e-10	1.888991234749750e-08	-6.436850207940650e-11
12	1.736498040397040e-10	1.106003127127480e-09	2.350168269709410e-11
13	-7.693121262340320e-11	1.752401085721140e-09	2.321358068727610e-11
14	3.485269197769610e-11	-1.364762944049400e-10	2.636593526158320e-12
15	-1.608506662519110e-11	2.000879783288790e-10	-1.139207052258690e-12
16	7.530478144378150e-12	-4.354349576970780e-11	-7.314416583435220e-13
17	-3.545863047530400e-12	2.738074123398660e-11	
18	1.631081082539700e-12	-8.687479490879170e-12	
19	-6.387767991337960e-13	4.196188738890250e-12	
20		-1.521565690726940e-12	
21		5.748616824737580e-13	
	u		
	1.060708119058860e-01	7.049238354832290e-01	9.715292650150570e-01
	k_1	k_1	k_1
	8.775453590729910e+02	-5.009576443446880e+01	6.414761023377960e+00
	k_2	k_2	k_2
	-1.150665798108190e+00	1.000000000000000e+00	-9.422665062905070e-01

TABLE 13
(cont.) Chebyshev coefficients c_n for $h = 1/10$.

n	right tail	right tail
0	1.167088563196570e+00	5.557949689428240e+00
1	4.028821977072450e-01	1.804403214930680e+00
2	1.589726864878320e-02	2.001076313509200e-02
3	-2.776444180529080e-03	-4.157908839745580e-03
4	5.440877740378380e-04	9.533639401005070e-04
5	-1.067963570631740e-04	-2.298471294547880e-04
6	1.602535986540860e-05	5.706424934572420e-05
7	3.639164819106400e-07	-1.443342632426860e-05
8	-1.502345300041770e-06	3.696661627610680e-06
9	6.684757371238390e-07	-9.553281498410910e-07
10	-1.716295249441850e-07	2.486726588153440e-07
11	1.635394935133220e-08	-6.518766056569640e-08
12	8.892938254607350e-09	1.724037249294330e-08
13	-5.718412804481970e-09	-4.621243803810750e-09
14	1.784898899321040e-09	1.266095041880910e-09
15	-2.594370983148820e-10	-3.591505441133870e-10
16	-6.261300169685750e-11	1.071702367595880e-10
17	5.827210983507840e-11	-3.409479146600350e-11
18	-2.189105354284160e-11	1.160098934787360e-11
19	4.514597736601780e-12	-4.170286799495250e-12
20	-6.083212355274480e-14	1.531989721713420e-12
21		-5.089272134222670e-13
	9.998315799958800e-01	
	k_1	k_1
	2.923879081718190e+00	7.878535911129940e-01
	k_2	k_2
	-1.885294461971110e+00	-1.777456775656590e+00

TABLE 14
Chebyshev coefficients c_n for $h = 1/20$.

n	left	central	middle
0	8.320108386176220e-04	1.028289222803410e-02	1.796716788945920e-01
1	3.797922844843720e-04	6.051387649842750e-03	9.215513210293030e-02
2	6.119152516315670e-06	2.386515701734710e-03	1.798443115218630e-02
3	-2.216499535843730e-06	9.149383182711970e-04	3.536164396647120e-04
4	3.549796569970470e-07	3.260804312989750e-04	-3.290230257519100e-04
5	-6.909777679284210e-08	1.174302244391960e-04	-9.190331115977200e-06
6	1.800406773387920e-08	4.046558068563540e-05	8.941392960865100e-06
7	-5.727807832664590e-09	1.430511004864880e-05	4.569100427021660e-07
8	2.048306829365090e-09	4.845772394724280e-06	-1.898690252517320e-07
9	-7.892933375352240e-10	1.708561223033980e-06	-1.470693084569350e-08
10	3.208272429161230e-10	5.709919634096540e-07	9.061517318686090e-10
11	-1.358581479450610e-10	2.027725977295490e-07	-4.996134827280970e-10
12	5.944136353935260e-11	6.667913363885630e-08	-3.085715272976990e-11
13	-2.671169627505600e-11	2.408641753810920e-08	8.541875621658270e-11
14	1.227327977365980e-11	7.729248497752890e-09	3.049756612877180e-11
15	-5.743936308401000e-12	2.879366774439790e-09	7.727805117204190e-13
16	2.726212185552570e-12	8.872469780543650e-10	-3.534457536346370e-12
17	-1.300587961514960e-12	3.484429145625870e-10	-1.357036283678540e-12
18	6.052241498351530e-13	1.001335286917030e-10	4.056653202382400e-14
19	-2.390157663283510e-13	4.301663419431590e-11	2.166251245948460e-13
20		1.093494057671210e-11	
21		5.462280485697060e-12	
22		1.109419945826560e-12	
23		6.264905101784660e-13	
	u		
	9.952451539818020e-02	7.959736941620220e-01	9.872109261016380e-01
	k_1	k_1	k_1
	3.350041337835460e+03	-6.091816627093630e+01	5.415831650268340e+00
	k_2	k_2	k_2
	-1.142970216093080e+00	9.99999999999990e-01	-6.895558541579670e-01

TABLE 14
(cont.) Chebyshev coefficients c_n for $h = 1/20$.

n	right tail	right tail
0	9.761057883039990e-01	5.196073467821080e+00
1	3.017284864244540e-01	1.831141920349900e+00
2	1.166946937938660e-02	2.543065037748800e-02
3	-1.687052247930830e-03	-5.741796704905520e-03
4	2.745955374164150e-04	1.425454072455170e-03
5	-4.255962891388790e-05	-3.709730129757980e-04
6	3.654738784807000e-06	9.914921759807340e-05
7	9.678759239832630e-07	-2.692978838795350e-05
8	-5.962323527180660e-07	7.390951335687150e-06
9	1.619073566570090e-07	-2.044323535428510e-06
10	-2.044848058779350e-08	5.700139242154520e-07
11	-3.557663286168380e-09	-1.608555974873110e-07
12	2.792106872070250e-09	4.637422326004230e-08
13	-8.014791797406380e-10	-1.388223005657000e-08
14	9.886383182987470e-11	4.408914855308610e-09
15	2.338331909817720e-11	-1.513613329915950e-09
16	-1.720362865683670e-11	5.636677579981080e-10
17	5.096915629190340e-12	-2.238514411774360e-10
18	-7.701281537440130e-13	9.204119152754320e-11
19		-3.802089545459430e-11
20		1.539622910176960e-11
21		-5.993091125355200e-12
22		2.193183001782910e-12
23		-6.910989846330220e-13
	9.997667653179200e-01	
	k_1	k_1
	3.745971846148320e+00	7.690538107824300e-01
	k_2	k_2
	-2.168616210929900e+00	-1.650521806358000e+00

TABLE 15
Chebyshev coefficients c_n for $h = 1/50$.

n	left	central	middle
0	3.342404855864130e-04	5.287504606339480e-03	1.679802218836370e-01
1	1.582119045977740e-04	3.609167042053250e-03	9.425159027828390e-02
2	-4.034459826869400e-06	1.936145076792520e-03	2.146641276528250e-02
3	-1.781674777546940e-06	9.633501098384940e-04	7.761771414171220e-04
4	6.111894067922420e-07	4.586062099584780e-04	-4.715700923865780e-04
5	-1.616413643230570e-07	2.128565367871240e-04	-2.911833910065400e-05
6	4.535507820139480e-08	9.711724060740940e-05	1.543681974168120e-05
7	-1.504566368490170e-08	4.380458926575550e-05	1.397441335389570e-06
8	5.916977370301490e-09	1.959490913685950e-05	-3.947158787904670e-07
9	-2.631104077272530e-09	8.713044455946110e-06	-4.582398590716490e-08
10	1.265674285428750e-09	3.857017778878410e-06	4.537121001350180e-09
11	-6.412984582939380e-10	1.701669482580570e-06	-8.587058106556170e-10
12	3.373488093146030e-10	7.488328990975590e-07	-3.395277343066420e-10
13	-1.827196103322590e-10	3.288850425725570e-07	1.497940638456500e-10
14	1.013577890763340e-10	1.442278857066740e-07	9.047367570431180e-11
15	-5.736165706600700e-11	6.317620038821080e-08	1.532712463574530e-11
16	3.301900838213170e-11	2.764873413720030e-08	-5.899234983630290e-12
17	-1.928175236669560e-11	1.209228320347630e-08	-4.759599480764640e-12
18	1.139207390775470e-11	5.285996098982320e-09	-9.845099825540210e-13
19	-6.784952996564550e-12	2.309885154214620e-09	3.353301735326350e-13
20	4.046041780101790e-12	1.009129182529960e-09	
21	-2.377799356621700e-12	4.407929681530880e-10	
22	1.318077536426880e-12	1.925241011297400e-10	
23	-5.870490384521500e-13	8.408559765252580e-11	
24		3.672433365477270e-11	
25		1.603764366665520e-11	
26		6.998237196315440e-12	
27		3.040158479208750e-12	
28		1.288881492848470e-12	
29		4.729004482220720e-13	
u			
	2.9311238965950420e-01	8.963482076412410e-01	9.952179896810610e-01
	k_1	k_1	k_1
	7.818489955336010e+03	-1.112036741342440e+02	4.876183772221110e+00
	k_2	k_2	k_2
	-1.055332320056090e+00	1.000000000000000e+00	-5.434844889094470e-01

TABLE 15
(cont.) Chebyshev coefficients c_n for $h = 1/50$.

n	right tail	right tail
0	9.761146326247330e-01	5.440971360286990e+00
1	3.016928648060250e-01	1.956911680269630e+00
2	1.167231718705550e-02	2.774260925258900e-02
3	-1.651276452041110e-03	-6.436890817427110e-03
4	2.666875570608340e-04	1.641299885337880e-03
5	-4.247191460497490e-05	-4.384480040071970e-04
6	4.247919767558590e-06	1.201938574075200e-04
7	7.240192379129270e-07	-3.345172414930230e-05
8	-5.468504974426770e-07	9.394648359883000e-06
9	1.621838761986780e-07	-2.653557174889410e-06
10	-2.469682517941960e-08	7.531228230971810e-07
11	-1.846812979021160e-09	-2.152447292666580e-07
12	2.453530993347940e-09	6.237985768142160e-08
13	-8.104795070564450e-10	-1.859198071101320e-08
14	1.328212021134190e-10	5.827250350019090e-09
15	9.746012118699450e-12	-1.970501685911350e-09
16	-1.445305942484290e-11	7.299803884539640e-10
17	5.164008080182300e-12	-2.939243341028580e-10
18	-1.029938970952770e-12	1.250293085781470e-10
19		-5.430549502597070e-11
20		2.340535807434650e-11
21		-9.802247791887960e-12
22		3.924623772975130e-12
23		-1.472095272217630e-12
24		4.733000270115350e-13
25		
26		
27		
28		
29		
	9.999145446729710e-01	
	k_1	k_1
	3.727057577727170e+00	7.200044464436850e-01
	k_2	k_2
	-2.179745438075220e+00	-1.614273003898510e+00

TABLE 16
Chebyshev coefficients c_n for $h = 1/100$.

n	left	central	middle
0	1.064576523939530e-04	7.757528496943130e-04	6.583911279090610e-02
1	4.967483886634590e-05	3.963182148041290e-04	4.630386572794740e-02
2	-2.574907330657650e-06	1.452820177102820e-04	1.757544141274230e-02
3	-5.303715403034560e-07	4.855954814287430e-05	3.315284363718880e-03
4	2.663871929167150e-07	1.531863558980870e-05	1.968319378136490e-05
5	-8.401958707782960e-08	4.676444520070540e-06	-1.223428005218250e-04
6	2.541840517940180e-08	1.394003778702580e-06	-1.557379115932900e-05
7	-8.458536138015860e-09	4.088490384098540e-07	3.231990249141240e-06
8	3.265291063082850e-09	1.184092050832930e-07	9.273005743030430e-07
9	-1.446267628365560e-09	3.397158988245310e-08	-3.854154049131550e-08
10	7.070186386866000e-10	9.672491318170320e-09	-3.568282952834910e-08
11	-3.686990455737450e-10	2.737461712291000e-09	-8.276509465005390e-10
12	2.008214150700500e-10	7.708833517653440e-10	1.206706537754180e-09
13	-1.129090416703240e-10	2.161982864910220e-10	9.225936702119910e-11
14	6.508194177274510e-11	6.042419184248020e-11	-3.617701898545360e-11
15	-3.828935422940620e-11	1.683809589516920e-11	-4.590404543093130e-12
16	2.291651606295020e-11	4.678693771234680e-12	9.605943640102260e-13
17	-1.391339883329400e-11	1.290808850907550e-12	1.614097426563680e-13
18	8.543046330402440e-12	3.320491288954080e-13	
19	-5.282416801082780e-12		
20	3.263505722460030e-12		
21	-1.979537858186990e-12		
22	1.125706972359250e-12		
23	-5.098805064619270e-13		
24			
25			
26			
27			
28			
29			
30			
u			
	3.364182499030230e-01	7.854302604129020e-01	9.936476554735930e-01
	k_1	k_1	k_1
	2.356466133610040e+04	-2.112823879640160e+02	4.261592636084800e+00
	k_2	k_2	k_2
	-1.042176040321580e+00	1.000000000000000e+00	2.136086687920960e-01

TABLE 16
(cont.) Chebyshev coefficients c_n for $h = 1/100$.

n	right tail	right tail
0	5.721713263001810e-01	5.012707101453440e+00
1	2.017820038440820e-01	2.062096651831810e+00
2	1.377375013917080e-02	3.999684930491530e-02
3	-1.806370775567440e-03	-1.094915283125730e-02
4	1.523593047177300e-04	3.280050342478840e-03
5	2.295752543436930e-05	-1.026359592164560e-03
6	-1.211645711839800e-05	3.290839108300630e-04
7	1.558915013492110e-06	-1.072510048733340e-04
8	3.379002506728430e-07	3.549425811224860e-05
9	-1.589627733030860e-07	-1.199878274669100e-05
10	8.281053242094140e-09	4.199796533313170e-06
11	9.754591213299930e-09	-1.552499344038120e-06
12	-2.587101485419130e-09	6.174229919308370e-07
13	-2.654922061326020e-10	-2.654025845860760e-07
14	2.854986006586110e-10	1.213436337756580e-07
15	-4.288462498279570e-11	-5.724458644126490e-08
16	-1.614286040010390e-11	2.696385391883720e-08
17	8.227664210952470e-12	-1.231399370142220e-08
18	-8.469562416364850e-13	5.303258910110760e-09
19		-2.080169945416400e-09
20		6.955732723896000e-10
21		-1.600540556356640e-10
22		-1.256262769207190e-11
23		4.730496708984270e-11
24		-3.958827080866930e-11
25		2.486066180938770e-11
26		-1.342780201739020e-11
27		6.510864817550600e-12
28		-2.877910389935850e-12
29		1.155822468250220e-12
30		-3.885406981704210e-13
	9.997327929473050e-01	
	k_1	k_1
	4.734018530749910e+00	6.757660555129490e-01
	k_2	k_2
	-1.873568041871660e+00	-1.410192678438050e+00

TABLE 17
Chebyshev coefficients c_n for $h = 1/200$.

n	left	central	middle
0	3.518991274756410e-05	8.392520820142320e-04	3.802327783487690e-02
1	1.590990829653510e-05	6.431136826076690e-04	2.293406644160830e-02
2	-1.491507257739220e-06	4.085596936397020e-04	6.950796412254640e-03
3	-9.066540515692110e-08	2.399296017984750e-04	1.080933113927390e-03
4	1.118185077651380e-07	1.344982201802300e-04	3.968276530040410e-05
5	-4.689629675507760e-08	7.316918708694770e-05	-1.510396050891140e-05
6	1.672578243190620e-08	3.898020499880180e-05	-2.164545910662930e-06
7	-5.962483120983330e-09	2.045075653316820e-05	1.031238628209580e-07
8	2.299928220409480e-09	1.060530105647130e-05	4.715822375760130e-08
9	-9.951311785026230e-10	5.449951689909780e-06	1.338195202962630e-09
10	4.813973704272410e-10	2.780434074253660e-06	-7.162524074055580e-10
11	-2.538921373245920e-10	1.410169685110300e-06	-5.838646258223070e-11
12	1.421639472958470e-10	7.117308974598160e-07	9.035922879320330e-12
13	-8.292852778673330e-11	3.577606972109210e-07	1.324669429761400e-12
14	4.981742953446680e-11	1.792155094219710e-07	-9.136939392295850e-14
15	-3.060881416945410e-11	8.951262809172500e-08	
16	1.915173995253600e-11	4.459614066323360e-08	
17	-1.216412493952420e-11	2.216977555006020e-08	
18	7.820244746397910e-12	1.100014354771840e-08	
19	-5.072097961571200e-12	5.448923967042200e-09	
20	3.302395224132890e-12	2.695162687572190e-09	
21	-2.138908948989580e-12	1.331357683924750e-09	
22	1.351588122026080e-12	6.569059660914260e-10	
23	-7.937121438141370e-13	3.237909926903940e-10	
24	3.670269446605750e-13	1.594506248721030e-10	
25		7.845610579728340e-11	
26		3.857391556723120e-11	
27		1.895058050737680e-11	
28		9.300136827782300e-12	
29		4.552865562504610e-12	
30		2.209843826831820e-12	
31		1.035453103819430e-12	
32		4.092881791896850e-13	
u			
	3.889455754261150e-01	9.290038930121230e-01	9.933230995102950e-01
k_1			
	6.580451400950010e+04	-2.484251686923060e+02	6.345255066723990e+00
k_2			
	-1.029129856396840e+00	1.000000000000000e+00	4.634771910249610e-01

TABLE 17
(cont.) Chebyshev coefficients c_n for $h = 1/200$.

n	right tail	right tail
0	4.996811103033990e-01	4.914258356400550e+00
1	2.283166265702920e-01	2.011738127244230e+00
2	2.514423513031150e-02	3.937356800757610e-02
3	-3.474198991631110e-03	-1.065266526129480e-02
4	5.077220214696990e-05	3.152291195579000e-03
5	1.613616422231280e-04	-9.738895553647930e-04
6	-3.880889586523480e-05	3.081786621477630e-04
7	-3.634159932107070e-06	-9.909792676876680e-05
8	3.510602114428830e-06	3.236113469325020e-05
9	-1.965557011348590e-07	-1.080367954217740e-05
10	-2.893679425553000e-07	3.742488200776480e-06
11	4.919338342933830e-08	-1.374128809584770e-06
12	2.766224437511820e-08	5.450001386646280e-07
13	-9.150633315570560e-09	-2.341737771120620e-07
14	-2.629338358854130e-09	1.069346503420290e-07
15	1.702910382225310e-09	-5.021967626980490e-08
16	1.193636414090970e-10	2.344515094335100e-08
17	-2.861147205442400e-10	-1.056108154875420e-08
18	3.711031444447810e-11	4.460714134159530e-09
19	3.822894605668730e-11	-1.700913808398100e-09
20	-1.452954868328450e-11	5.418507670597160e-10
21	-2.818928436440390e-12	-1.082511209350420e-10
22	3.052195946657310e-12	-2.332308071729190e-11
23	-4.763636711850320e-13	4.458678049756930e-11
24		-3.438522185303330e-11
25		2.066800196185070e-11
26		-1.078966568122660e-11
27		5.070919968888780e-12
28		-2.172493412014030e-12
29		8.448217334599220e-13
30		-2.756966775927990e-13
31		
32		
	9.998681694019440e-01	
	k_1	k_1
	3.821761784764750e+00	6.915167979999310e-01
	k_2	k_2
	-1.323148927258810e+00	-1.420354956151160e+00

TABLE 18
Chebyshev coefficients c_n for $h = 1/500$.

n	left	central	middle
0	5.483749876010110e-06	6.081052138201630e-05	5.473769059145160e-02
1	2.486444309865320e-06	3.802911084933040e-05	4.351538755149600e-02
2	-2.246254082499010e-07	1.823368632895480e-05	2.198780054496340e-02
3	-1.578587968151560e-08	7.946990081244110e-06	6.662984075703530e-03
4	1.732923293003170e-08	3.273356396625710e-06	7.907173467155090e-04
5	-7.081399642607440e-09	1.301100356483330e-06	-2.243067264619820e-04
6	2.482198403770580e-09	5.043448241124090e-07	-1.032261735179890e-04
7	-8.749831841180770e-10	1.919418161993120e-07	-5.350827374548080e-06
8	3.358446096487070e-10	7.202571800642060e-08	6.032870474106270e-06
9	-1.452715547964040e-10	2.672894811858390e-08	1.389775608451330e-06
10	7.036053028305950e-11	9.830459878805920e-09	-1.667794341081260e-07
11	-3.712078515936340e-11	3.588823452512350e-09	-1.098049445185060e-07
12	2.075613750341240e-11	1.302082454421860e-09	-3.990118701505280e-09
13	-1.206646596058050e-11	4.699379616814380e-10	6.210083081288950e-09
14	7.203733700544880e-12	1.688418171221930e-10	9.633344895225680e-10
15	-4.375271295344380e-12	6.042392709176170e-11	-2.609783367202760e-10
16	2.674170121231750e-12	2.154618744858790e-11	-8.315421351488390e-11
17	-1.612760826306620e-12	7.648543523947050e-12	6.884100040797630e-12
18	9.148126116574220e-13	2.675596311035590e-12	5.334393632012140e-12
19	-4.140244318492860e-13	8.418748326551260e-13	8.096094478676190e-14
20			
21			
22			
23			
24			
25			
26			
27			
28			
u			
	3.765509769494760e-01	8.507269533566090e-01	9.987527542914820e-01
	k_1	k_1	k_1
	4.258473700427800e+05	-4.473698477162510e+02	3.134901409944510e+00
	k_2	k_2	k_2
	-1.030074288714920e+00	1.000000000000000e+00	4.184273889203900e-01

TABLE 18
(cont.) Chebyshev coefficients c_n for $h = 1/500$.

n	right tail	right tail
0	5.722628305041320e-01	4.619812351486580e+00
1	2.017761232436850e-01	1.860589481022910e+00
2	1.372549559855640e-02	3.705233566867140e-02
3	-1.799486944230340e-03	-9.679912077752170e-03
4	1.548179312896890e-04	2.763008630922080e-03
5	2.188831960478410e-05	-8.227338295193510e-04
6	-1.205509962337280e-05	2.508114545966230e-04
7	1.626588892457300e-06	-7.771817988229730e-05
8	3.184920827863750e-07	2.450094311357910e-05
9	-1.604199428018640e-07	-7.933144007790290e-06
10	1.026914924420960e-08	2.688223932510620e-06
11	9.459364972251830e-09	-9.765416694004470e-07
12	-2.712392941794810e-09	3.865875322747190e-07
13	-2.064497813254320e-10	-1.657778704727940e-07
14	2.839303432413100e-10	7.480889417663450e-08
15	-4.871222002206250e-11	-3.419915104148750e-08
16	-1.444200355589120e-11	1.528919983568170e-08
17	8.372113940734360e-12	-6.479029251360280e-09
18	-8.215034741114160e-13	2.513840140749050e-09
19	-5.718274703852940e-13	-8.420176316921800e-10
20		2.056434736961990e-10
21		-1.906441397640450e-12
22		-4.118010901086650e-11
23		3.573866647613250e-11
24		-2.210862584205230e-11
25		1.157843167001790e-11
26		-5.392753508375620e-12
27		2.255758034817050e-12
28		-7.825720526313930e-13
	9.999476900342120e-01	
	k_1	k_1
	4.729614165580610e+00	7.444073462053960e-01
	k_2	k_2
	-1.877416447914540e+00	-1.452884710450130e+00

TABLE 19
Chebyshev coefficients c_n for $h = 1/1000$.

n	left	central	middle
0	1.702183541035500e-06	4.683227357260460e-05	5.536218616018370e-02
1	7.420902874786450e-07	3.703626675908400e-05	4.374721584420760e-02
2	-9.865066726948370e-08	2.459788457587220e-05	2.175988835715660e-02
3	2.116960181208090e-09	1.509706997971100e-05	6.418561137830710e-03
4	5.497757664443220e-09	8.833813587467830e-06	7.077802624591750e-04
5	-3.075679409634450e-09	5.007785871509330e-06	-2.234688941525440e-04
6	1.295461350315470e-09	2.775387397751700e-06	-9.419306294251860e-05
7	-5.101921537607570e-10	1.512369265686630e-06	-3.360150759204170e-06
8	2.046470586232400e-10	8.133846678811100e-07	5.606215973335830e-06
9	-8.795781406451580e-11	4.329046589636930e-07	1.138744283796750e-06
10	4.150674524923850e-11	2.284469855279910e-07	-1.744975342137310e-07
11	-2.146959372032940e-11	1.197027748370630e-07	-9.175604868426630e-08
12	1.195357510557570e-11	6.234932494901730e-08	-9.405807379254040e-10
13	-7.007921488895000e-12	3.231076406508420e-08	5.303111119723840e-09
14	4.242800470479290e-12	1.667069009839600e-08	6.408776988724730e-10
15	-2.605046952660340e-12	8.568338007765290e-09	-2.359584489072000e-10
16	1.583112277512220e-12	4.389129098487210e-09	-5.912784735389670e-11
17	-9.048703171667920e-13	2.241645822968350e-09	7.661640011719350e-12
18	4.117767633668480e-13	1.141836261366420e-09	3.874828519769490e-12
19		5.802414152021560e-10	-1.166357191529640e-13
20		2.942280531036410e-10	
21		1.489078538692040e-10	
22		7.522864040175020e-11	
23		3.794343618365480e-11	
24		1.910697269597880e-11	
25		9.603319488497670e-12	
26		4.810076959555690e-12	
27		2.385153926155570e-12	
28		1.138578899937890e-12	
29		4.560886440536520e-13	
	u		
	4.174876557129840e-01	9.322059315659190e-01	9.993778254256840e-01
	k_1	k_1	k_1
	1.251565690963700e+06	-5.828431086945030e+02	3.197606134309120e+00
	k_2	k_2	k_2
	-1.022376759557920e+00	1.000000000000000e+00	4.064120883541780e-01

TABLE 19
(cont.) Chebyshev coefficients c_n for $h = 1/1000$.

n	right tail	right tail
0	5.722747148899260e-01	4.619756015894430e+00
1	2.017753450395620e-01	1.860594275953970e+00
2	1.371924357276870e-02	3.708005345183760e-02
3	-1.798581149904210e-03	-9.684906797069420e-03
4	1.551213775007570e-04	2.763643547482780e-03
5	2.175254385332560e-05	-8.226383894790440e-04
6	-1.204645343665130e-05	2.506774823695980e-04
7	1.634965165513770e-06	-7.763711144862420e-05
8	3.159981622016720e-07	2.446026791697170e-05
9	-1.605777694467310e-07	-7.914262660093390e-06
10	1.051874919029200e-08	2.679801742363770e-06
11	9.419608354447810e-09	-9.728790947989900e-07
12	-2.727465609582260e-09	3.850313981959300e-07
13	-1.988937692998890e-10	-1.651364788520010e-07
14	2.836178919653520e-10	7.455668628814360e-08
15	-4.943002831236940e-11	-3.410750194426710e-08
16	-1.421606720565170e-11	1.526049674013000e-08
17	8.387073685132130e-12	-6.472921009013150e-09
18	-8.503982177047610e-13	2.514557909430010e-09
19	-5.640963743958310e-13	-8.439824101491250e-10
20		2.072428649649560e-10
21		-2.907032521718900e-12
22		-4.063479916620080e-11
23		3.546906613254100e-11
24		-2.198580726676460e-11
25		1.152667195366090e-11
26		-5.372666511779410e-12
27		2.248692740626720e-12
28		-7.804828886326530e-13
29		
	9.999739151276640e-01	
	k_1	k_1
	4.729078684657730e+00	7.443447629709830e-01
	k_2	k_2
	-1.877882960729700e+00	-1.452971340318820e+00

TABLE 20
Chebyshev coefficients c_n for $h = 1/2000$.

n	left	central	middle
0	8.340782562108640e-08	2.468455017350810e-06	2.280294691861460e-02
1	3.790348335769390e-08	1.808380820210540e-06	1.944720833702610e-02
2	6.055403556177730e-10	9.977786192716350e-07	1.206597650481480e-02
3	-2.457590587255690e-10	5.095262839987460e-07	5.365044701332920e-03
4	3.852931864752020e-11	2.442450448287350e-07	1.591201684585550e-03
5	-7.060509039767990e-12	1.138166487478510e-07	2.189680324488170e-04
6	1.745854017090550e-12	5.143505829362970e-08	-5.028795904628400e-05
7	-4.817127130663810e-13	2.294108192095970e-08	-3.473771288547360e-05
8		1.003514899934200e-08	-6.612748781444730e-06
9		4.362945792279890e-09	8.987877800239300e-07
10		1.869145494199760e-09	7.769588194187460e-07
11		7.993315810705090e-10	1.334497286164700e-07
12		3.374445612260970e-10	-2.638905677337210e-08
13		1.426920238747580e-10	-1.641293598763500e-08
14		5.956301256742110e-11	-1.798371164119150e-09
15		2.498973580154360e-11	8.162891792784310e-10
16		1.032764886165960e-11	3.081840920792170e-10
17		4.294120630111010e-12	5.391475739175650e-12
18		1.719237245981870e-12	-2.108451751530640e-11
19		6.120456681919280e-13	-4.569166977955490e-12
20			5.618348229993250e-13
21			
22			
23			
24			
25			
26			
27			
28			
	u		
	7.747528004946140e-02	8.259386083799630e-01	9.993395585026600e-01
	k_1	k_1	k_1
	3.425124201204160e+07	-5.668468349121090e+02	2.690942655592710e+00
	k_2	k_2	k_2
	-1.151540996208610e+00	1.000000000000000e+00	7.708355493813890e-01

TABLE 20
(cont.) Chebyshev coefficients c_n for $h = 1/2000$.

n	right tail	right tail
0	4.997785332154780e-01	4.423666819273100e+00
1	2.283167712864420e-01	1.759820399395020e+00
2	2.509022440364520e-02	3.541998526121500e-02
3	-3.473302792894470e-03	-9.020823900527130e-03
4	5.642398807896150e-05	2.508301403041810e-03
5	1.601477839497730e-04	-7.271867741631950e-04
6	-3.917135579658680e-05	2.157837314850230e-04
7	-3.440824241326100e-06	-6.511087849455140e-05
8	3.519318737665770e-06	2.002320021389290e-05
9	-2.194212259839990e-07	-6.350484440175690e-06
10	-2.877017875529090e-07	2.122832316166750e-06
11	5.198973063531290e-08	-7.670810351604760e-07
12	2.710916358293470e-08	3.034734463075500e-07
13	-9.510243857620720e-09	-1.296599648285690e-07
14	-2.488075646152630e-09	5.774831521471910e-08
15	1.740766101870470e-09	-2.574755859857430e-08
16	8.803780581176810e-11	1.108702976174020e-08
17	-2.866253352551910e-10	-4.459918192937890e-09
18	4.280148433910300e-11	1.605691932192970e-09
19	3.704110753342700e-11	-4.731139230730710e-10
20	-1.527178121204120e-11	7.876459425075560e-11
21	-2.422082175650230e-12	2.822685782970870e-11
22	3.088328322933470e-12	-3.938365394966460e-11
23	-5.645136949758680e-13	2.737131256274080e-11
24		-1.510876686567670e-11
25		7.257145569467040e-12
26		-3.126553351859840e-12
27		1.213046040716080e-12
28		-3.939886674131800e-13
	9.999869750663500e-01	
	k_1	k_1
	3.820640730812540e+00	7.845522141906270e-01
	k_2	k_2
	-1.325371123114800e+00	-1.477505002954480e+00